Evaluation of a Nordic Seas 4 km numerical ocean model hindcast archive (SVIM), 1960–2011

Article · January 2013

CITATIONS
29

READS
435

5 authors, including:

Vidar Surén Lien
Institute of Marine Research in Norway
33 PUBLICATIONS **922** CITATIONS
SEE PROFILE

Yvonne Gusdal
Norwegian Meteorological Institute
8 PUBLICATIONS **210** CITATIONS
SEE PROFILE

Jon Albretsen
Institute of Marine Research in Norway
78 PUBLICATIONS **909** CITATIONS
SEE PROFILE

Arne Melsom
Norwegian Meteorological Institute
48 PUBLICATIONS **637** CITATIONS
SEE PROFILE

FISKEN OG HAVET

nr. 7-2013

Evaluation of a Nordic Seas 4 km numerical ocean model hindcast archive (SVIM), 1960-2011

Vidar S. Lien[1]*, Yvonne Gusdal[2], Jon Albretsen[1], Arne Melsom[2] and Frode B. Vikebø[1]

[1] Institute of Marine Research, Bergen, Norway

[2] Meteorological Institute, Oslo, Norway

HAVFORSKNINGSINSTITUTTET
INSTITUTE OF MARINE RESEARCH

Evaluation of a Nordic Seas 4 km numerical ocean model hindcast archive (SVIM), 1960-2011

by
Vidar S. Lien[1]*, Yvonne Gusdal[2], Jon Albretsen[1],
Arne Melsom[2] and Frode B. Vikebø[1]
[1]Institute of Marine Research, Bergen, Norway
[2] Meteorological Institute, Oslo, Norway

* Corresponding author: vidar.lien@imr.no

HAVFORSKNINGSINSTITUTTET
INSTITUTE OF MARINE RESEARCH

Meteorologisk institutt

Contents

Abstract

A 52 year (1960-2011) numerical ocean model hindcast archive is evaluated. Overall, we find that the water masses that are directly influenced by Atlantic Water are realistically represented in the model, both in terms of advection/transport and hydrographic and dynamic variability. Inshore of the Norwegian Atlantic slope Current, the salt relaxation scheme applied negates variability in salinity within the Norwegian Coastal Current. This is most pronounced in the upper part of the water column. The modelled temperature variability in the near-shore waters is, however, in close agreement with observations. Within the two Norwegian Sea basins, the heat/freshwater content is unrealistically low/high, probably due to too little slope-basin eddy-fluxexchange between the slope current and the interior basins. In shelf areas (e.g. the Barents Sea and the North Sea), we find that the model to a large degree resembles the variability within the Atlantic-influenced water masses, while the salinity relaxation inhibits variability in the salinity within water masses dominated by coastal water.

1 Introduction

Numerical ocean models cannot replace but rather be a supplement to observations by filling in gaps in the observational data coverage. In addition, models allow for advanced cause-effect process studies that would require non-feasible observation campaigns. Here, we present the evaluation of a numerical ocean model hindcast, that simulates the Nordic and Barents seas during the period 1960-2011 at a spatial resolution of 4 km. The aim of the evaluation is to assess the quality of the model results and identify areas where the model can be expected to add information of high quality and where the model likely adds information of little value only.The focus in the current model simulation is an adequate representation of the Atlantic influenced water masses within the Nordic Seas. Less emphasize has been put on the areas downstream of the Arctic bound Atlantic Water flow, i.e. the Arctic Ocean and the Greenland Sea. These areas would require a different approach in terms of e.g. boundary values.

The aim of the current simulation is to provide a standard model product to be used as boundary values for smaller scale model studies, a dataset for process studies within physical oceanography, as well as a representation of the oceanographic conditions on which other model applications are based, such as primary production models and individual-based models for zoo- and ichtyoplankton. Therefore, the simulation will be continuously updated and maintained, at least at annual time scales, as well as further developed and improved. The model results are available at the original model grid through the Meteorological Institute web services: ftp://ftp.met.no:/projects/SVIM-public/SVIMresults. Model results will also be made available at standard depths and regular grid through the Institute of Marine Research web services.

Any queries, requests, suggestions or notifications on the model simulation, such as data requests or data quality assessments, may be directed to the corresponding author.

2 Model Description

The Regional Ocean Modeling System (ROMS) is a three dimensional baroclinic ocean general circulation model which uses topography-following s-coordinates in the vertical (Shchepetkin and McWilliams 2005). This ensures high vertical resolution in shallow areas such as shelf seas and coastal areas. Here, the model is run on a grid with 32 sigma layers in the vertical and a minimum depth of 10 meter. The latter ensures that bank structures as shallow as 10 meter are represented in the model. In the horizontal, the grid resolution is 4 km and covers the Nordic, Barents and Kara seas, as well as parts of the Arctic Ocean (Figure 2.1). This means that, according to the Nyquist-criterion structures and processes larger than ~10 km in horizontal extent are represented in the model, while structures larger than ~25 km are adequately resolved. In the Barents Sea, the Rossby radius of deformation can be as small as 1-2 km (e.g. Lien and Ådlandsvik (2011)). Thus, the model is barely within the eddy-permitting regime in the northern parts of the domain, while it is closer to eddy-resolving in the Norwegian Sea.

The NORA10 (NOrwegian ReAnalysis 10km) high resolution atmospheric re-analysis archive (Reistad et al. 2011) has been applied as atmospheric forcing, providing information on atmospheric variables at 6 hour temporal resolution (00, 06, 12 and 18 UTC). The archive is a dynamic downscaling based on the ERA40 re-analysis (Uppala et al. 2005) for the period January 1958 to August 2002 and analysis from the European Centre for Medium Range Weather Forecast (ECMWF) from September 2002 and onwards. As the archive only covers the interior of the ocean model domain, it has been expanded with ERA40 and EC-analysis. Variables include surface winds, temperature, pressure, humidity, cloud cover and accumulated precipitation. Short and net long wave radiation terms are analytically calculated internally.

Figure 2.1. Model domain.

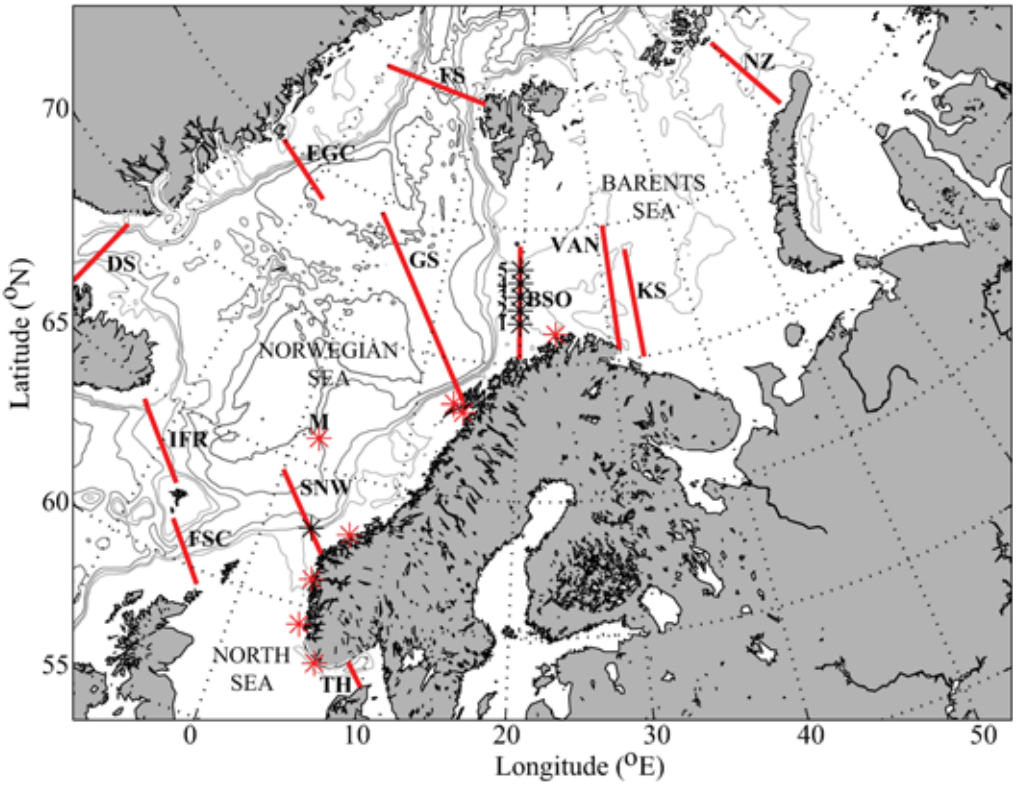

Figure 2.2. Map of the Nordic and Barents seas. Gray contours show (from light to dark, respectively) the 300, 500, 1000, 2000, and 3000 meter model bathymetry isobaths. Sections are shown by red lines: DS: Denmark Strait; IFR: Iceland-Faroe Ridge; FSC: Faroe-Shetland Channel; TH: Torungen-Hirtshals; SNW: Svinøy Northwest; GS: Gimsøy section; BSO: Barents Sea Opening; VAN: Vardø North; KS: Kola Section; NZ Novaya Zemlya - Franz Josef Land; FS: Fram Strait; EGC: East Greenland Current. Black stars indicate position of current meter moorings. Red stars show position of coastal fixed stations and station MIKE (denoted by 'M').

The Simple Ocean Data Assimilation dataset version 2.1.6 (SODA 2.1.6; Carton et al. (2000), Carton and Giese (2008)) was used both for initial and boundary values, by applying the radiation and nudging boundary conditions scheme proposed by Marchesiello et al. (2001). The nudging time scales are 0.25 days and 25 days for incoming and outgoing information, respectively. For sea ice, initial and boundary values were taken from a regional simulation using the ocean model MICOM (Sandø et al. 2012). The sea-ice model used is similar to the module described in Budgell (2005). In addition, tidal forcing based on a global ocean tides model (TPXO4) was included by imposing surface elevation and corresponding barotropic velocity components at the open boundaries, as proposed by Flather (1976) and Chapman (1985), respectively. Regarding freshwater input from rivers, the model use monthly mean climatological values of river runoff. Inter-annual variability has been accounted for by scaling the climatological values based on precipitation-extent from the ERA40 and ERA Interim (Uppala et al. 2008) re-analyses.

Due to spurious drift in the upper-ocean salinity in the Norwegian Sea in earlier simulations, a sea surface salinity relaxation scheme has been applied by nudging towards the monthly sea surface salinity from the SODA-dataset with an e-folding time of 180 days. This prevents drift in the sea surface salinity, while still allowing for interannual variation. To account for model spin up, the first two years (1958-1959) are neglected in the following analysis.

A third-order upstream scheme was applied for horizontal advection of tracers and momentum. Due to the diffusive nature of this advection scheme, the explicit horizontal mixing and viscosity coefficients were set to zero. For vertical advection of momentum and tracers, a non-diffusive 4^{th} order centered scheme was applied. The diffusive nature of the upstream advection scheme has been demonstrated to produce spurious diapycnal mixing in sigma-coordinate models (Marchesiello et al. 2009). This will tend to erode vertical gradients in temperature and salinity. Marchesiello et al. (2009) suggest a solution where the advection is split into its purely advective and diffusive parts and then the diffusion operator is rotated along geopotential surfaces. Here, the standard upstream scheme implemented in ROMS is applied. As a consequence, the simulation is susceptible to spurious diapycnal mixing affecting the water mass characteristics, especially in areas where vertical hydrographic gradients overlay steep topography. Therefore, the scheme proposed by Marchesiello et al. (2009) should be considered in future applications.

The Generic Length Scale (GLS) mixing scheme (Umlauf and Burchard 2003, Umlauf et al. 2003) was used for calculating the sub-gridscale parameterization of vertical turbulent mixing of momentum and tracers, using the $k - \omega$ set-up. The GLS mixing scheme has been evaluated and found to produce realistic results e.g. in coastal applications where tidal mixing is important (Warner et al. 2005a,b). However, improved methods should be considered in future applications (J. Röhrs, pers. comm.).

3 Data and Methods

3.1 Hydrographic Data

Hydrographic data based on CTD-measurements (Conductivity-Temperature-Depth) were obtained from the Norwegian Marine Data Center. The data are concentrated in repeatedly monitored sections. The sections investigated are shown in figure 2.2 (for positions, see table 3.1), and the analysis carried out is listed in Table 3.2.

A hydrographic atlas for the Barents Sea (Sigrid Gjessing Lind; Pers. comm.) based on CTD-observations are used for evaluating the modelled horizontal distribution and variability of temperature and salinity. Observations from August through October have been compiled into yearly averages by the use of the objective analysis toolkit DIVA (Troupin et al. 2012), and represents summer conditions.

Table 3.1. Section positions.

Section	Latitude	Longitude	Pos. Dir.
Faroe-Shetland Channel	61° 18'N - 59° 30'N	6° 30'W - 3°W	N
Iceland-Faroe Ridge	64° 30'N - 62° 30'N	13°W - 7° 30'W	N
Denmark Strait	69°N - 66°N	24°W	N
Torungen-Hirtshals	58° 24'N - 57° 35'N	8° 47'E - 9° 58'E	N
Svinøy Section	64° 30'N - 62°N	0°E - 5°E	N
Gimsøy Northwest	74° 30'N - 69° 12'N	0°E - 15°E	N
Barents Sea Opening	74° 21'N - 70° 12'N	19° 30'E - 20°E	E
Vardø North	75°N - 70° 24'N	31°E	E
Kola Section	74°N - 70°N	33° 30'E	E
Novaya Zemlya - Franz Josef Land	79° 48'N - 76° 30'N	60°E - 63°E	NE
Fram Strait	79° 24'N	10°W - 11°E	N
East Greenland Current	75°N - 74°N	17°W - 8°W	S

Table 3.2. Analysis included for various sections.

Section	Volume and heat	Hydrography
Faroe-Shetland Channel	x	
Iceland-Faroe Ridge	x	
Denmark Strait	x	
Torungen-Hirtshals		x
Svinøy Section	x	x
Gimsøy Northwest		x
Barents Sea Opening	x	x
Vardø North		x
Kola Section		x
Novaya Zemlya - Franz Josef Land	x	
Fram Strait	x	
East Greenland Current	x	

3.1.1 Repeated Sections

Hydrographic measurements from repeatedly monitored sections, sampled 2-12 times a year, are used to evaluate the modelled water mass distribution and variability. Climatological mean and standard deviation of temperature and salinity in the sections during the period 1980-2009 are calculated using the methods described in Kangas et al. (2006). Similarly, daily averages from the model output are compiled into climatological means and standard deviations by sampling the model both temporally and spatially according to the actual observations.

3.1.2 Coastal Fixed Stations

Hydrographic data from 7 coastal fixed stations were obtained from the Norwegian Marine Data Center (Sætre et al. 2003). The data were interpolated to fixed depths in space and the 15th day of each month in time, using linear interpolation. For the period 1960-2005, data corrected by J. Blindheim were used (available on CD-ROM). After 2005, standard calibrations were used where available. Elsewhere, raw data were used. Clearly erroneous values/spikes have been removed manually.

3.1.3 Ocean Weather Station MIKE

Hydrographic data at standard depths and monthly temporal resolution at Ocean Weather Station Mike (66N, 2E) were utilized for comparison between modelled and observed hydrography in intermediate and deep water masses in the Norwegian Sea.

3.2 Current Meter Data

In sections within the Nordic and Barents seas where observational-based estimates of volume and heat transports are available, we compared the model results with transport estimates found in the literature. Generally, we adopted the water mass definitions used in literature (Table 3.3) and compared within the periods of observation. When estimating the heat transports, we used a reference temperature of -0.1 ^{o}C, which is widely used as a common reference temperature for water masses leaving the Arctic Ocean (Aagaard and Greisman 1975). Although this method can be questioned (see e.g. Schauer and Beszczynska-Möller (2009) for a thorough discussion), it enables a consistent comparison between modelled and observed heat transports.

3.2.1 Barents Sea Opening

For comparison between modelled and observed volume and heat transports through the Barents Sea Opening, we used monthly averages based on direct current measurements (Ingvaldsen et al. 2004). For comparison between modelled and observed current speed and direction, hourly observations of *u* and *v* from the current meters were averaged to daily mean values. Corresponding modelled daily averages were found using nearest neighbour interpolation from the native model grid.

3.2.2 Svinøy Section

In the Svinøy section, a different approach was chosen. Orvik and Skagseth (2003) proposed a method for estimating the volume transport of the Norwegian Atlantic slope Current based on a single current meter only by indentifying the position which to the largest degree resembled the total variation in the flow. Here, we have identified the position in the monthly averaged model section that yields the highest correlation with the observation-based time series, after the hourly observations were filtered using a 720 hour moving average and then resampled every 15th day of each month. In addition, we have compared the average modelled volume transport of Atlantic water masses with observation-based estimates from the complete array of instruments found in literature (e.g. Orvik et al. (2001)).

Table 3.3. Water mass definitions. [1]Restricted by 72^{o} 30' N.

	Atlantic water		Coastal water	
Section	Temp	Salt	Temp	Salt
Faroe-Shetland Channel	> 5 ^{o}C	> 34.9	-	-
Iceland-Faroe Ridge	> 5 ^{o}C	> 34.9	-	-
Denmark Strait	> 5 ^{o}C	> 34.9	-	-
Svinøy Section	> 5 ^{o}C	> 34.9	-	<34.8
Gimsøy Northwest	> 4 ^{o}C	> 34.9	-	<34.8
Barents Sea Opening	> 3 ^{o}C	> 34.9	-[1]	<34.9
Novaya Zemlya - Franz Josef Land	> 0 ^{o}C	> 34.75	-	-
Fram Strait	> 2 ^{o}C	-	-	-
East Greenland Current	> 0 ^{o}C	-	-	-

3.3 Sea-ice data

Sea-ice concentration observations are available from the Ocean and Sea Ice Satellite Application Facility (OSI-SAF) High Latitude Processing Center. The observations are derived from Special Sensor Microwave/Imager (SSM/I) data, and have been gridded onto a polar stereographic projection with a horizontal resolution of 10 km. Details about the data processing are given by Andersen et al. (2012) and Eastwood et al. (2011).

Sea-ice concentrations have been interpolated/extrapolated onto regions where observations have originally been discarded due to cloud contamination. Here, daily sea-ice concentration values that covers the present model domain for the period 2000-2001 are used. Due to operational issues, no SSM/I observations exist for the northern hemisphere from 2000-12-01. As a consequence of this, results from 2000-12-01 and 2000-12-02 are discarded in the present analysis.

The present analysis takes advantage of a product that is post-processed so that the masking is time-invariant. When examining sea-ice results, we project all results on the coarsest resolution, which is here the 10 km grid of the OSI-SAF product.

4 Results and Discussion

In the following chapter, the model results are compared with direct observations. To improve the readability, the results are discussed when presented. A paragraph summarizing the main conclusions following the comparison is given at the end of each main section.

4.1 Hydrography

4.1.1 Horizontal distribution and variability in the Barents Sea

To evaluate the general features of the modelled hydrography, we compare the model results to the horizontal distribution of temperature and salinity at 50 meter depth in the hydrographic atlas of the Barents Sea. Both the atlas and the model represent hydrographic conditions in late summer, August-October. The atlas also provides similar information on winter conditions (February-April), but due to less coverage in winter, especially in northern areas, we limit our analysis to the summer conditions. It should be noted, however, that the atlas is based on observations unevenly distributed in both space and time. Consequently, the observations provide less details than the high resolution model results. Moreover, while the model averages are always representative for the whole three-month period in every grid point, the representativeness of the observations may be biased towards the early or the late part of the period. Therefore, focus should be on the larger patterns rather than the details.

The observed and modelled climatological temperature at 50 meter depth in the Barents Sea is displayed in figure 4.1.

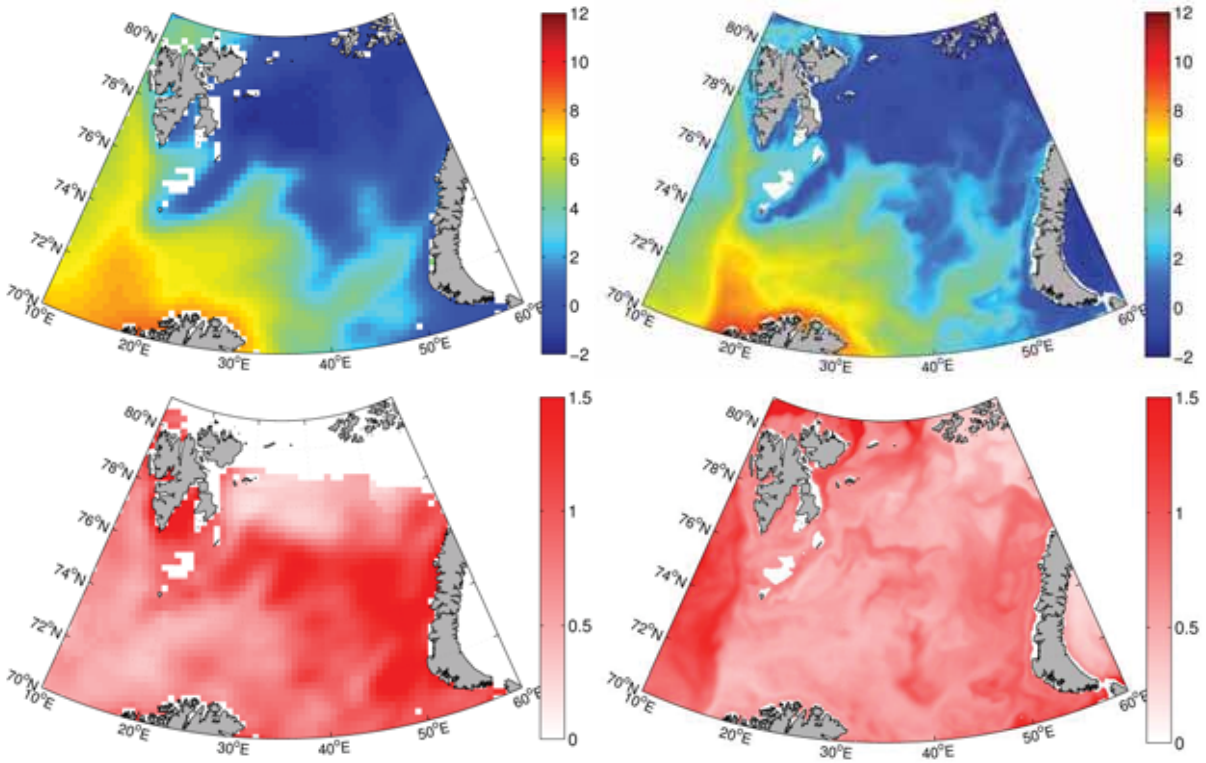

Figure 4.1. Climatological temperature (top) and corresponding standard deviation (bottom) in summer (August-October) from observations (left; 1980-2008) and model (right; 1980-2009) at 50 meter depth. Units are ^{o}C.

Although the higher resolution in the model results allows for more details, we clearly recognize the observed features. Atlantic Water is dominating the southwestern part, while the temperature in the northeastern part is typically around or below 0 ^{o}C. The flow of Atlantic Water around the Murman Rise, through Sentralbassenget and further northward around the Novaya Zemlya Bank is well captured in the model. Also the inflow of Atlantic Water into Hopendjupet with extensions eastward between Sentralbanken and Storbanken is represented in the model at realistic temperatures. Moreover, the southwestward-flowing Bjørnøya Current, transporting cold and low-salinity Polar Water, is well defined along the eastern slope of Svalbardbanken. There are, however, also some differences. The most noticeable is the substantially lower modelled temperatures in the Norwegian Sea, probably owing to unrealistically low cross-slope eddy heat transport in the model (see further discussion in section 4.1.2). On the other hand, the model seems to slightly overestimate the temperature in the Norwegian Coastal Current. There is also an indication that the model overestimates the southward flow of Atlantic Water between Nordaustlandet and Kvitøya, although the observational data coverage in this area is probably very limited.

Focussing on the variability, the observations indicate that the model grossly underestimate the interannual variability in temperature in the interior Barents Sea, especially in the southeastern parts. This area represents the eastern part of the Polar Front, i.e. the frontal zone between the warm Atlantic Water and the cold Polar Water. However, it should be noted that although both datasets represent three-month averages, the observations consist of snapshots compiled into longer term averages. And as a consequence, the observations are expected to display larger variability. However, the narrow bands of higher variability along the Polar front seen in the model, indicate a relatively strong topographical control of the front also in the eastern Barents Sea, although observations indicate less topographical control here compared to further west (Jakobsen and Ozhigin 2011). In the Norwegian Sea, the model displays larger than observed variability. This can be explained by the lower temperature in the model. That is, in the model, the 50 meter depth is closer to the gradient representing the transition zone between Atlantic Water and intermediate waters within the Norwegian Sea. Consequently, the model is more susceptible to variability due to vertical perturbations. Also, the model indicate a relatively large variability both in the trench between Nordaustlandet and Kvitøya and in the Franz Victoria Trough, indicating that, according to the model, southward flow of Atlantic Water here is a variable rather than a permanent feature.

As for the temperature, the general patterns of the modelled salinity are similar to the observations in terms of horizontal distribution (Figure 4.2). In the Norwegian Sea and the inflow area in the western parts of the Barents Sea, the salinity is lower in the model than in the observations, whereas in the eastern Barents Sea, the modelled and observed Atlantic Water salinity are comparable. The modelled salinity clearly shows the Atlantic Water flow along Nordaustlandet. Furthermore, the model indicates a narrow and relatively fresh Novaya Zemlya Coastal Current that most likely due to poor resolution is not present in the observations. The coastal current does, however, appear in observations along the Novaya Zemlya Coast (see e.g. Jakobsen and Ozhigin (2011)). On the contrary, the salinity in the Norwegian Coastal Current is grossly overestimated in the model.

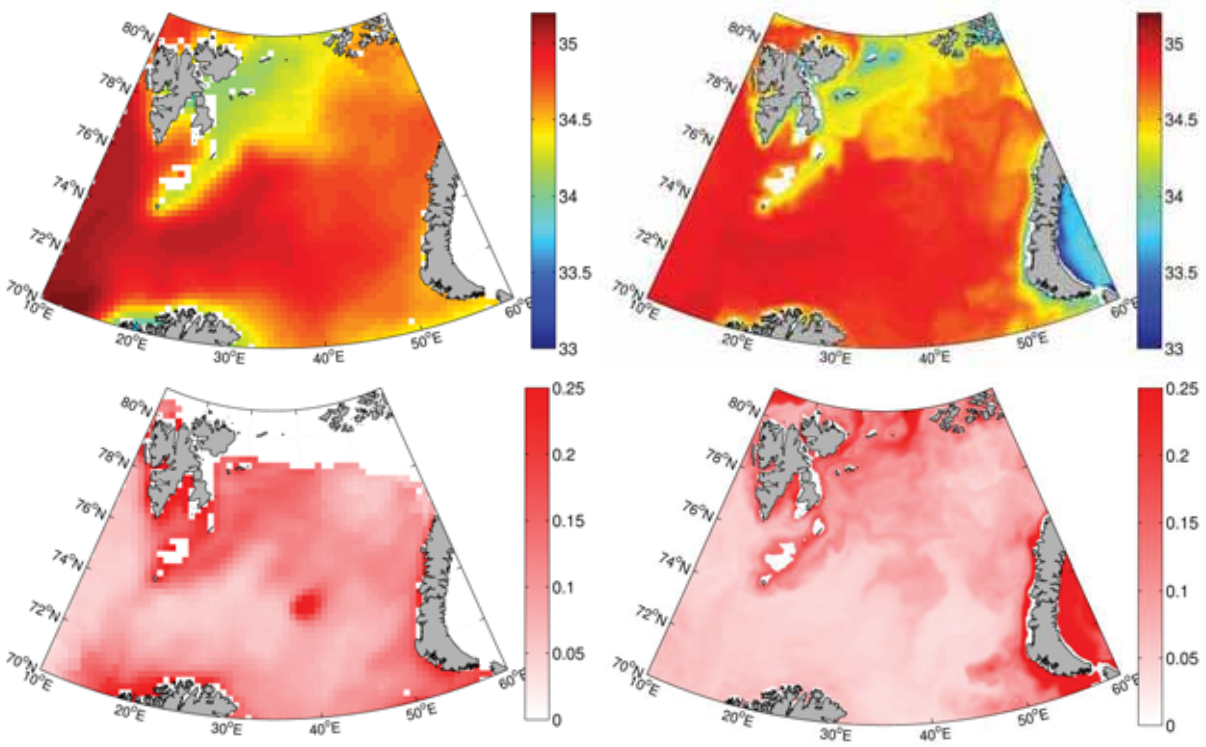

Figure 4.2. Climatological salinity (top) and corresponding standard deviation (bottom) in summer (August-October) from observations (left; 1980-2008) and model (right; 1980-2009) at 50 meter depth. Units are practical salinity units (psu).

In terms of variability, both the model and the observations indicate less variability in the southern, Atlantic Water dominated part compared to the northern, Polar Water dominated part of the Barents Sea (Figure 4.2; the small area of large observed variabilty immediately east of Sentralbanken is probably due to an erroneus value). There is also a relatively large variability in the salinity at and around Svalbardbanken. A striking difference occurs in the coastal regions. In the observations, there is a large variability in the Norwegian Coastal Current which is absent in the model, likely due to the salinity relaxation applied in the model. On the contrary, the model indicates a large variability in the Novaya Zemlya Coastal Current, which is less pronounced in the observations. As mentioned above, the resolution of the observations is likely too coarse to resolve the narrow Novaya Zemlya Coastal Current. As opposed to the Norwegian Coastal Current, which is distantly fed by freshwater input into the Skagerak in the North Sea, the Novaya Zemlya Coastal Current is fed by the nearby Kara Sea through the Kara Gate. Therefore, the salinity relaxation scheme is too slow to destroy the salinity signature of the Novaya Zemlya coastal water.

The Polar Front is a prominent feature in the Barents Sea. In addition to representing the transition zone between the warm and saline Atlantic Water and the cold and less saline Arctic and Polar waters, it also has large biological implications (Jakobsen and Ozhigin 2011). It is most pronounced in the Svalbardbanken area, which is clearly seen in both the observations and in the model (Figure 4.3). In this area, the front is tightly locked to the topography (e.g. Johannessen and Foster (1978)). In the eastern Barents Sea, the front is typically more variable, which is partly indicated by the less pronounced temperature and especially salinity gradients here in both the observations and the model. Not surprisingly, due

to the higher resolution, the model results display stronger gradients in both temperature and salinity than do the observations. However, the observations clearly indicate elevated gradients in most areas where relatively strong gradients appear in the model. This suggests that the position of the Polar Front is realistic in the model results.

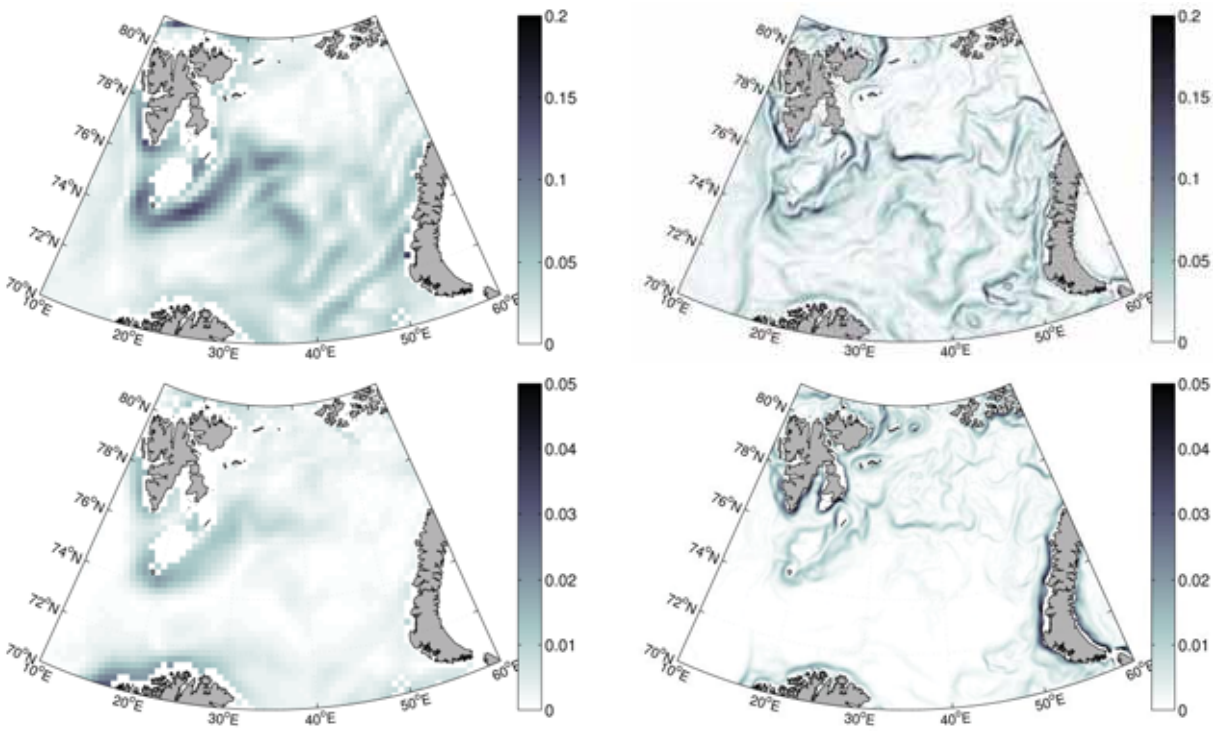

Figure 4.3. Gradients in climatological temperature (top; ^{o}C/km) and salinity (bottom; psu/km) in summer (August-October) from observations (left; 1980-2008) and model (right; 1980-2009) at 50 meter depth

4.1.2 Heat content

The basin scale heat content, i.e. the total amount of heat within the basin relative to a chosen reference temperature, represents the integrated or accumulated effect of changes in the net heat transport and fluxes into the basin. It dampens the high-frequency variability in heat transport and fluxes and is a measure on the climatic state of the ocean. Therefore, it also represents a robust measure for evaluating the model's performance in terms of lateral heat exchange between the sources and sinks of heat (usually currents along the basin rim), vertical heat fluxes (interaction with the atmosphere) and the interior heat storage within the ocean basins.

For direct comparison with observations, we apply a method for computing heat content similar to that proposed by Palmer and Haines (2009), which has also been used to estimate the heat content of the Norwegian Sea (Skagseth and Mork 2012). Following this approach, we calculate the heat content above a reference density using the temperature in the water column relative to the temperature at the reference density surface. For further details on the procedure, see Skagseth and Mork (2012). Here, we use a reference density of $\sigma\theta$ = 27.95. Comparing the average depth of the reference level (Figure 4.4) with an observation-based average depth (Skagseth and Mork (2012) and their Figure 4.a), we find some common

patterns as well as some striking differences. Although the observations represent April through June averages for the years 1995-2010 only, the comparison should still be valid due to the large inertia. Moreover, Skagseth and Mork (2012) use a reference density of $\sigma\theta$ = 27.90. We have chosen a slightly higher reference density for better comparison with observations (based on visual inspection). Similar to the observations, the model shows a deepening of the isopycnals in the advection area of the Norwegian Atlantic Current and a general shoaling towards the west. Furthermore, in accordance with the observations, the modelled reference density is more shallow in the Norwegian Basin (southern Norwegian Sea) compared to the Lofoten Basin (northern Norwegian Sea).

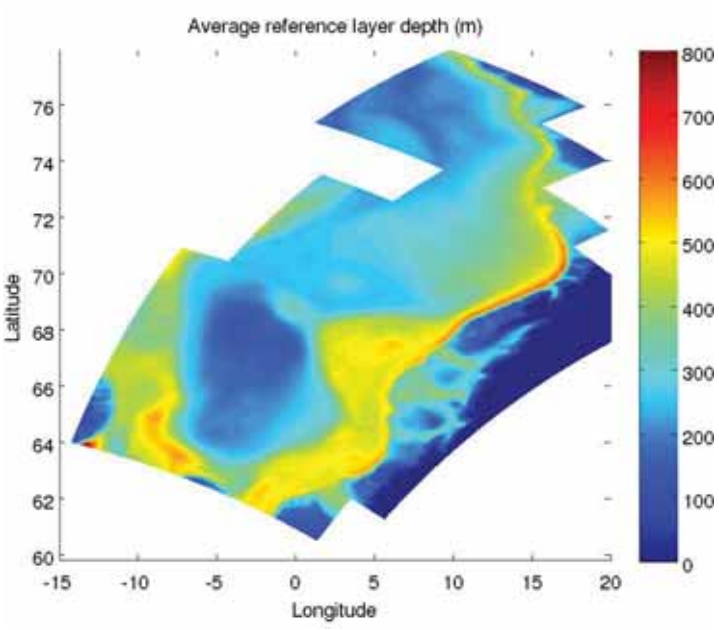

Figure 4.4. Average depth of the density level $\sigma\theta$ = 27.95 in the model.

The most striking difference between the model and observations, is the depth of the reference density layer in the Lofoten Basin. The observations show a substantial deepening, indicating a pool of Atlantic Water extending down to about 700 m depth. In the model, however, there is no clear evidence of such an Atlantic Water pool, and the reference density layer is located at 300 meter depth or less within the Lofoten Basin. Isachsen et al. (2012), using ROMS with a slightly different set up, found that the modelled eddy heat fluxes between the shelf slope and the Lofoten Basin were too small and that the model eddies were too strongly influenced by the bathymetry. The lack of an Atlantic Water pool in the Lofoten Basin indicates that this is also a problem in this model simulation.

Note that our choice of a slightly higher reference density implies that the actual difference between modelled and observed vertical extent of Atlantic Water is even larger. However, the net effect of the negative biases in modelled temperature and salinity within the Atlantic Water (see section 4.1.4) is an increase of the Atlantic Water density. Hence, the different choices of reference density defining the Atlantic Water in the model and the observations are comparable.

Figure 4.5 clearly demonstrate the difference between modelled and observed climatic temperature and salinity in the Lofoten Basin. Most notably, the Atlantic Water is mostly confined to the slope in the model, which results in strong horizontal gradients in both temperature and salinity, compared to the vertical gradients seen in the observations. As a consequence, there is a lack of Atlantic Water (usually defined as T >5 ^{o}C) at depth within the Lofoten basin.

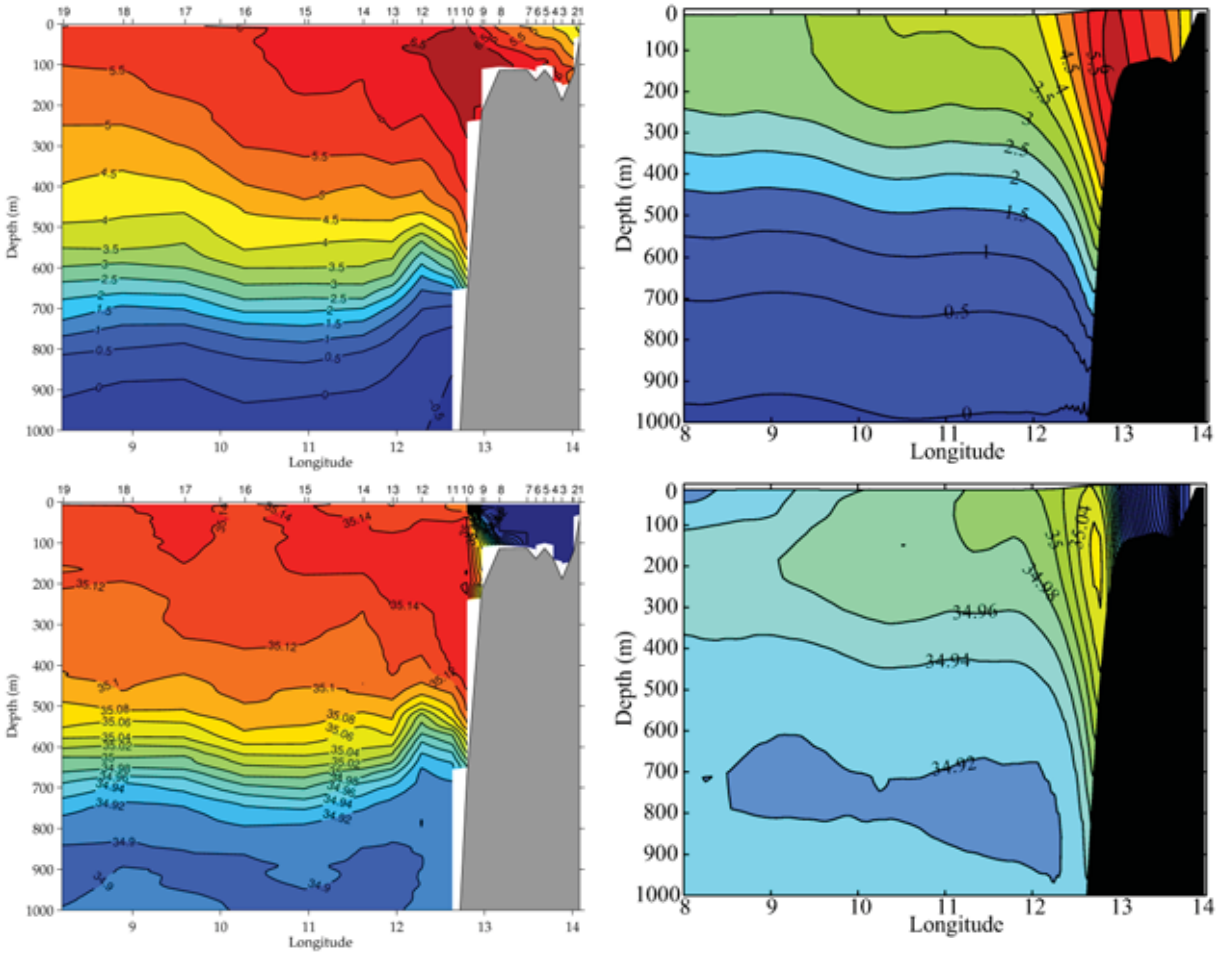

Figure 4.5. Climatological temperature (top) and salinity (bottom) in March in the Gimsøy Northwest section from observations (left; 1980-2010) and model (right; 1980-2009).

4.1.3 Freshwater content

During initial runs, difficulties in getting realistic salinity distribution in the southern Norwegian Sea were encountered. The problem was manifested through apparently exaggerated freshwater transport in the East Icelandic Current from the Iceland Sea to the Norwegian Sea. This resulted in a negative trend in sea surface salinity and subsequently also in subsurface layers within the Norwegian Sea. To correct the spurious trend, a sea surface salinity relaxation scheme was applied. As a result, the salt budget in the model is not mass-conserving. Therefore, changes in modelled freshwater content has not been estimated.

4.1.4 Repeated sections

Torungen-Hirtshals

The Torungen-Hirtshals section crosses the Skagerrak from the southern coast of Norway to the northwestern coast of Denmark. It is sampled monthly, 12 times a year. Hence, the temporal data coverage is very good for variability on time scales down to seasons.

Table 4.1. Water mass definitions in the Torungen-Hirtshals section.

Water mass	Depth (m)	Distance from coast (nm)
Norwegian Coastal Water	0-20	0-5 (from Norway)
Danish Coastal Water	0-20	3-8 (from Denmark)
Atlantic water	100-200	30-35 (from Norway)
Skagerrak Bottom Water	400-600	15-20 (from Norway)

In the following comparison between modelled and observed hydrography, the section is divided into four boxes representing different water masses (see Table 4.1). The characteristic of each water mass consists of a weighted mean of the temperature and salinity within each box. Then, monthly anomalies relative to the monthly 1980-2009 average are computed for each water mass.

Starting with the Atlantic Water in Skagerrak, Figure 4.6 shows that the model resembles the observed variability, especially at interannual time scales, in both temperature and salinity (R = 0.80; $p < 0.01$ and R = 0.62; $p < 0.01$, respectively). Furthermore, Figure 4.11 shows that the distribution of modelled salinity within the box representing Atlantic Water matches the observed distribution closely. This is also so in temperature (Figure 4.10), although the model diplays a slightly larger spread towards higher temperatures, which is also reflected in the root mean square error *rmse* = 0.59 between the model and the observations.

In the Norwegian Coastal Current, the modelled and observed temperature are highly correlated (R = 0.98; $p < 0.01$; Figure 4.7). This is also reflected in the close agreement between the modelled and observed probability density functions (Figure 4.10), with the exception that the model is missing the highest temperatures (*rmse* = 1.05). For salinity, there is much less agreement between the model and the observations (R = 0.37; $p < 0.01$). Most strikingly, the model displays a far too narrow salinity range, with an overrepresentation of the highest salinities (Figure 4.11) which is also reflected in the large difference between model and observations (*rmse* = 2.58).

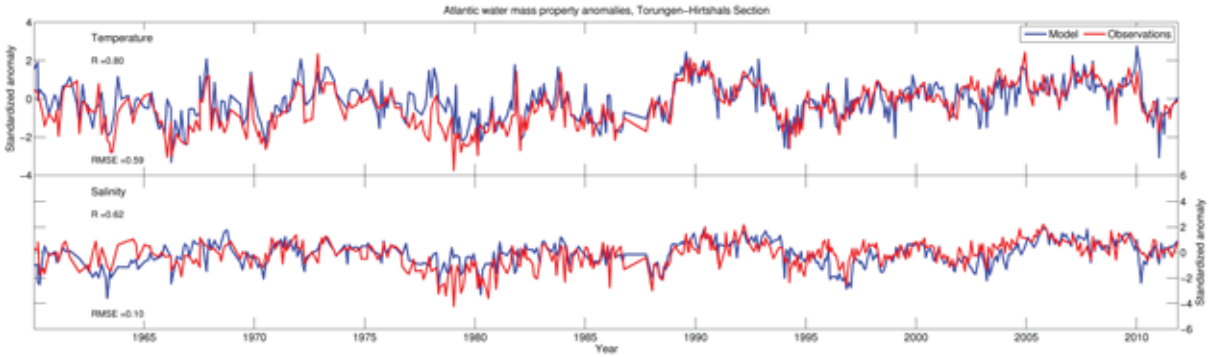

Figure 4.6. Temperature (top) and salinity (bottom) anomalies in the Atlantic Water in Skagerrak relative to the 1980-2009 average from model (blue) and observations (red).

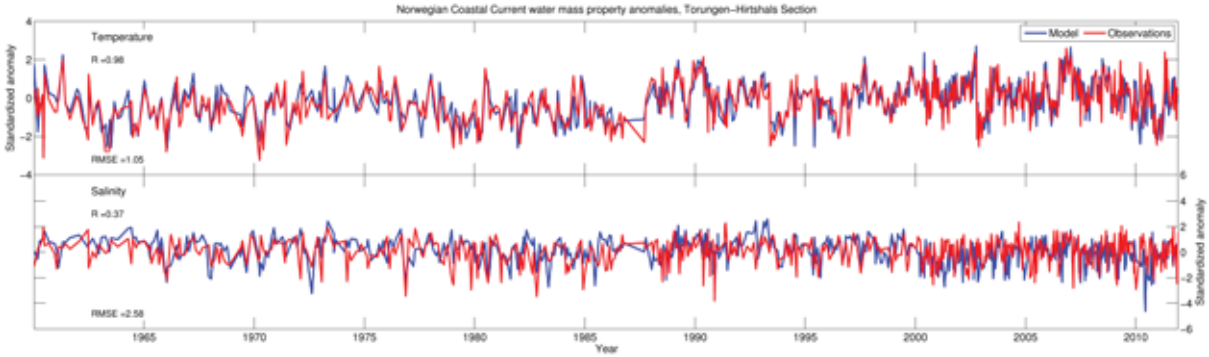

Figure 4.7. Temperature (top) and salinity (bottom) anomalies in the Norwegian Coastal Water relative to the 1980-2009 average from model (blue) and observations (red).

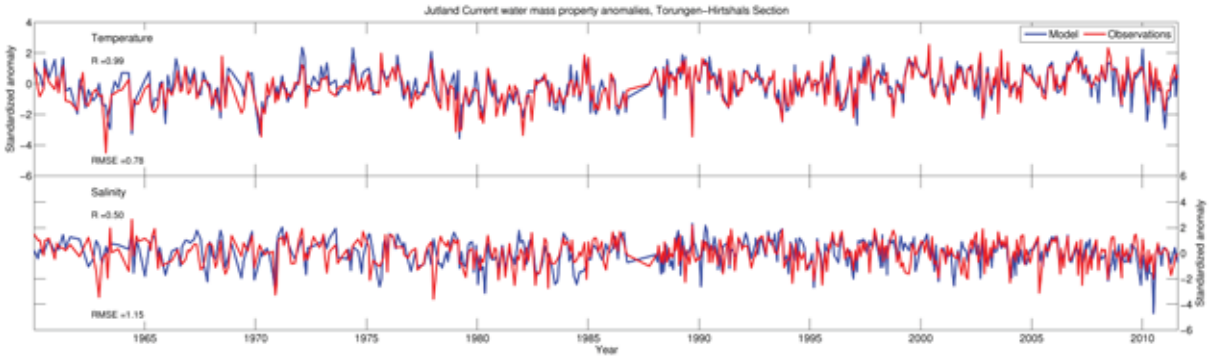

Figure 4.8..Temperature (top) and salinity (bottom) anomalies in the Danish Coastal Water relative to the 1980-2009 average from model (blue) and observations (red).

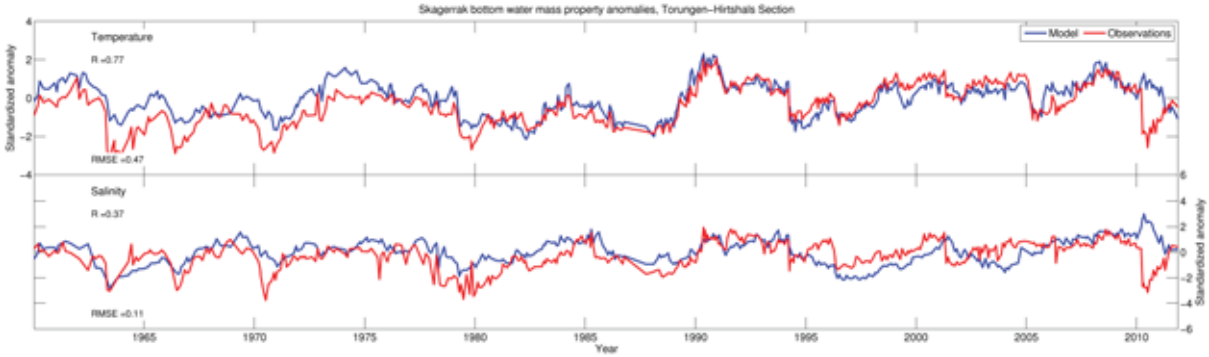

Figure 4.9. Temperature (top) and salinity (bottom) anomalies in the Skagerrak Bottom Water relative to the 1980-2009 average from model (blue) and observations (red).

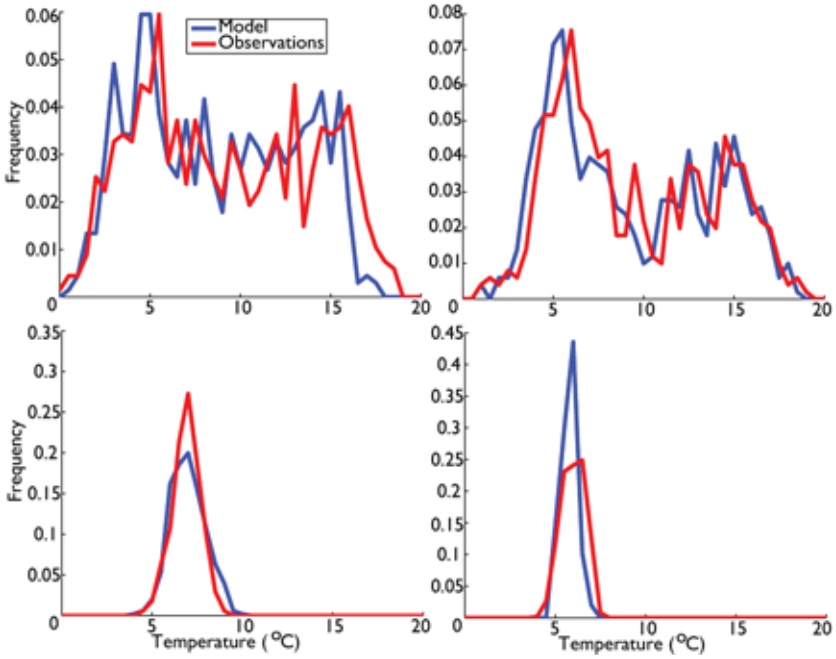

Figure 4.10. Probability density functions for temperature from model (blue) and observations (red) for Norwegian Coastal Water (top left), Danish Coastal Water (top right), Skagerrak Atlantic Water (bottom left) and Skagerrak Bottom Water (bottom right).

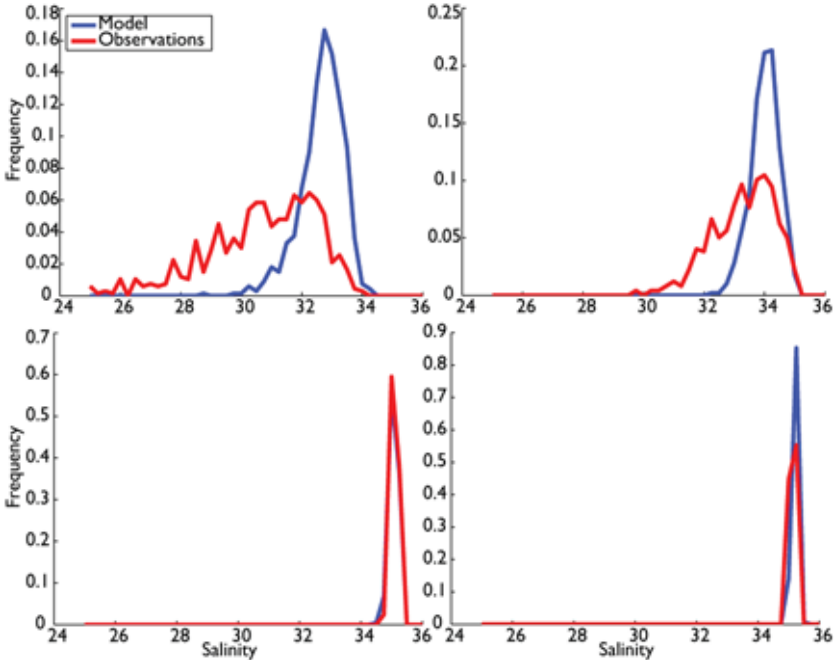

Figure 4.11. Probability density functions for salinity from model (blue) and observations (red) for Norwegian Coastal Water (top left), Danish Coastal Water (top right), Skagerrak Atlantic Water (bottom left) and Skagerrak Bottom Water (bottom right).

In the Danish Coastal Water the modelled temperature follows the observed values closely (R = 0.99; p < 0.01; Figure 4.8). There is also a close agreement between the modelled and observed probability density functions for temperature (Figure 4.10), in which the model resembles the observed distribution. However, although there is a close agreement between modelled and observed variability, there is a bias between the two (*rmse* = 0.78). Similar to the Norwegian Coastal Current, the modelled salinity show less variability than observations, which is reflected in both the correlation (R = 0.50; p < 0.01) and a more narrow probability density function compared to observations, with the higher salinities being overrepresented in the model (Figure 4.11). This is reflected in the large difference between modelled and observed salinity (*rmse* = 1.15).

Figure 4.9 shows the modelled and observed temperature and salinity of the bottom water in Skagerrak. The model closely resembles the observed temperatures (R = 0.77; p < 0.01), especially at interannual time scales, except for some severe cold spells in the 1960s, 1970s and in 2010, which are not very well captured in the model. The probability density function (Figure 4.10) shows that the model also resembles the temperature distribution, although the model probability density function is slightly more narrow and concentrated around the lower end compared to that based on observations. The model also captures, to some degree, the observed interannual variability in salinity (R = 0.37; p < 0.01), except for some striking features. The well-known Great Salinity Anomaly of the 1970s (e.g. Dickson et al. (1988)) is easily distinguishable as a negative salinity anomaly around 1980 in the observations, but is less severe in the model. On the other hand, a similar salinity anomaly in the late 1990s (Belkin 2004) is more pronounced in the model, as well as a slightly less distinct anomaly in the mid-2000s. However, the most striking feature is the dramatic drop in bottom water salinity during the severe winter of 2009-10, which to the contrary represents a distinct peak in the modelled salinity.

Svinøy Section

The Svinøy section intersects with the northward flow of Atlantic Water along the Norwegian continental slope (Figure 2.2). It has been regularly monitored by hydrographic measurements (CTD) since the 1970s, although earlier measurements using e.g. STD also exist. The Norwegian Atlantic Current displays a two-branch structure in the Svinøy section (Orvik et al. 2001). Here we focus on the innermost (eastern) branch commonly termed the Norwegian Atlantic slope Current (e.g. Orvik and Skagseth (2005)).

The Atlantic Water is easily distinguishable at the Norwegian continental slope and the model resembles its characteristics (Figure 4.12, 4.13; top), although the temperature and salinity are both biased low in the model (-1.25 and -0.12, respectively; Table 4.2). Despite the bias in water mass characteristics, the distribution of the Atlantic Water in the Norwegian Sea in the model compares well with the observations, although the interface between the Atlantic Water and the Norwegian Sea Intermediate Water is smoother than observed. The bias in modelled temperature and salinity is also seen in Figure 4.16 (top), along with a larger spread in the model. On the other hand, the modelled distribution of anomalies is comparable to observations (Figure 4.18).

Table 4.2. Root mean square error and bias of modelled water mass properties relative to corresponding observations in the Svinøy section. The calculations are based on daily averages from the model.

	Atlantic water		Coastal water	
	rmse	bias	rmse	bias
Temperature	1.56	-1.25	0.82	0.26
Salinity	0.14	-0.12	0.77	0.70

In the coastal water, the model tends to overestimate the temperature (*rmse* = 0.82) and the salinity (*rmse* = 0.77). This is also evident in the climatology (Figure 4.12, 4.13), showing less freshwater content in the Norwegian Coastal Current in the model. As a result, the front

towards the Norwegian Atlantic slope Current is less pronounced and also smoother in the model, although its location and wedge shape compares well with the observations.

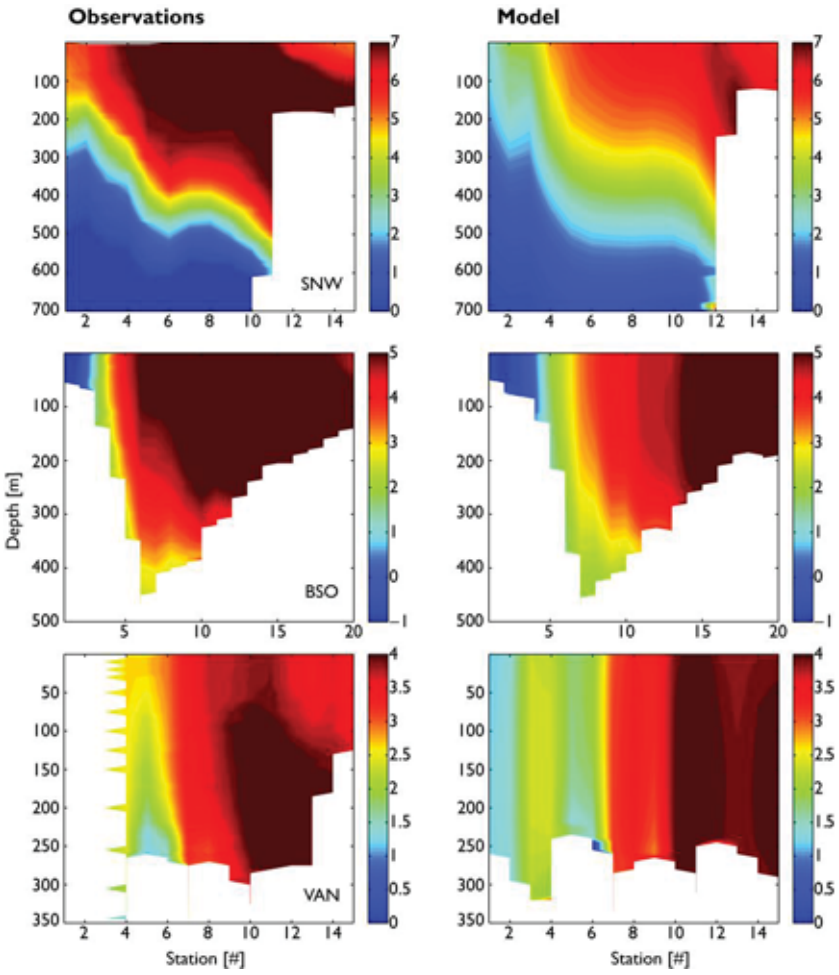

Figure 4.12. Observed (left) and modelled (right) temperature climatology in March 1980-2009 in the Svinøy section (top), Barents Sea Opening (middle) and Vardø North section (bottom).

Focussing on the temperature variability (Figure 4.14), we find that the model to a large degree resembles the observed pattern. According to the observations, the largest variability is ocurring at the interface between the Atlantic Water and the Norwegian Sea Intermediate Water. This is also clearly seen in the model, especially along the continental slope. Moreover, a slightly less variable interface at station 8-9 is also indicated by the model. A striking difference, however, is associated with the western extent of the Atlantic Water. In the model, there is a vertical region with a large standard deviation in temperature indicating that the western extent of the Atlantic Water is varying quite a bit. In the observations, there is a large variability in westward extent in sub-surface layers (below 200 meter depth), while there is only little temperature variability in this region in the upper 100 meter.

Looking at the variability in salinity, by far the largest variability is taking place within the Norwegian Coastal Current (Figure 4.15). However, there is also clearly variability associated with a varying depth of the Atlantic Water, as also seen in temperature. The largest variability is taking place in the Norwegian Coastal Current also in the model. But there is no trace of any significant variability associated with the depth of the Atlantic Water, except along the

continental slope where there is indication of an elevated standard deviation down to ~700 meter depth, similar to that of temperature.

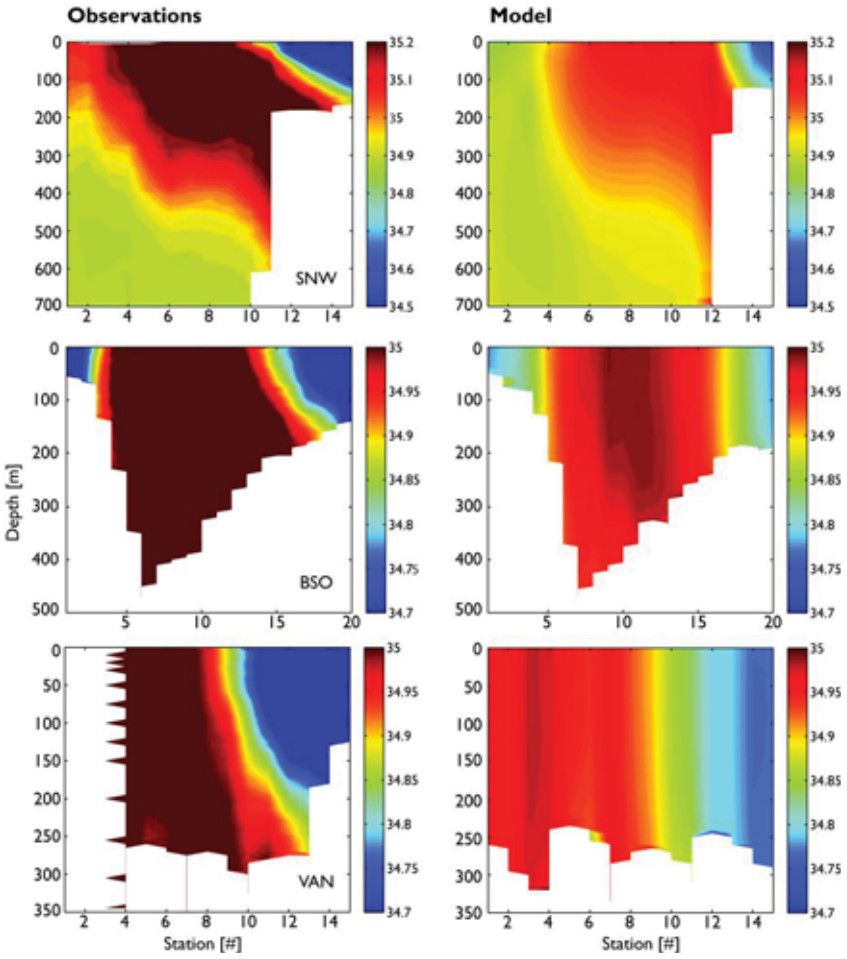

Figure 4.13. Observed (left) and modelled (right) salinity climatology in March 1980-2009 in the Svinøy section (top), Barents Sea Opening (middle) and Vardø North section (bottom).

Barents Sea Opening

The Barents Sea Opening (Norwegian coast to Bjørnøya) is sampled by CTD-measurements at 20 stations six times a year since 1977. For a consistent comparison between the model and the observations in terms of spatial variability, both the visualization of the temperature and salinity distribution within the vertical section and the probability density function analysis is based on synoptic in situ observations and modelled daily averages at similar dates.

The Barents Sea Opening is dominated by the inflow of Atlantic Water in the central parts of the section (Figure 4.12, 4.13). It is bounded to the south by the less saline Norwegian Coastal Current, which flows eastward along the Norwegian coast, and to the north by cold and less saline Polar Water flowing westward into the Norwegian Sea. From the observations, we see that the buoyant Norwegian Coastal Current is forming a wedge-shaped front by overlying the more dense Atlantic Water. In the model, however, this front is weaker and more or less vertical, indicating that the Norwegian coastal water is well-mixed to the bottom (Figure 4.13). As for the Svinøy Northwest section, the fronts separating the Atlantic Water from colder and less saline water masses (Norwegian Coastal Water and Polar Water) are considerably smoother in the model compared to the observed hydrography.

In terms of variability, the model generally displays a pattern of elevated standard deviations at depth in the central parts of the section as well as in the Barents Sea Polar Front area along the Bjørnøya slope (Figure 4.14).

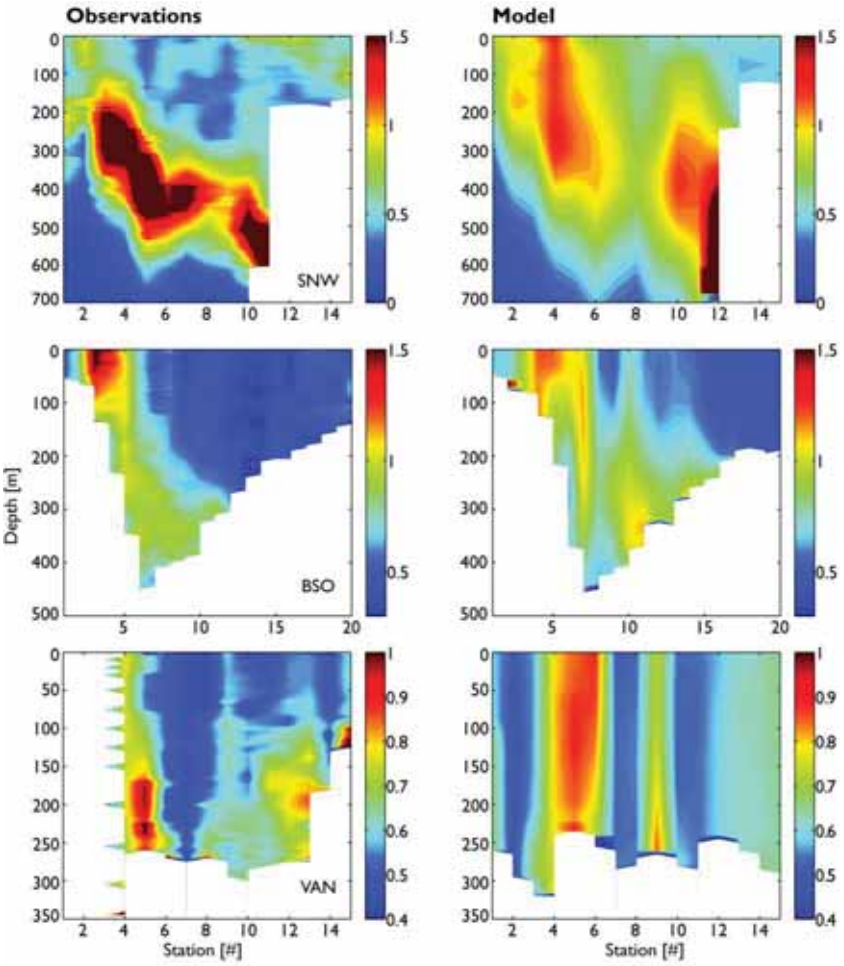

Figure 4.14. Observed (left) and modelled (right) temperature climatology standard deviation in March 1980-2009 in the Svinøy section (top), Barents Sea Opening (middle) and Vardø North section (bottom).

This pattern is also seen in the observations, although the observed variability is larger on the upper slope than in the deeper parts of the Barents Sea Opening. The variability is consistent with the varying width of the North Cape Current (Ingvaldsen 2005) and transient flow reversals on the Bjørnøya slope (Lien et al. 2013). Also the variability in salinity is confined to the frontal areas. However, the front between Atlantic Water and Norwegian Coastal Water is mainly due to differences in salinity. This is reflected in the large standard deviation in salinity in the Norweigan Coastal Current. In the model, the variability in salinity is largest in the frontal areas, although the absolute values of the variability are lower. A possible explanation for this is the sea surface salinity relaxation that tend to dampen the variability in salinity.

The comparison of modelled and observed probability density functions for temperature and salinity (Figure 4.16, 4.17) reveals that the model spread of temperature is in agreement with observations, although the model tends to be on the low side in the Atlantic Water (note that daily averages from the model are used in this comparison). For salinity, the model displays a wider range and a tendency to be on the lower side in the Atlantic Water, and oppositely a more narrow range on the higher side in the Norwegian Coastal Current. This is also reflected

in the negative bias for both temperature (-0.80) and salinity (-0.08) in the Atlantic Water (based on daily averages). In the Norwegian coastal water, the bias is -0.15 for temperature and 0.39 for salinity (Table 4.3).

Based on the same CTD-measurements, an integrated index of temperature and salinity of the inflowing Atlantic Water is calculated by averaging the observations in the depth range 50 to 200 m between 71^{o} 30'N and 73^{o} 30'N (Blindheim and Loeng 1981). The resulting time series are compared with the model results by linearly interpolating the modelled monthly averages to the time of the observations. As a consequence, the observations may reflect temporal variability at short time scales (~days), while such variability (e.g. eddies) are filtered out in the model results. However, the latter analysis involves investigation of an integrated measure and therefore small-scale variability is reduced also in the observations.

Table 4.3. Root mean square error and bias of modelled water mass properties relative to corresponding observations in the Barents Sea Opening. The calculations are based on daily averages from the model.

	Atlantic water		Coastal water	
	rmse	bias	rmse	bias
Temperature	0.96	-0.80	0.50	-0.15
Salinity	0.09	-0.08	0.42	0.39

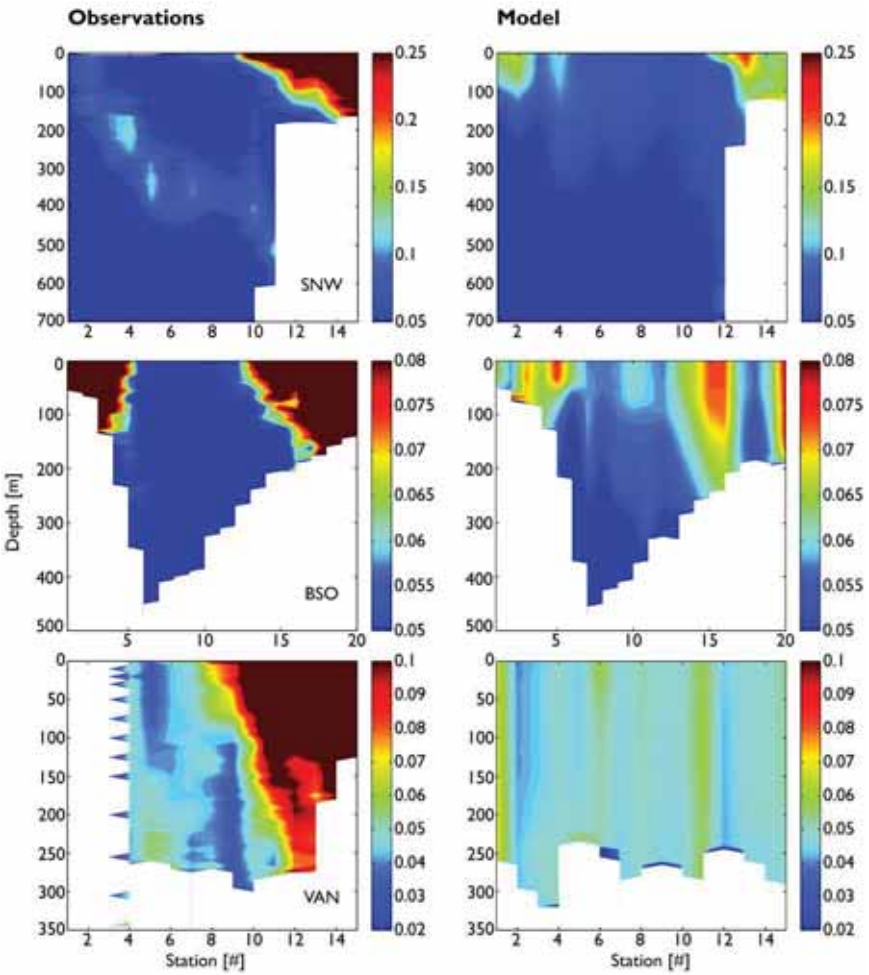

Figure 4.15. Observed (left) and modelled (right) salinity climatology standard deviation in March 1980-2009 in the Svinøy section (top), Barents Sea Opening (middle) and Vardø North section (bottom).

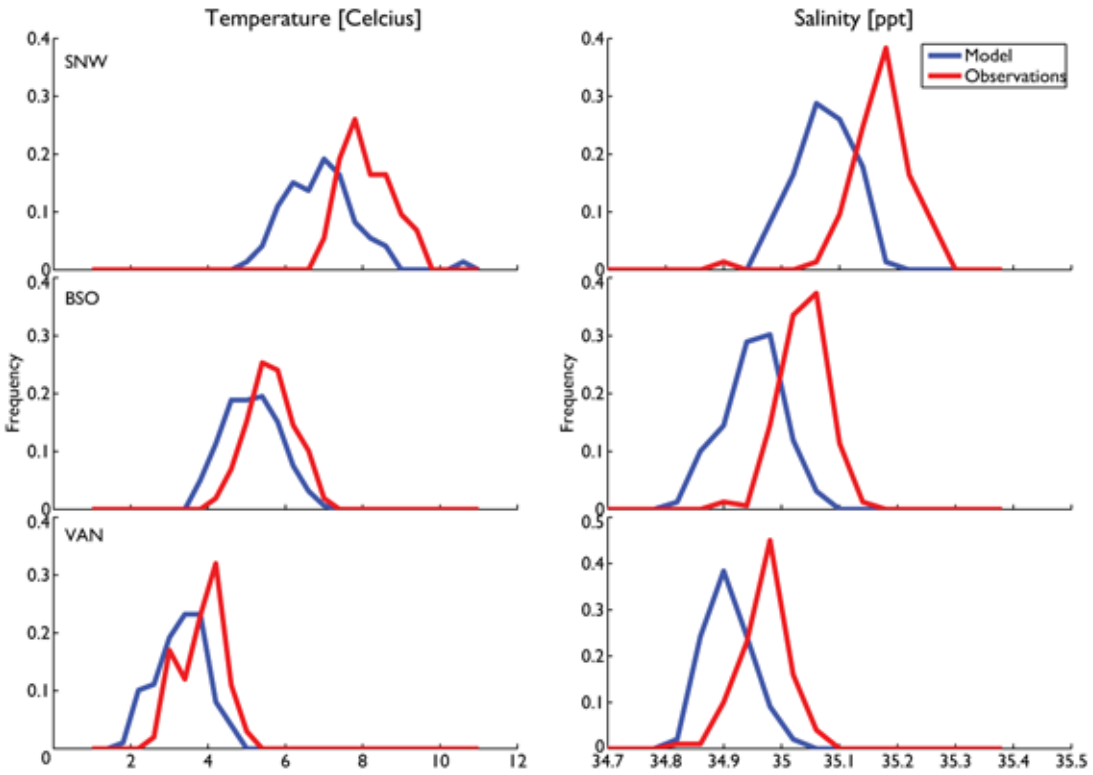

Figure 4.16. Probability density functions for observed (red) and modelled (blue) temperature (left) and salinity (right) within the Atlantic Water in the Svinøy section (top), Barents Sea Opening (middle) and Vardø North (bottom).

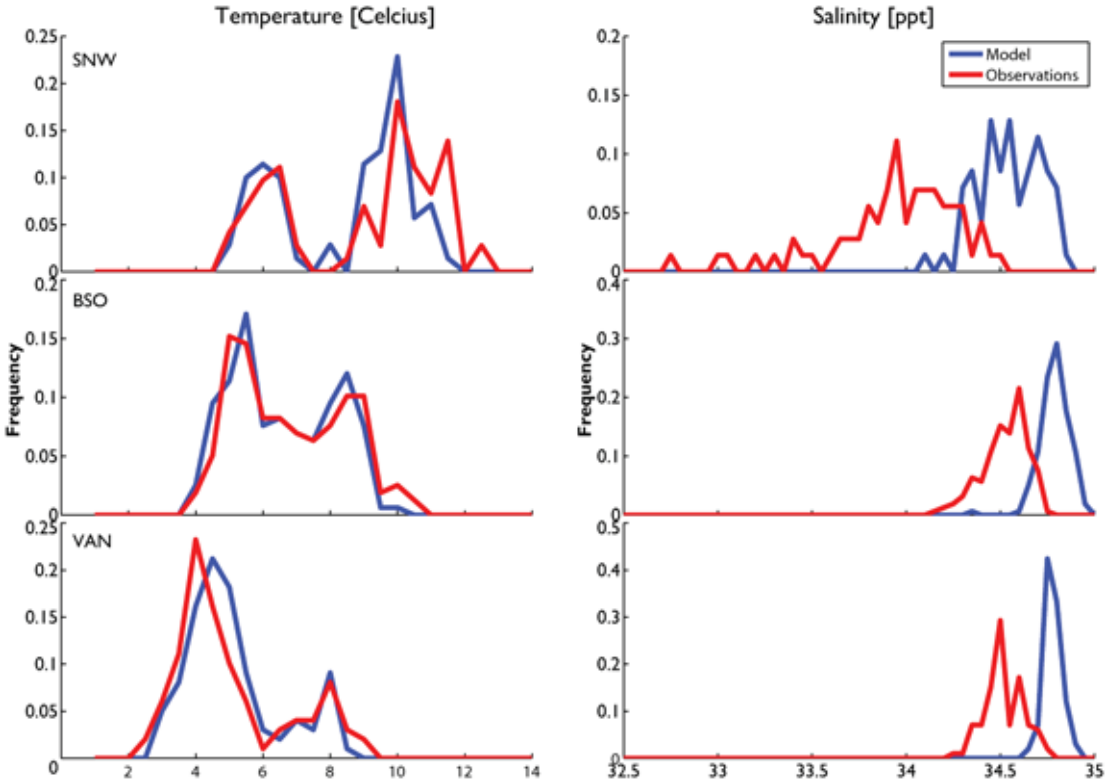

Figure 4.17. Probability density functions for observed (red) and modelled (blue) temperature (left) and salinity (right) within the Norwegian Coastal Current in the Svinøy section (top), Barents Sea Opening (middle) and Vardø North (bottom).

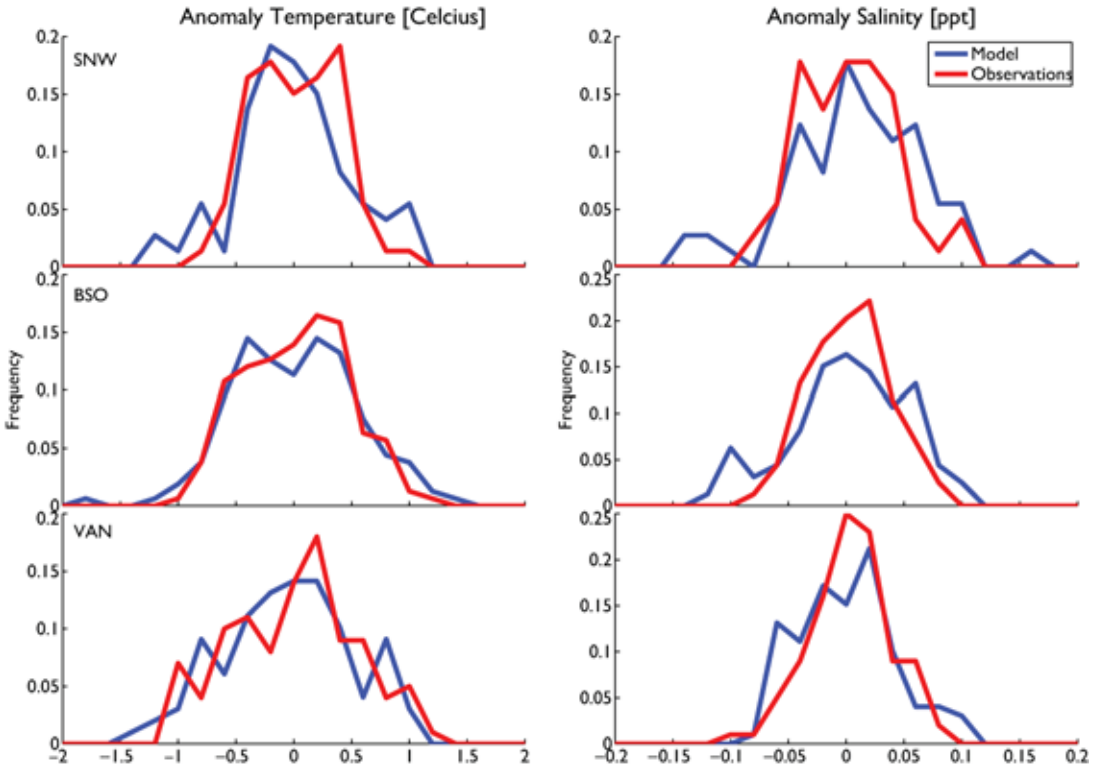

Figure 4.18. Probability density functions for observed (red) and modelled (blue) temperature (left) and salinity (right) anomaly within the Atlantic Water in the Svinøy section (top), Barents Sea Opening (middle) and Vardø North (bottom).

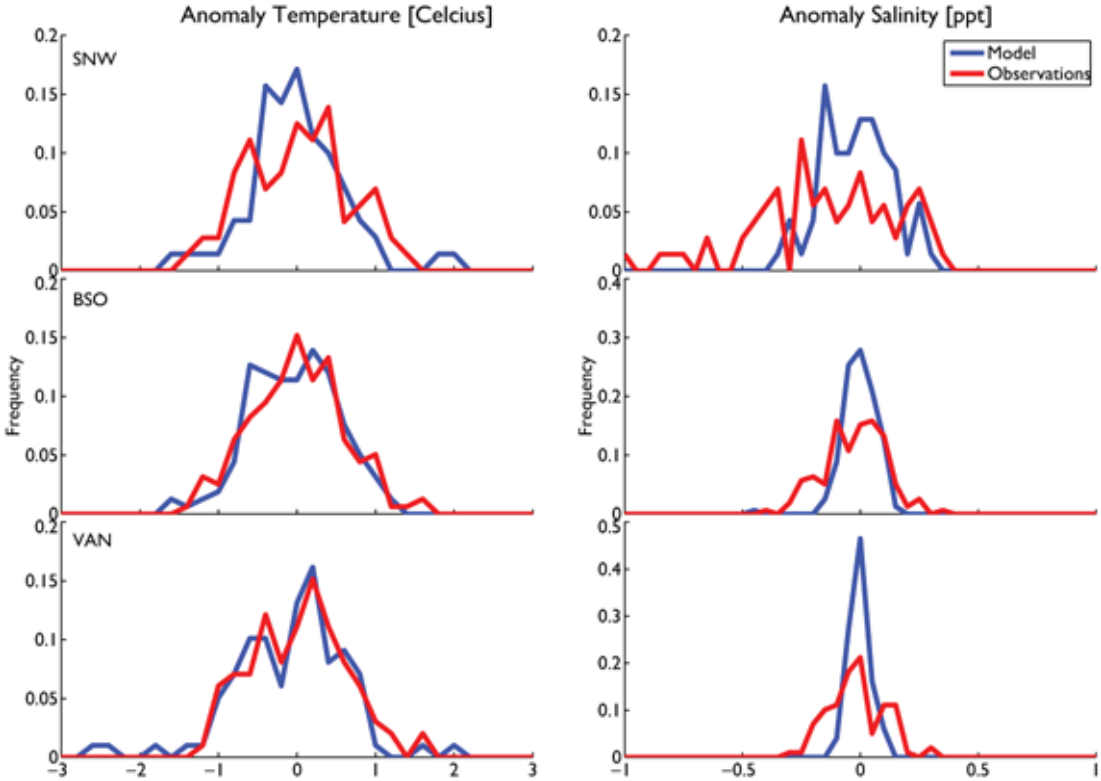

Figure 4.19. Probability density functions for observed (red) and modelled (blue) temperature (left) and salinity (right) anomaly within the Norwegian Coastal Current in the Svinøy section (top), Barents Sea Opening (middle) and Vardø North (bottom).

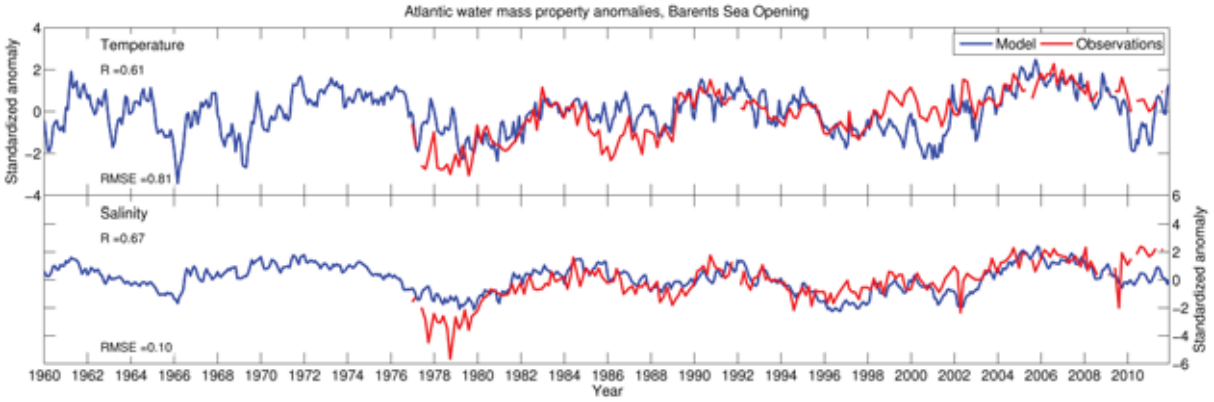

Figure 4.20. Average temperature (top) and salinity (bottom) of the Atlantic Water in the Barents Sea Opening from model (blue) and observations (red). The correlation and rmse are based on monthly averages from the model.

The time series of modelled and observed salinity and temperature of the Atlantic Water are shown in Figure 4.20. The model resembles a substantial part of the variability in both temperature and salinity, especially at interannual to decadal time scales, with correlation coefficients of $R = 0.61$ ($p < 0.01$) and $R = 0.67$ ($p < 0.01$), respectively. There are, however, some differences also on the multi-year time scale. The Great Salinity Anomaly of the 1970s, which entered the Barents Sea Opening in the late 1970s, is less pronounced in the model than in the observations. In the late 1990s and especially the early 2000s, however, the model seems to exaggerate the impact of similar large scale temperature and salinity anomalies.

Vardø North

The Vardø North section is sampled four times a year since 1977. Here, we use the temperature index based on Blindheim and Loeng (1981), representing the integrated temperature between 50 to 200 m depth from 72^o 15'N to 74^o 15'N. The model results are based on monthly averages interpolated to the time of the obseravtions by linear interpolation. Hence, variability on timescales shorter than approximately 1 month (e.g. eddies) is filtered out in the model results while present in the observations. Moreover, while the spacing between observation stations is approximately 25 km, the model results are interpolated from the native 4 km grid onto a 2 km section grid using linear interpolation. For the probability density function analysis, daily averages from the model are compared with observations. As a result, more high-frequency variability is allowed in the model results in the latter analysis.

From the temperature and salinity climatology for March, 1980-2009 (Figure 4.12, 4.13) it is evident that the vertical mixing in the model is too strong, at least during winter which is depicted here. A likely explanation for the lack of stratification within the Norwegian Coastal Current is the relaxation towards the sea surface salinity from SODA. The coarse resolution of the SODA data likely fails to resolve the Norwegian Coastal Current. As a consequence, the coastal water is more saline and therefore also less buoyant in the model and vertical mixing is more likely to occur. Apart from the differences in stratification, the modelled horizontal distribution of the water masses and the fronts separating them are generally in agreement with observations, also in terms of the horizontal gradients through the fronts.

The effect of the sea surface salinity relaxation is also clearly seen in the variability in salinity (Figure 4.15). The large observed variability associated with the Norwegian Coastal Current is absent in the model results, even at 250 meter depth. The observed temperature variability associated with the northward extent of the Atlantic Water is well represented in the model. Also, the model indicate somewhat larger temperature variability towards the coast, in agreement with the observations.

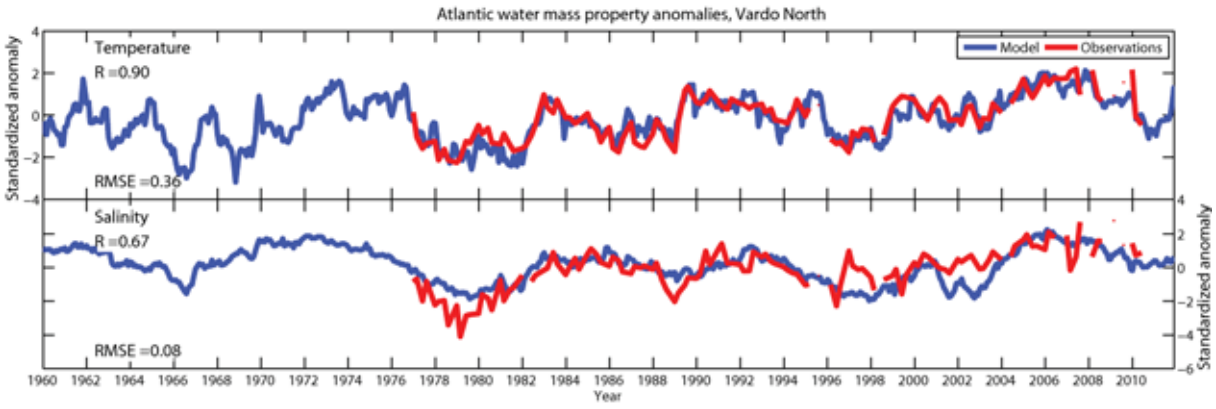

Figure 4.21. Average temperature (top) and salinity (bottom) of the Atlantic Water in the Vardø North section from model (blue) and observations (red). The correlation and rmse are based on monthly averages from the model.

The time series of integrated temperature reveals a very close agreement between the observations and the model with respect to variability on timescales from seasons to decades (R = 0.90; p < 0.01). For salinity, the correlation is lower (R = 0.67; p < 0.01) and the model is clearly representing the multi-year variability well, while the annual to intra-annual variability is less well represented (Figure 4.21). The model is generally warmer in winter and colder in summer/autumn (not shown; *rmse* = 0.36 ^{o}C). For salinity, *rmse* = 0.08 and the model is more or less uniformly biased low throughout the year (not shown). Using daily averages from the model and considering only Atlantic Water, the *rmse* for temperature increases to 0.66, while for salinity it remains at 0.08. For Coastal water, the corresponding numbers are 0.74 and 0.36, respectively (Table 4.4).

Table 4.4. Root mean square error and bias of modelled water mass properties relative to corresponding observations in the Vardø North section. The calculations are based on daily averages from the model.

	Atlantic water		Coastal water	
	rmse	bias	rmse	bias
Temperature	0.66	-0.45	0.74	0.05
Salinity	0.08	-0.07	0.36	0.35

Kola section

The Kola section is sampled monthly and provides time series of temperature and salinity dating back to the early 1900s (Bochkov 1982, Tereshchenko 1997). The section consists of 10 stations at fixed positions, with stations 1-3 (south) being occupied by coastal water masses and stations 8-10 (north) being occupied by Atlantic water masses. Here, we have

used the average between 50-200 m depth at the stations 3-7 (70° 30'N to 72° 30'N) for temperature, and the average between the surface to 200 m depth at the stations 8-10 (73°N to 74°N) for salinity. While the observations are based on a few stations, we have used all model grid points within the latitudinal boundaries interpolated onto a 2 km section grid using linear interpolation when calculating the model-based values.

Figure 4.22 shows that the model follows the observed temperature very closely from decadal to intra-annual timescales (R = 0.87; p < 0.01). However, the model is biased high during winter and low during summer (not shown; *rmse* = 0.38 °C). For salinity, the correlation is lower (R = 0.59; p < 0.01). Visually, we see that this is due to a lack of coherence on shorter time scales; while the model clearly follows the decadal and multi-year oscillations in observed salinity, there is less agreement on annual and intra-annual time scales. In addition, the model is biased low in salinity throughout the year (*rmse* = 0.07).

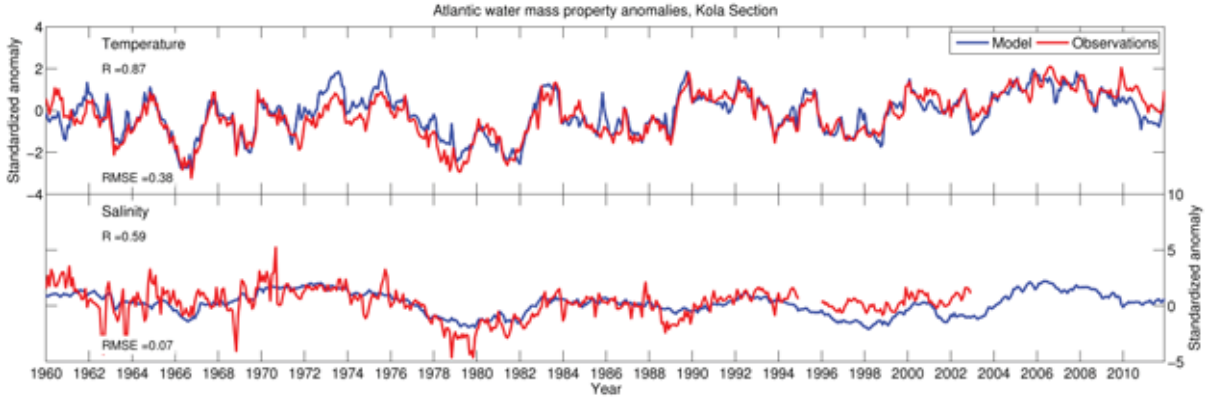

Figure 4.22. Average temperature (top) and salinity (bottom) of the Atlantic Water in the Kola section from model (blue) and observations (red). The correlation and rmse are based on monthly averages from the model.

4.1.5 Coastal Fixed Stations

CTD-observations at fixed stations operated by the Institute of Marine Research along the Norwegian coast provide information on temperature and salinity at standard depths and weekly to monthly time resolution for the whole period covered by the model simulation. Due to some irregularities in depth and timing, the observations are interpolated to predefined standard depths in space and to the 15th of each month by the use of linear interpolation. Climatologies for each separate depth and each month of the year are then computed at each station for the 30-year period 1980-2009. The climatologies are then subtracted from the timeseries to obtain anomalies for the whole period 1960-2011. For comparison, modelled monthly average temperature and salinity at gridpoints representative for the positions of the coastal fixed stations are interpolated in the vertical to standard depths using linear interpolation.

Lista

Station Lista is located off the southernmost part of Norway, within the Norwegian Coastal Current. The surface layer exhibits very low salinity (S ~ 30), and during winter the

temperature may reach the freezing point. At depth, the station is influenced by Atlantic water circulating within the Norwegian Trench.

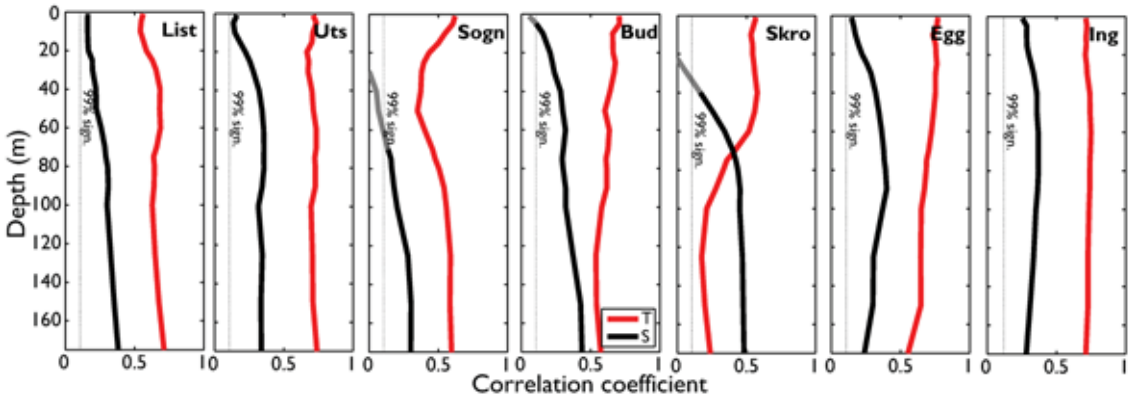

Figure 4.23. Correlation between observed and modelled temperature (red) and salinity (black) at the coastal fixed stations. The whole model period 1960-2011 is used. Dotted line indicate the 99% confidence level using a double-sided t-test. Non-significant values are shown in gray/pink.

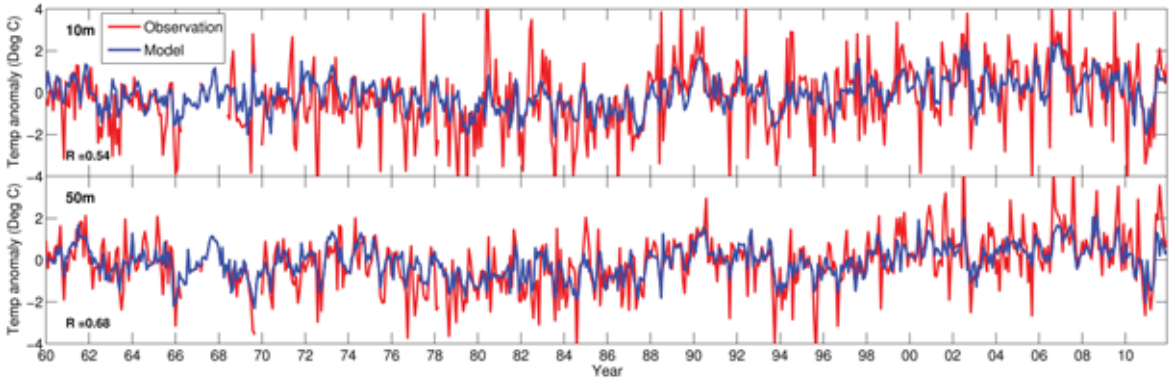

Figure 4.24. Temperature anomalies at 10 meter depth (top) and 50 meter depth (bottom) at station Lista from model (blue) and observations (red).

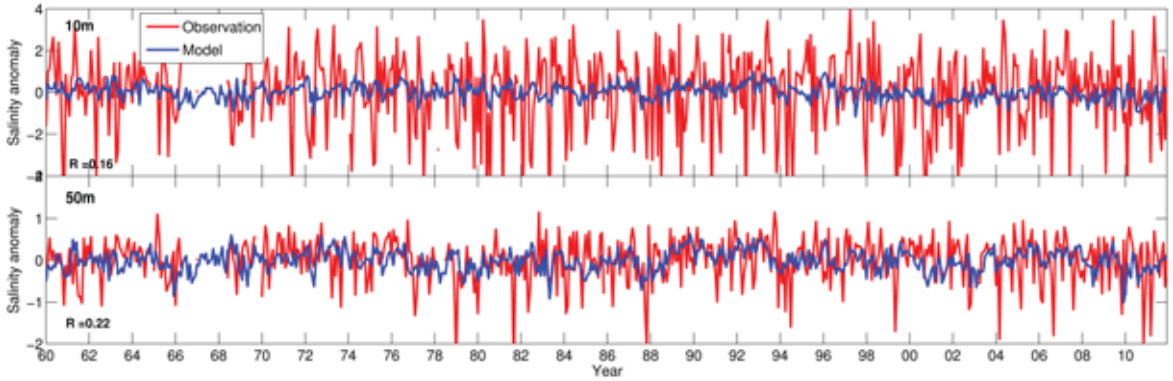

Figure 4.25. Salinity anomalies at 10 meter depth (top) and 50 meter depth (bottom) at station Lista from model (blue) and observations (red).

The modelled and observed temperature and salinity anomalies at station Lista are shown in Figures 4.24 and 4.25. Generally, the observations display a larger short term variability than the model, especially at 10 m. Hence, the model misses events with extreme temperature and salinity anomalies in the surface layer. On longer inter-annual timescales, there is a relatively

close agreement between modelled and observed temperature. In salinity, however, the correlations between modelled and observed values are low, although there is a slight increase with depth (Figure 4.23).

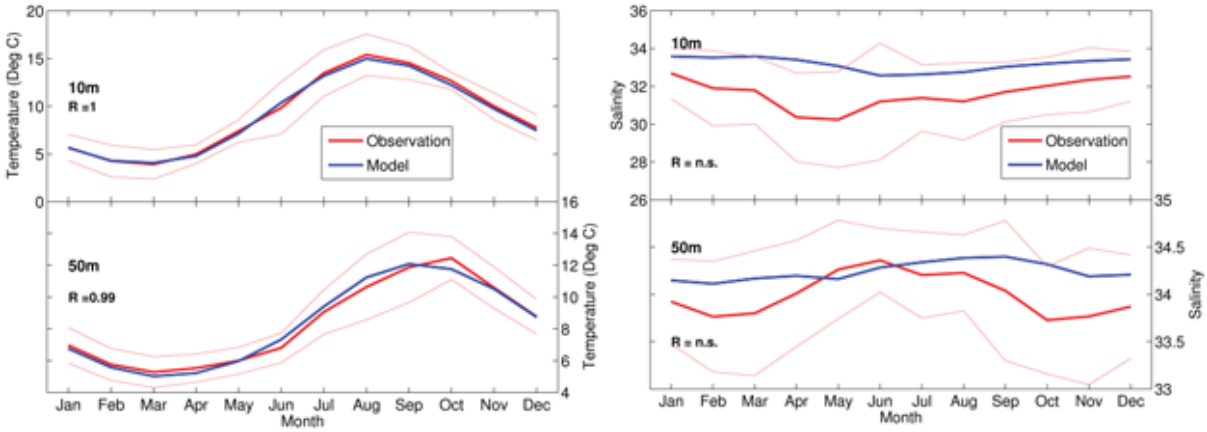

Figure 4.26. Seasonal cycle of temperature (left) and salinity (right) at station Lista from model (blue) and observations (red). Only data from the climatological period 1980-2009 are used.

Although the model lacks the observed variability on shorter time scales, the modelled average temperature and seasonal cycle are close to the observations at both 10 m and 50 m depth (Figure 4.26). Here, only the years within the climatological period (1980-2009) are included.

The modelled salinity is too high, especially near the surface. The seasonal cycle in salinity is to some degree resembled in the model, but the low number of points (N = 12) put strong constraints on the significance of the correlation (R = 0.71 needed for 99% significance).

Utsira

At Utsira, which is an island located within the Norwegian Coastal Current, two stations are operated, namely one inshore of the island and one further offshore. In the following analysis, we use the outermost station, which exhibits Atlantic Water at depth.

The temperature variability at station Utsira is well resembled in the model throughout the water column (Figure 4.23, 4.27). However, on short time scales (month), the model misses most extreme values in both temperature and salinity (Figure 4.27, 4.28). From Figure 4.23 we see that the correspondence between modelled and observed salinity is lowest in the top 20 m, while the correlation is ~0.35 from 50 m and downwards.

The model closely resembles the observed seasonal cycle in temperature both at 10 m and 50 m depth (Figure 4.29). For salinity, the model only to some degree captures the seasonal patterns.

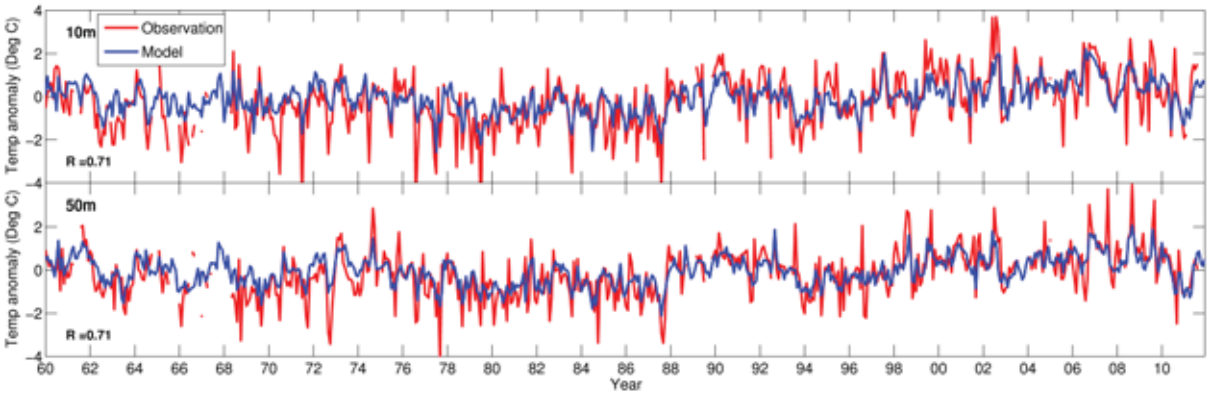

Figure 4.27. Temperature anomalies at 10 meter depth (top) and 50 meter depth (bottom) at station Utsira from model (blue) and observations (red).

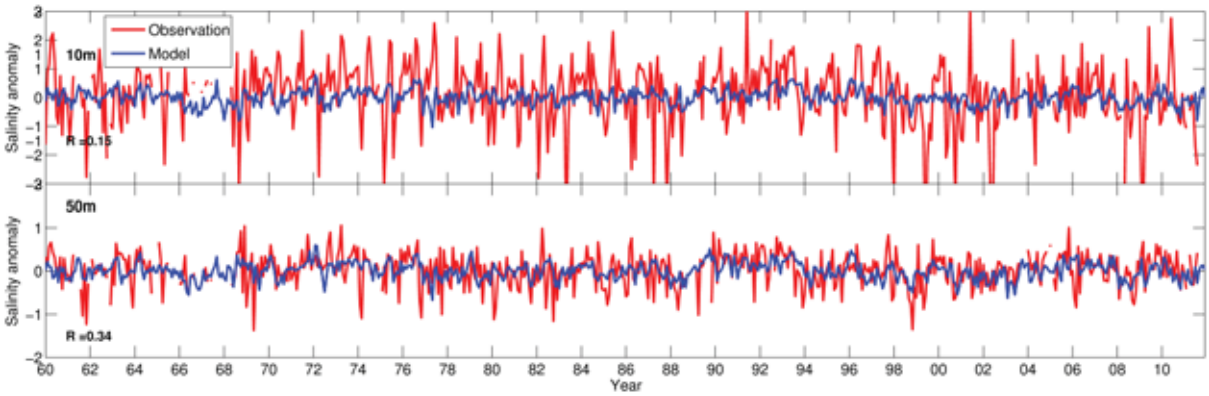

Figure 4.28. Salinity anomalies at 10 meter depth (top) and 50 meter depth (bottom) at station Utsira from model (blue) and observations (red).

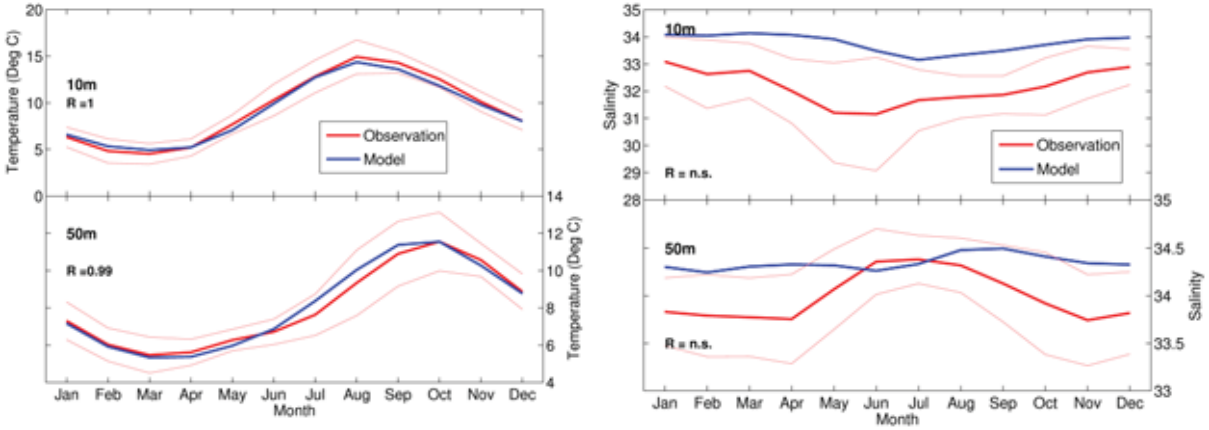

Figure 4.29. Seasonal cycle of temperature (left) and salinity (right) at station Utsira from model (blue) and observations (red). Only data from the climatological period 1980-2009 are used. In addition, the model exhibits too high salinity, especially at 10 m depth.

Sognesjøen

Station Sognesjøen is located at the mouth of Sognefjorden, and is influenced both from advected water masses from the surface layers in the fjord, coastal water and Atlantic Water deeper below. Therefore, especially the surface layers experience large seasonal and year to year variations e.g. due to interannual variability in freshwater runoff from land.

The modelled and observed temperature and salinity anomalies at station Sognesjøen are shown in Figures 4.30 and 4.31. As for the stations further south, the model resembles the temperature variations at seasonal to annual time scales and longer, while the more short-term variability, and especially the extreme values, are lacking in the model. There is a distinct minimum in the correlation between the model and the observations in the depth interval 10 m to 100 m. This is even more so in terms of salinity, where significant correlation between model and observations is found only below ~70 m depth. A possible explanation of the pattern in the correlation vs. depth analysis, could be the sill depth of 100-200 m inshore of the station. This influences the circulation, resulting in the advection above 100 m playing a dominant role. Circulation within the fjord is not expected to be adequately resolved in a model with 4 km horizontal resolution. Near the surface, the atmosphere is the most important forcing, which explains the relatively high correlation between observed and modelled temperature in the top 10 meters.

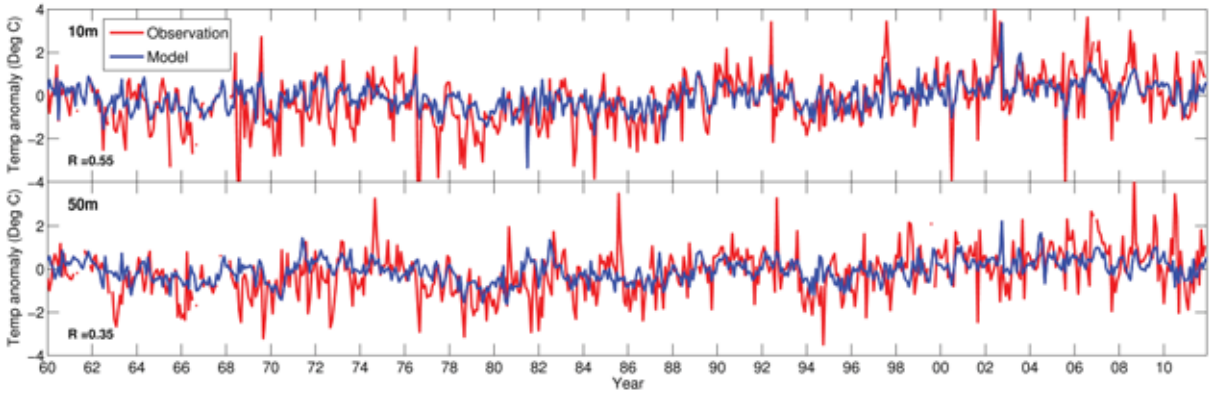

Figure 4.30. Temperature anomalies at 10 meter depth (top) and 50 meter depth (bottom) at station Sognesjøen from model (blue) and observations (red).

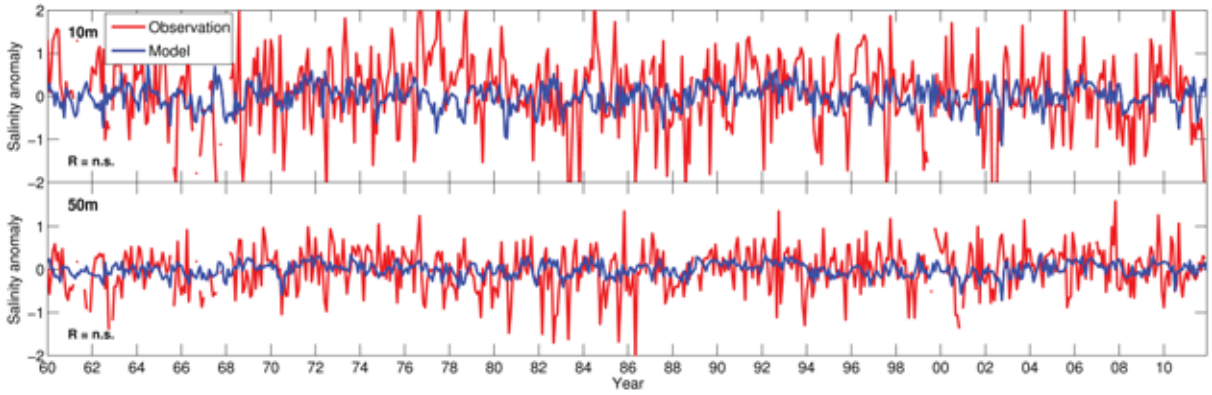

Figure 4.31. Salinity anomalies at 10 meter depth (top) and 50 meter depth (bottom) at station Sognesjøen from model (blue) and observations (red).

In terms of seasonal variation, we find that the model closely resembles the observed seasonal temperature pattern, although there are some discrepancies at 50 m depth (Figure 4.32). Especially the seasonal maximum temperature at 50 meter depth in October is underestimated in the model. For salinity, there is less agreement between the model and observations, and generally the model is too saline, being more than one standard deviation above the observed mean in all seasons. Moreover, the seasonal amplitude is underestimated in the model.

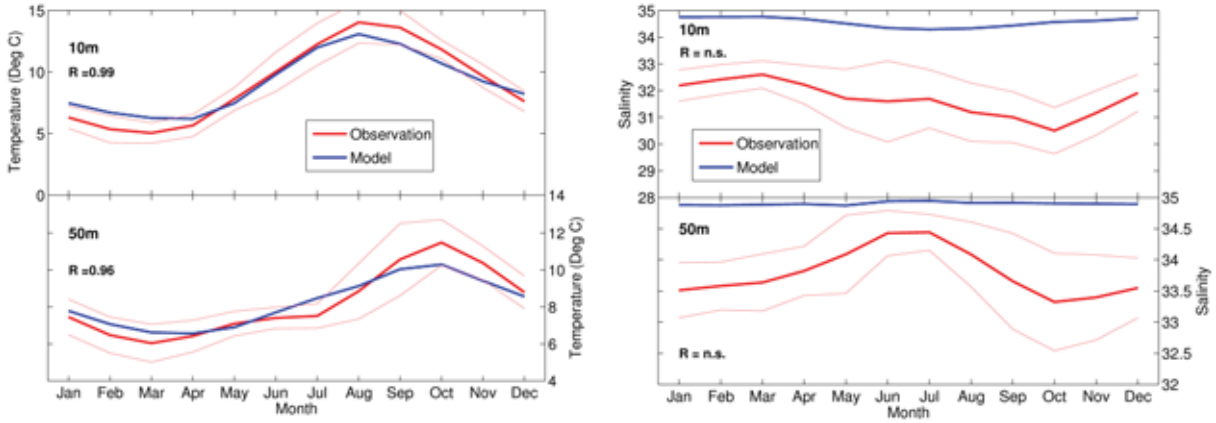

Figure 4.32. Seasonal cycle of temperature (left) and salinity (right) at station Sognesjøen from model (blue) and observations (red). Only data from the climatological period 1980-2009 are used.

Bud

Station Bud is located within the Norwegian Coastal Current, resulting in low salinities in the upper layers. At depth, however, influence from the Norwegian Atlantic slope Current results in the salinity increasing with depth.

The modelled variability in temperature is comparable with observations, except that the model underestimates some of the extreme values (Figure 4.33). Generally, the correlation between modelled and observed temperature is $0.60 < R < 0.70$, but slightly decreasing with depth (Figure 4.23). For salinity, there is less agreement between model and observations (Figure 4.34), although the correlation is increasing with depth and is close to $R = 0.5$ at 180 m depth.

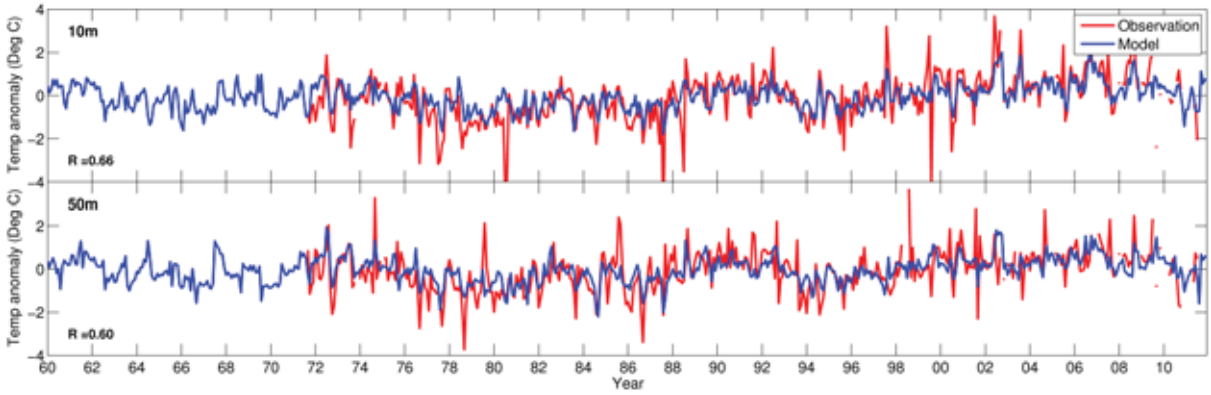

Figure 4.33. Temperature anomalies at 10 meter depth (top) and 50 meter depth (bottom) at station Bud from model (blue) and observations (red).

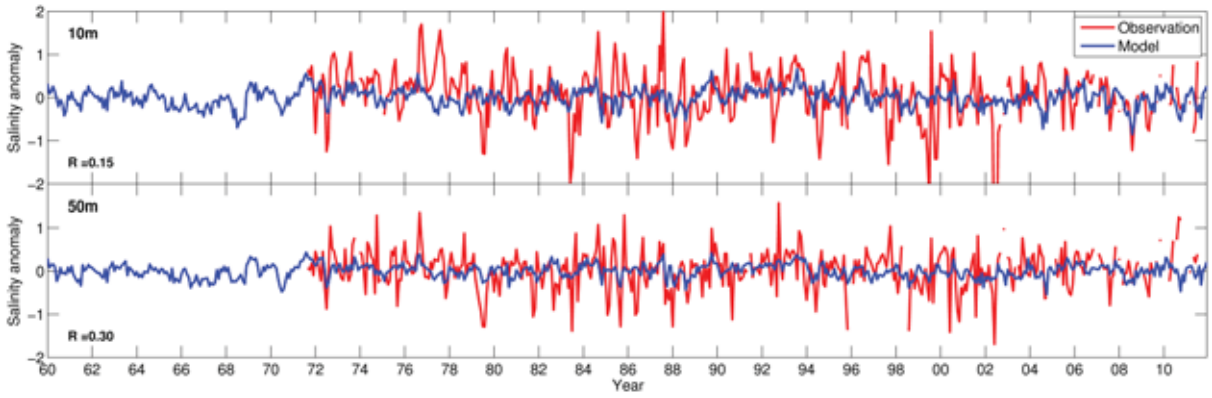

Figure 4.34. Salinity anomalies at 10 meter depth (top) and 50 meter depth (bottom) at station Bud from model (blue) and observations (red).

The modelled seasonal temperature cycle is in close agreement with observations, except for a shorter heating seson in the model (winter minimum later and summer maximum earlier than observed; Figure 4.35). Also, in winter, the model tends to be warmer and lying outside the one standard deviation range compared to observations. The modelled seasonal salinity cycle is in agreement with observations in the upper 10 m, although the model is considerably more saline. At 50 m, however, the modelled seasonal minimum (summer) appears two months too early (August vs. October), and also the seasonal maximum is skewed in the model (April) compared to observations (July).

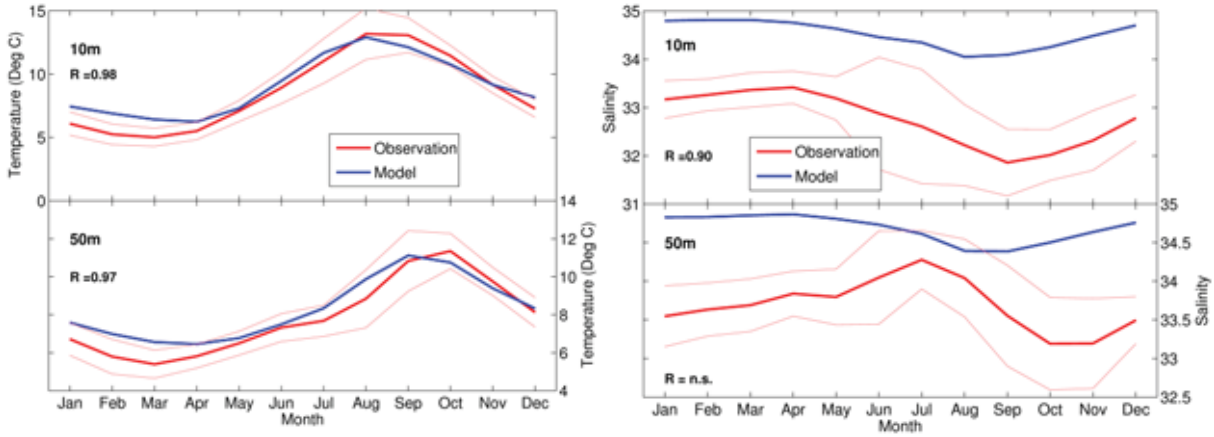

Figure 4.35. Seasonal cycle of temperature (left) and salinity (right) at station Bud from model (blue) and observations (red). Only data from the climatological period 1980-2009 are used.

Skrova

Station Skrova is located at the inshore side of the Lofoten archipelago. The surface layers are dominated by coastal water, while the deeper parts are occupied by Atlantic Water. Due to a threshold depth of 220 m further offshore, the temporal variations within the Atlantic layer are small, while the transition depth between coastal and Atlantic water can vary substantially even at short time scales (~days).

At both 10 m and 50 m depth, the model resembles the temporal variations in temperature fairly well ($0.5 < R < 0.6$; Figure 4.36). Below approximately 100 meter depth (influenced by Atlantic Water), however, the correlation between modelled and observed temperature is substantially lower. For salinity, the relation is opposite (Figure 4.37), with no significant correlation above 40 m depth (coastal water), but increasing to R~0.5 below 80 m depth (Atlantic Water).

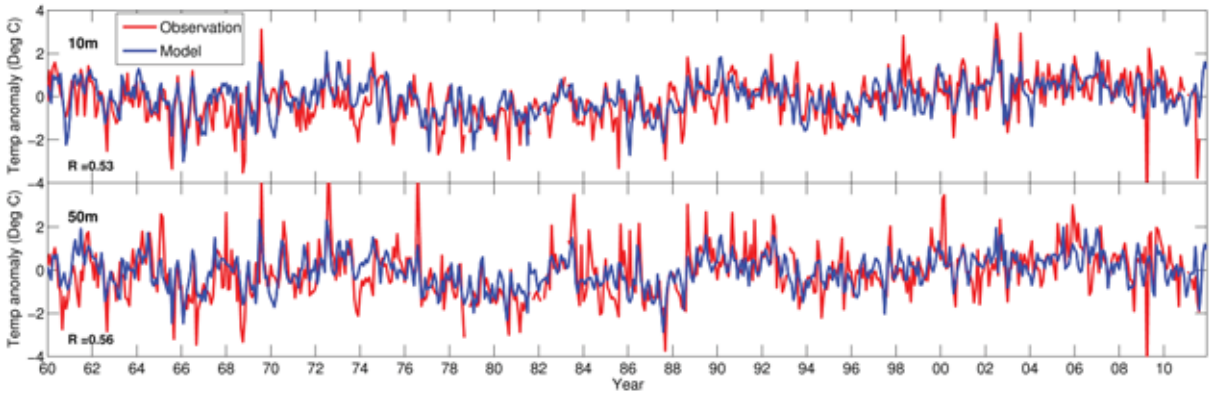

Figure 4.36. Temperature anomalies at 10 meter depth (top) and 50 meter depth (bottom) at station Skrova from model (blue) and observations (red).

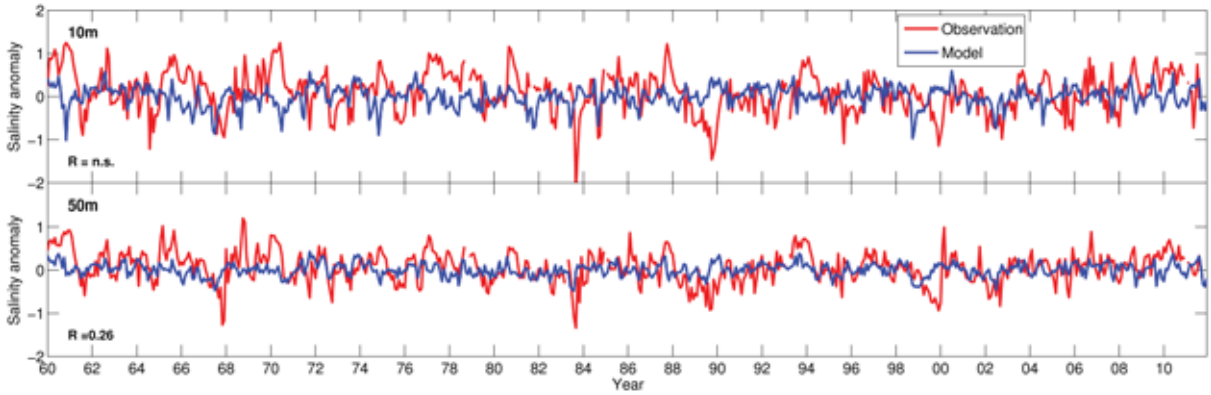

Figure 4.37. Salinity anomalies at 10 meter depth (top) and 50 meter depth (bottom) at station Skrova from model (blue) and observations (red).

Both the salinity and especially the temperature seasonal cycle is well represented in the model (Figure 4.38). However, the model tends to overestimate the temperature in winter (10 m depth) and throughout the year (50 m depth). And again, the model is biased high in salinity, although the seasonal amplitude is realistic.

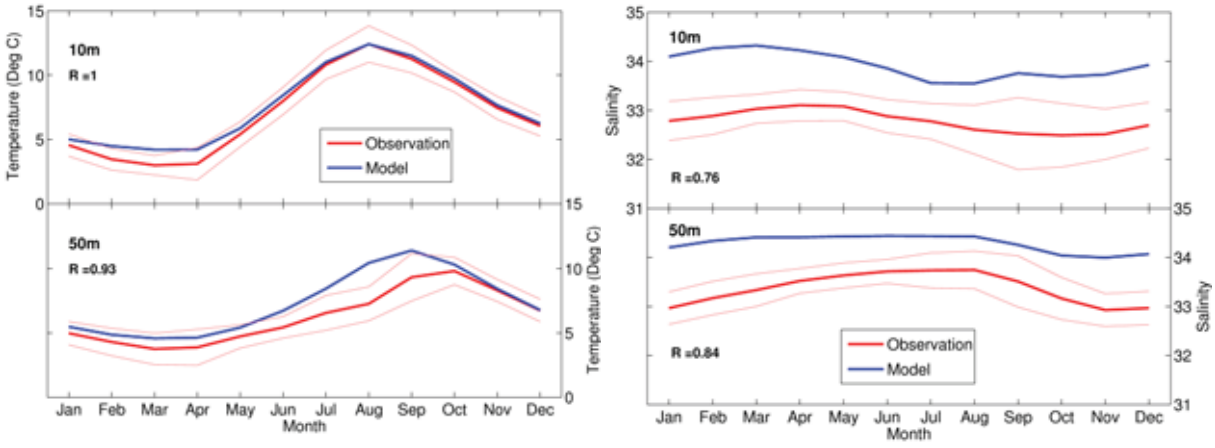

Figure 4.38. Seasonal cycle of temperature (left) and salinity (right) at station Skrova from model (blue) and observations (red). Only data from the climatological period 1980-2009 are used.

Both the salinity and especially the temperature seasonal cycle is well represented in the model (Figure 4.38). However, the model tends to overestimate the temperature in winter (10 m depth) and throughout the year (50 m depth). And again, the model is biased high in salinity, although the seasonal amplitude is realistic.

Eggum

Station Eggum is located at the outer side of the Lofoten archipelago. The upper layers are occupied by coastal water, while the deeper layers are influenced by Atlantic Water.

At station Eggum, the model resembles the temperature variations at both 10 m and 50 m depth (Figure 4.39), although the model misses some of the extreme values. Moreover, the correlation decreases slightly with depth (Figure 4.23). For salinity, the highest correlation (R~0.4) is found at around 80 m depth, decreasing both up- and downwards. Evidently, the model displays far less variability than seen in observations (Figure 4.40).

Except for an overestimation of the seasonal maximum temperature at 50 m depth, the modelled seasonal temperature cycle is within one standard deviation of the observed values. The model also represents the seasonal salinity cycle fairly well, although it is somewhat skewed in the model. Also, the modelled salinity is substantially higher than observed.

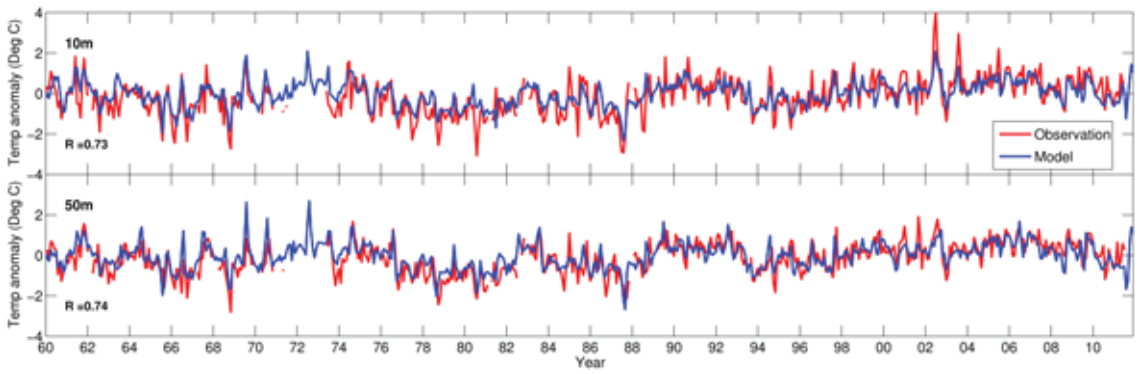

Figure 4.39. Temperature anomalies at 10 meter depth (top) and 50 meter depth (bottom) at station Eggum from model (blue) and observations (red).

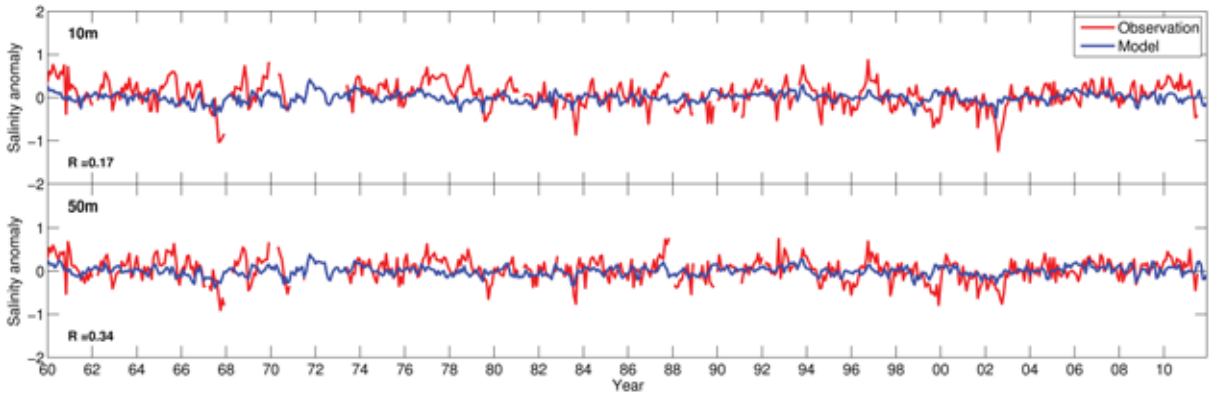

Figure 4.40. Salinity anomalies at 10 meter depth (top) and 50 meter depth (bottom) at station Eggum from model (blue) and observations (red).

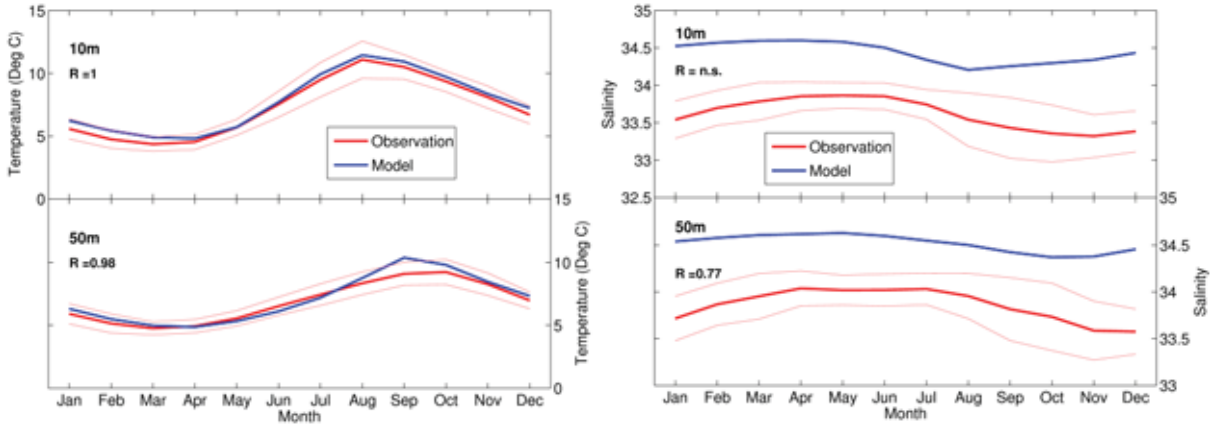

Figure 4.41. Seasonal cycle of temperature (left) and salinity (right) at station Eggum from model (blue) and observations (red). Only data from the climatological period 1980-2009 are used.

Ingøy

Station Ingøy is located outside the northern tip of Norway, and is the station which is most influenced by Atlantic Water and shows the least vertical stratification.

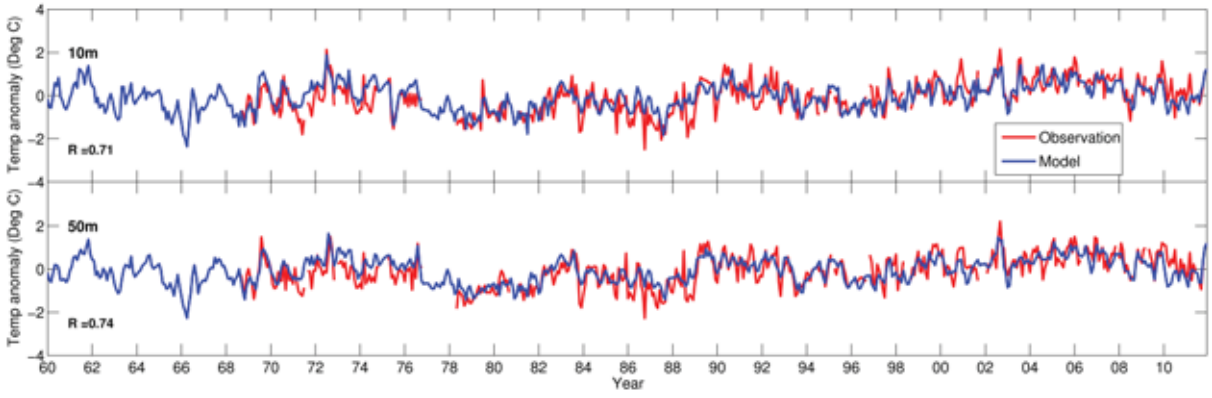

Figure 4.42. Temperature anomalies at 10 meter depth (top) and 50 meter depth (bottom) at station Ingøy from model (blue) and observations (red).

The correlation between modelled and observed temperature at Ingøy is *R* ~0.7 throughout the water column (Figure 4.23). Also for salinity, there is a significant correlation between the model results and the observations throughout the water column, although the correlation is

lower (R ~0.3; Figure 4.23). Furthermore, the model exhibits very small temporal variations in salinity compared to observations both at 10 m depth and 50 m depth. This may reflect an accumulated response from the relaxation towards the sea surface salinity in the SODA dataset as the coastal water masses are advected northward along the Norwegian coast.

At station Ingøy, the model resembles the seasonal variation in both temperature and salinity to a very high degree, with the correlations exceeding $R > 0.9$ at both 10 m and 50 m depth (Figure 4.44). However, as for the stations further south, the model overestimate the salinity substantially, and the seasonal amplitude is somewhat lower in the model compared to the observations. For temperature, the model tends to be on the high side compared to the observations, yet mostly within one standard deviation from observed values.

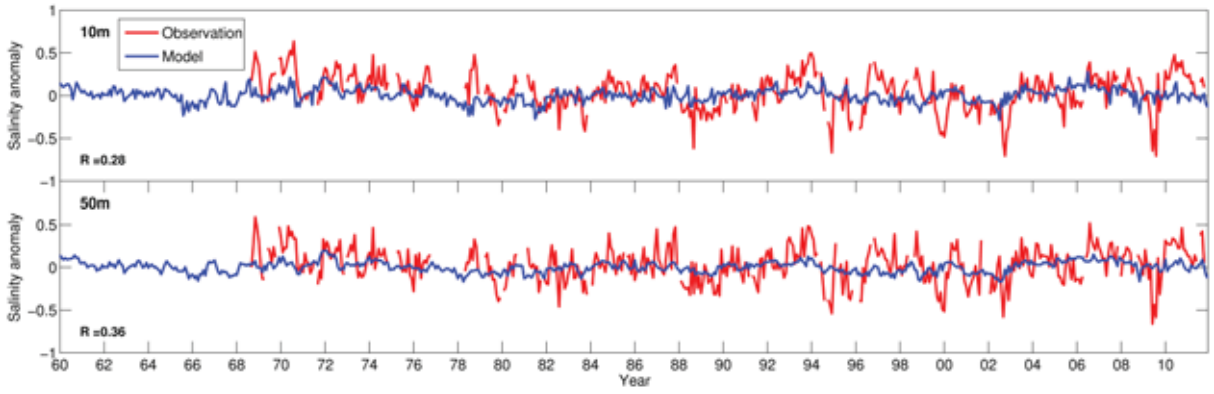

Figure 4.43. Salinity anomalies at 10 meter depth (top) and 50 meter depth (bottom) at station Ingøy from model (blue) and observations (red).

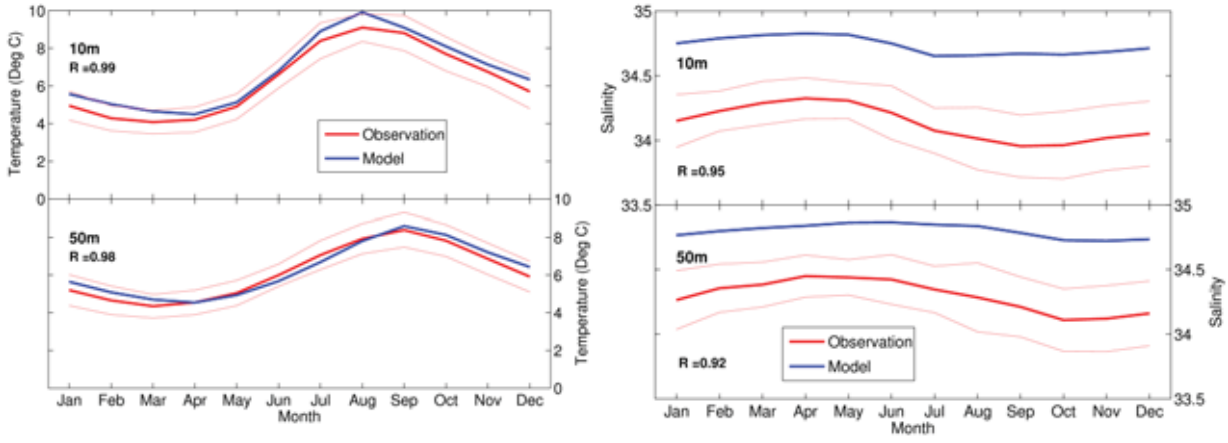

Figure 4.44. Seasonal cycle of temperature (left) and salinity (right) at station Ingøy from model (blue) and observations (red). Only data from the climatological period 1980-2009 are used.

4.1.6 Ocean Weather Station M

The Ocean Weather Station MIKE (OWSM) was initiated in 1948. It is located at 66°N, 2°E in the frontal zone between the northward flowing Atlantic Water and the colder and less saline water masses of the Norwegian Sea. The bottom depth at the station is 2000 meter, and thus, it constitutes the longest deep-ocean hydrographic time series in the world, with a temporal resolution of one month.

Figure 4.45 shows the modelled and observed hydrographic properties at intermediate and deep levels in the Norwegian Sea. Generally, the model is biased high in both temperature (0.2-0.4, decreasing with depth) and salinity (0.01-0.02). In terms of density, the biases in temperature and salinity contribute in opposite directions, yet a small bias remains also in density, with the modelled intermediate and deep water being slightly denser in the model.

Figures 4.46 to 4.49 show time series of temperature and salinity at depths 800 - 2000 m, based on observations and model results. As seen in the T-S diagrams, the model is generally biased high in both temperature and salinity. Moreover, the model generally displays less variability than do the observations.

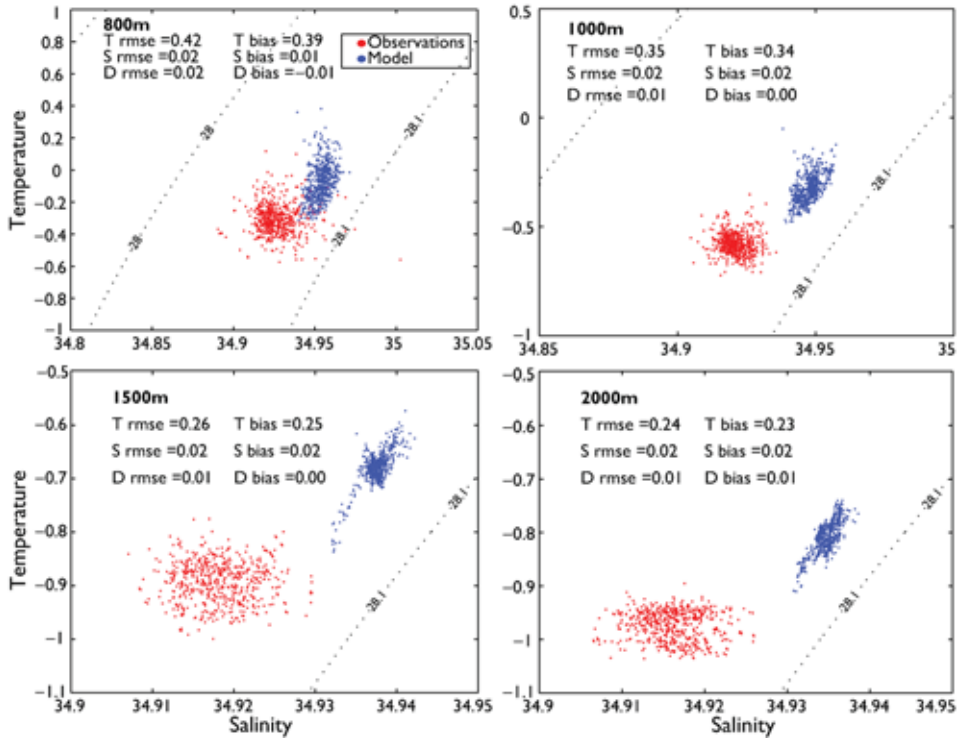

Figure 4.45. Temperature-Salinity diagrams at Ocean Weather Station Mike from observations (red) and model (blue) at 800 m (top, left), 1000 m (top, right), 1500 m (bottom, left) and 2000 m depth (bottom, right). Note the different scales.

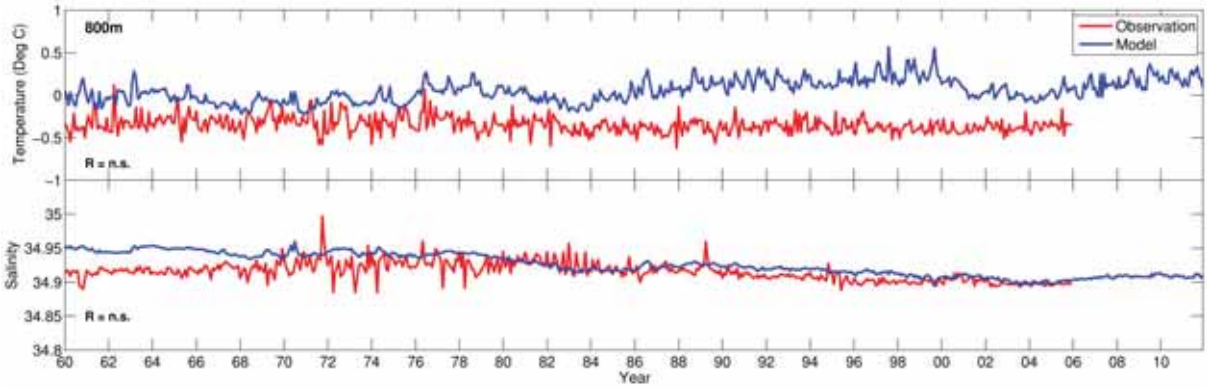

Figure 4.46. Temperature (top) and salinity (bottom) at Ocean Weather Station Mike from observations (red) and model (blue) at 800 m depth.

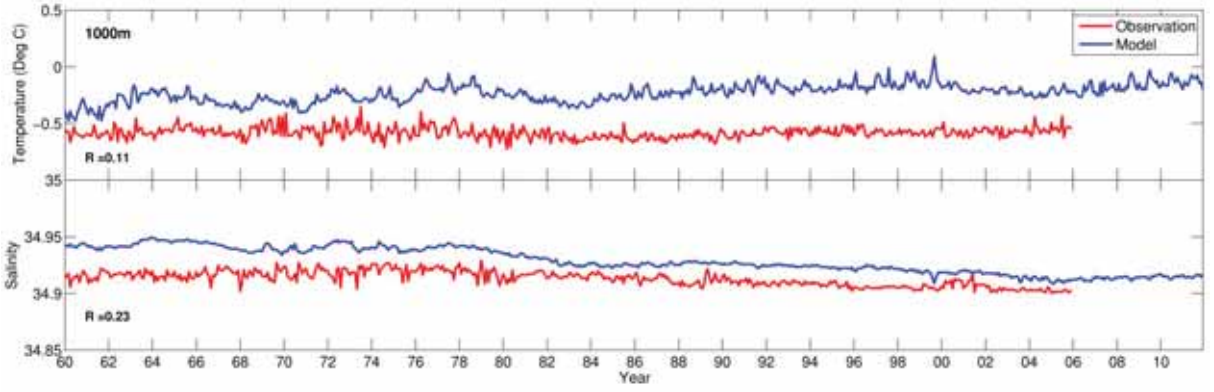

Figure 4.47. Temperature (top) and salinity (bottom) at Ocean Weather Station Mike from observations (red) and model (blue) at 1000 m depth.

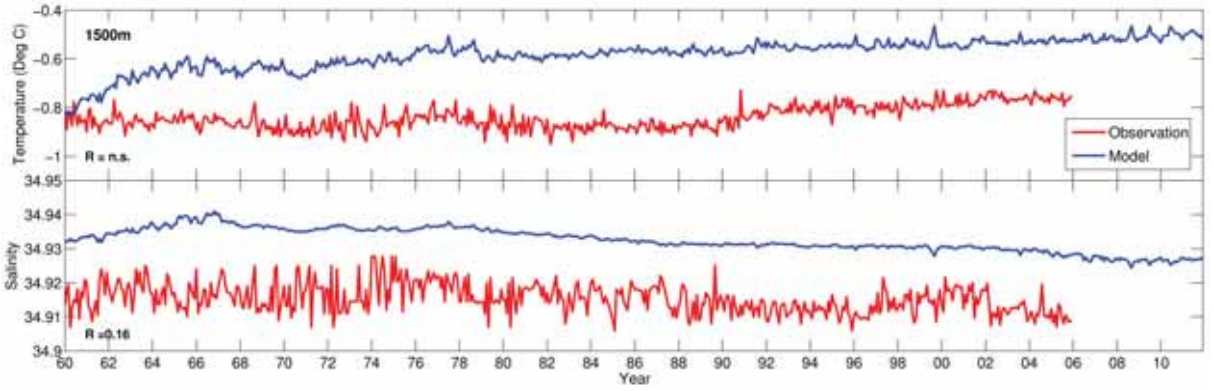

Figure 4.48. Temperature (top) and salinity (bottom) at Ocean Weather Station Mike from observations (red) and model (blue) at 1500 m depth.

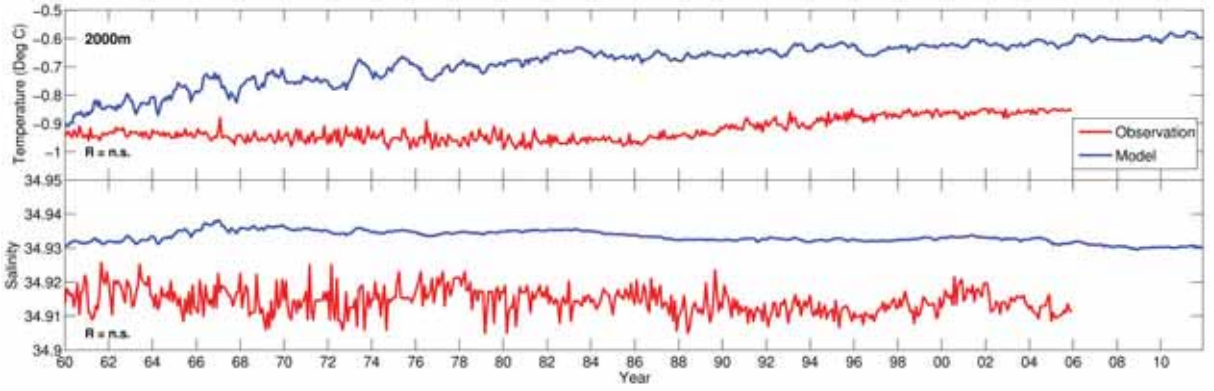

Figure 4.49. Temperature (top) and salinity (bottom) at Ocean Weather Station Mike from observations (red) and model (blue) at 2000 m depth.

Within the Norwegian Sea Deep Water at 1500 m and 2000 m depth, there is a clear trend in modelled temperature from the start of the time series and continuing for 10-20 years. A trend in the deep water temperature at OWSM has been observed after 1980 (Østerhus and Gammelsrød 1999). Such a trend is also seen in the model results, although representing a slower transition than the trend earlier in the model period. The deep basins require long time to spin up, and the initial trend could possibly be due to adjustments during the spinup phase of the simulation. Another issue concerning temperature and salinity trends in sigma-coordinate numerical ocean models (such as ROMS) is spurious diapycnal mixing. In the

current simulation, numerical diapycnal diffusion may occur in regions with a sloping bottom. For a discussion on this matter, see Marchesiello et al. (2009).

4.1.7 Short Summary: Hydrography

To summarize the comparison of modelled and observed hydrography, the model is generally biased low in both temperature (~0.5 ^{o}C) and salinity (~0.1) within the Atlantic Water. In terms of variability, the model resembles observed patterns at inter-annual timescales and longer and especially in shelf areas, where air-sea interactions become important. The Norwegian Coastal Current is too saline due to relaxation towards sea surface salinity from the SODA dataset, while its variability in temperature is well captured at seasonal to annual timescales and longer. At shorter time scales, the model misses the extreme anomalies in both temperature and salinity. The lack of variability in the model could be partly explained by the fact that model results are based on monthly averages while observations are based on instantaneous values. Furthermore, the model represents 4 by 4 km averages, in addition to the modelled sea surface salinity being relaxed towards the values from the SODA dataset.

In the Barents Sea, the model resembles the main observed patterns in terms of horizontal temperature and salinity distribution and variability. Additionally, the Polar Front is realistically represented in the model.

The modelled heat content within the Norwegian Sea is substantially lower than observed, due to a too shallow transition zone between Atlantic Water and colder and less saline intermediate water masses. A possible explanation is too little eddy-generated cross-slope exchange in the model.

4.2 Currents

4.2.1 Svinøy Section

The Atlantic inflow over the Greenland-Scotland Ridge and into the Nordic Seas is steered by the topography and flows northward along the Norwegian continental slope as the Norwegian Atlantic Current (Orvik and Niiler 2002). In the southern part of the Norwegian Sea, south of the Lofoten archipelago, the Norwegian Atlantic Current consists of two branches: a near-barotropic and topographically locked eastern branch flowing along the Norwegian continental slope, and an unstable frontal jet located further west, approximately above the 2000 m isobath (Orvik et al. 2001).

Figure 4.50 shows the probability density function for cross section velocity at 100 m depth in the core of the Norwegian Atlantic slope Current in the Svinøy section. Clearly, the model tends to underestimate the current speed. Although the width of the modelled range is similar to the observation-based results, the model overestimate the frequency of the lower current speeds and underestimate the frequency of the higher current speeds. Furthermore, the modelled current is less unidirectional (Figure 4.51), although a strong topographical steering prevails also in the model, especially at high current speeds.

When considering the differences in modelled and observed current speed, it should be taken into account that the observations represent a point measurement while the modelled speed represents the average within a 4 by 4 km grid cell. According to Orvik et al. (2001), the width of the Norwegian Atlantic slope Current core is ~10 km. Hence, small displacements of the current in the model (e.g. due to differences in bathymetry) will affect the model observation comparison in terms of current speed. Regarding direction, the discrepancy between model and observations suggests a less stable current in the model, which could arise from overestimated eddy activity, unrealistic temporal displacements of the Norwegian Atlantic slope Current, or both.

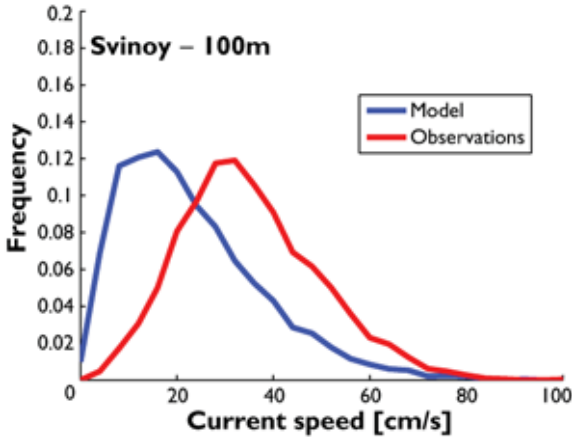

Figure 4.50. Probability density function of speed at 100 meter depth in the Svinøy section from model (blue) and observations (red).

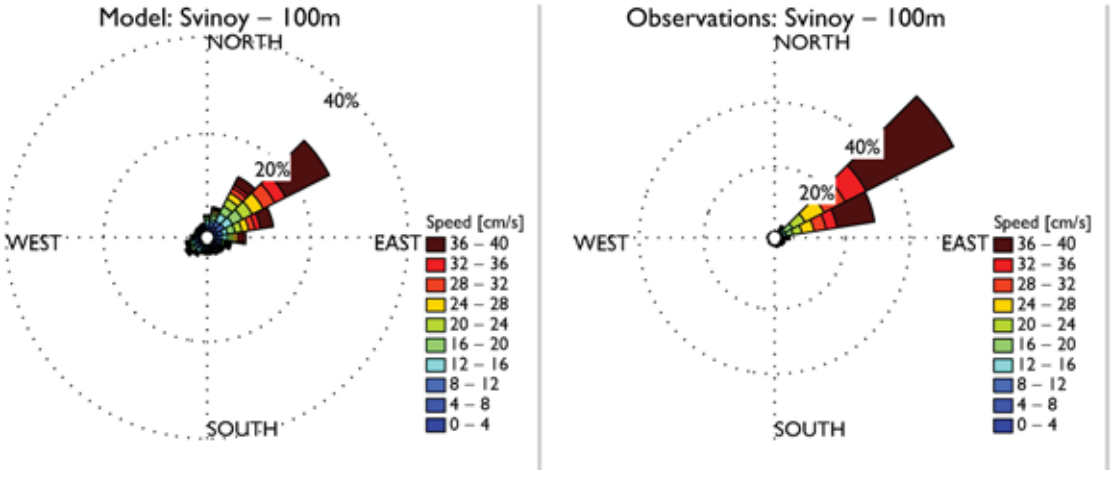

Figure 4.51. Current distribution at 100 meter depth in the Norwegian Atlantic slope Current in the Svinøy section from model (left) and observations (right).

4.2.2 Barents Sea Opening

The Barents Sea Opening has been continuously monitored by moored direct current meters since 1997 (Skagseth et al. 2008). The inflow of Atlantic Water to the Barents Sea consists of two branches along the southern slope (Ingvaldsen et al. 2004), although a third branch occasionally occupies the more narrow northern slope (Lien et al. 2013).

Figure 4.52 shows the probability density functions for modelled and observed current speeds in the Fugløya-Bjørnøya section at 50 meter depth. Generally, there is a close agreement between the model and the observations, and especially at mooring position 3 (CM3), which represents the core of the Atlantic Water inflow to the Barents Sea (Ingvaldsen et al. 2004). In the southern part of the section (CM1), the model tends to slightly overestimate the occurrences of higher current speeds, while the frequency of the lower current speeds is too low. At the rest of the CMs further north in the section, the range of the modelled current speeds tend to be slightly too narrow, indicating slightly lower current speeds in the model. Hence, the weaker currents are slightly overrepresented in the model, while the events of stronger currents are underrepresented. However, one must keep in mind that the model results represents 4 by 4 km areas, which are compared with point measurements. Thus, such a skewness is expected, especially when taking into account the relatively small dynamical length scale (typically below 10 km) in this region.

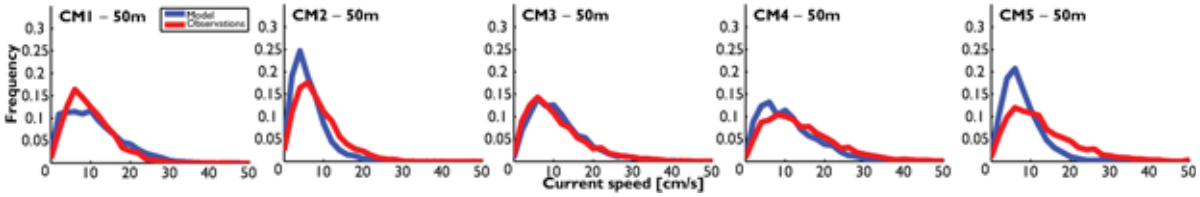

Figure 4.52. Probability density functions of speed in the Fugløya-Bjørnøya section from model (blue) and observations (red) at 50 meter depth. The locations refer to current meter mooring positions 1-5 (see Figure 2.2 for positions).

At mooring position 1 the model results are in close agreement with the observations in terms of current direction (Figure 4.53), although the model overestimates the topographical steering along the southeastward directed slope on the northern side of Tromsøflaket. This results in a more unidirectional flow in the model compared to the observations, especially in deeper layers and at high current speeds. Moreover, the modelled current tends to be directed more towards southeast than the eastward-directed observed current. This implies that the slope of the local model bathymetry in this area differs from reality.

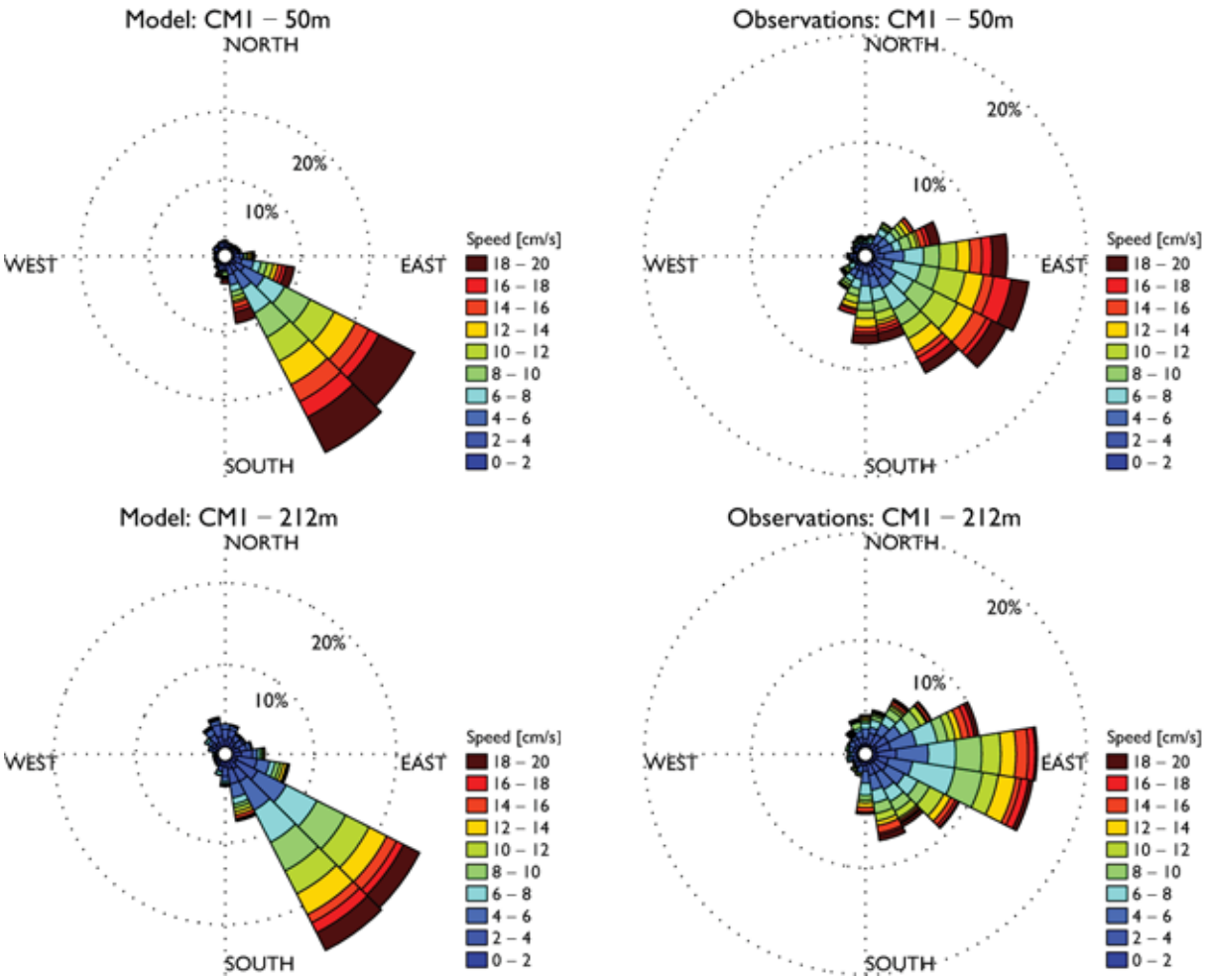

Figure 4.53. Current distribution at 50 meter depth (top) and near the sea floor (bottom) from model (left) and observations(right) at mooring station 1 in the Barents Sea Opening.

At mooring position 2 the flow is less unidirectional than at CM1 (Figure 4.54), and the model displays a larger spread than do the observations. However, there is a tendency of a prevailing southeastward flow in the model, which is also seen in the observations. We suspect that the dominating east-west flow seen in the observations at depth is caused by an error in the data processing, although its cause remains unknown.

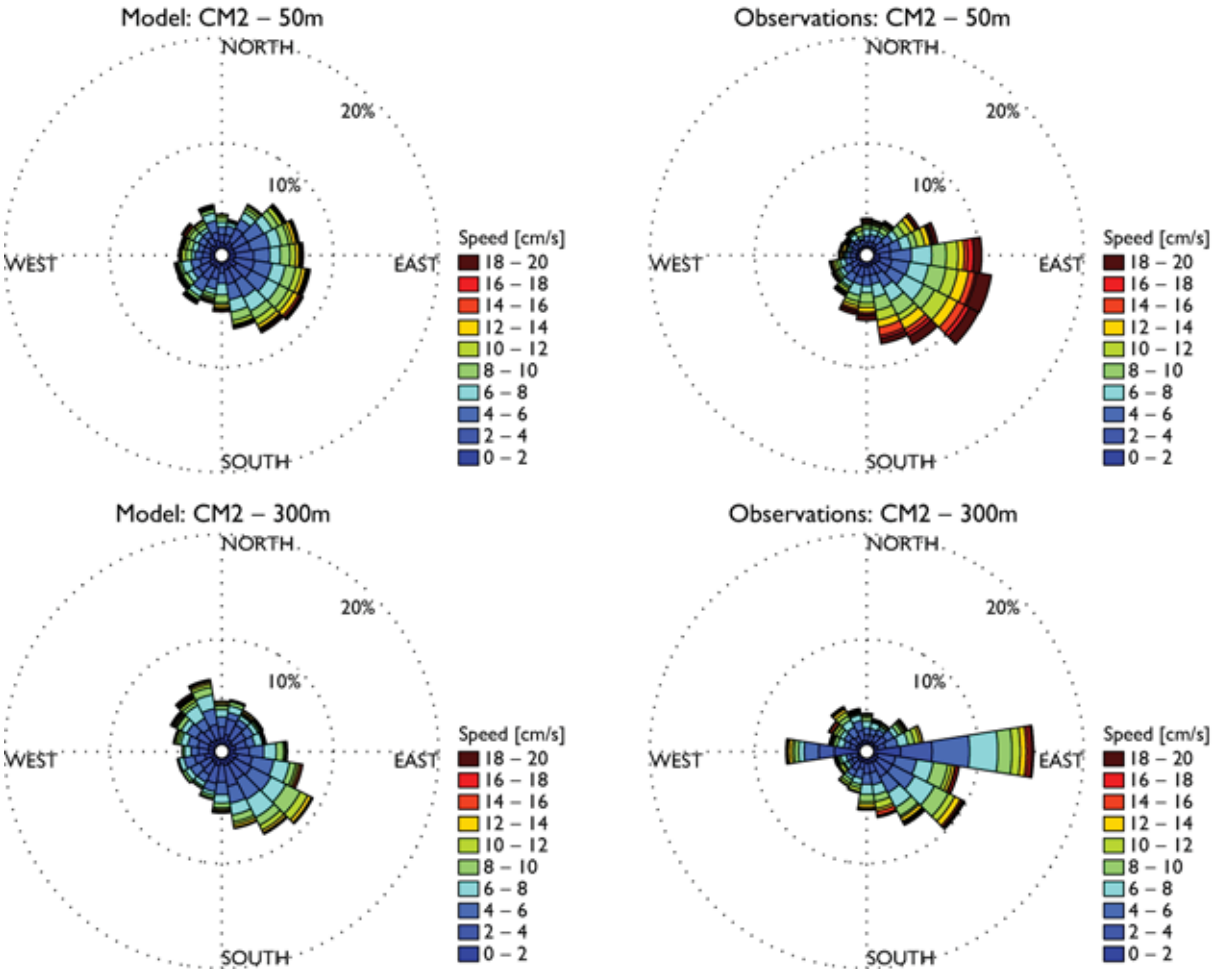

Figure 4.54. Current distribution at 50 meter depth (top) and near the sea floor (bottom) from model (left) and observations(right) at mooring station 2 in the Barents Sea Opening.

Mooring position 3 is located at 72^{o} 30'N, within the core of the Atlantic Water inflow to the Barents Sea. This is reflected in the observed current direction, which shows a prevailing eastward flow (Figure 4.55). However, there is a relatively large spread in the observed current directions, indicating frequent reversals of the flow, as well as vigorous eddy activity. In the model, the current direction is mainly varying between east and south, indicating stronger topographical steering.

Mooring position 4 at 73^{o}N, is located in the Bjørnøya Trough and close to the Polar Front, which separates the eastward flowing Atlantic Water from colder and less saline westward flowing water masses. According to the observations, the flow is multidirectional in this part of the section but with a weak tendency of an overall southeastward flow (Figure 4.56). In the upper part of the water column, the modelled current is directed eastward, as opposed to the

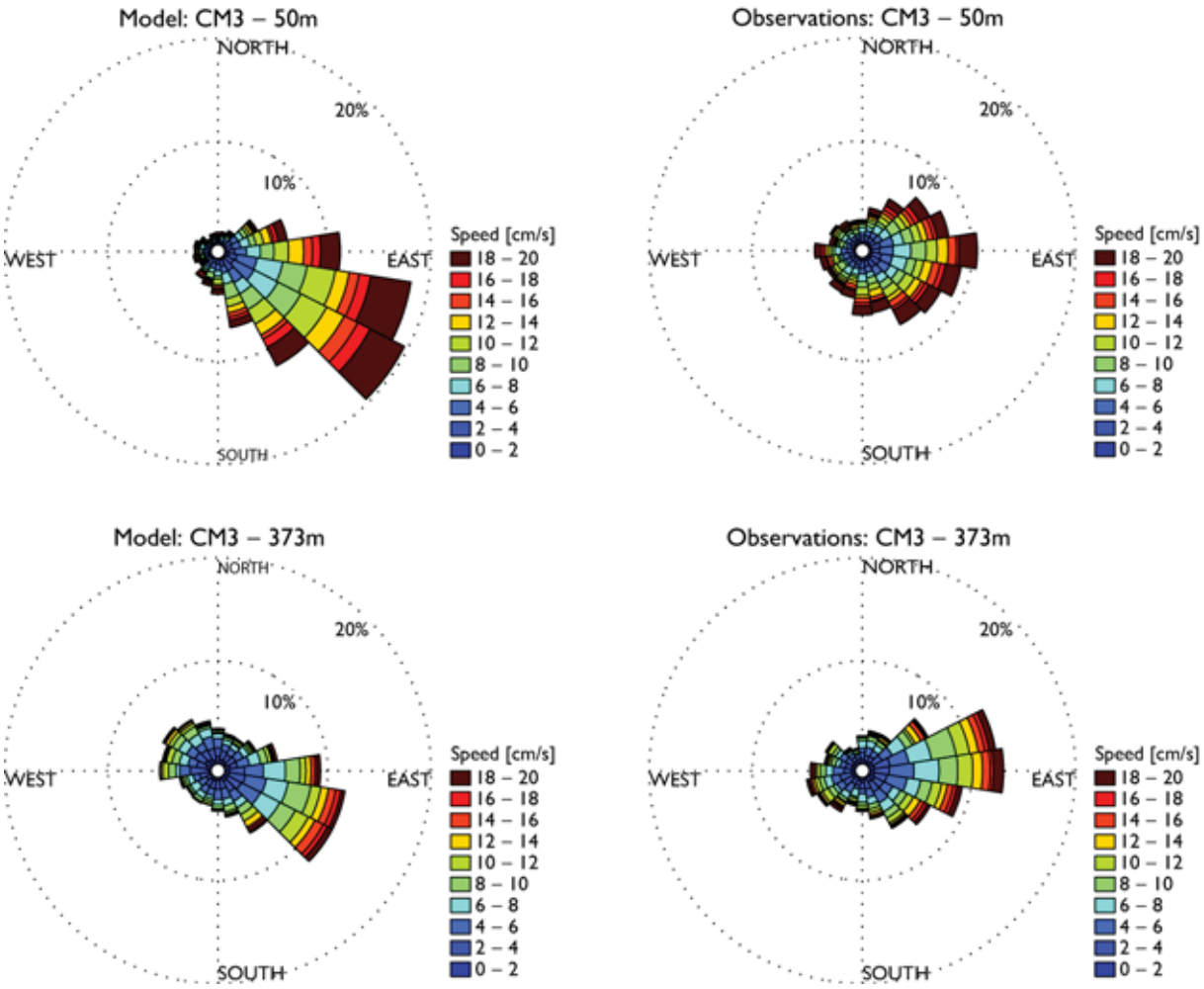

Figure 4.55. Current distribution at 50 meter depth (top) and near the sea floor (bottom) from model (left) and observations(right) at mooring station 3 in the Barents Sea Opening.

multidirectional pattern seen in the observations. The multidirectional spread of the higher velocities in the upper layers indicate vigorous eddy activity in this area, which is not reflected in the model results. In the deeper layers, however, the model resembles the multidirectional flow pattern seen in the observations, which indicates frequent fluctuations between inflow and outflow near the bottom. Thus, the topographical steering is over-estimated in the model.

This could be an indication that the Polar Front is positioned further north in the model, whereas in the observations, the front frequently reaches south to 73°N. Another explanation is that the model does not resolve synoptic scale dynamics, such as eddies close to the size of the internal Rossby radius.

Mooring position 5 is located in the northern part of the Barents Sea Opening, at the base of the slope rising towards Bjørnøya. Similar to CM4, the observations show multidirectional flow in the upper layers at CM5 (Figure 4.57). However, there is a a weak dominance by southwestward flow, following the general features of the bathymetry. At depth, there is a stronger dominance of southwestward flow, indicative of a vertically sheared flow. Baroclinic westward flow of dense bottom water in this area was reported by Blindheim (1989), and was

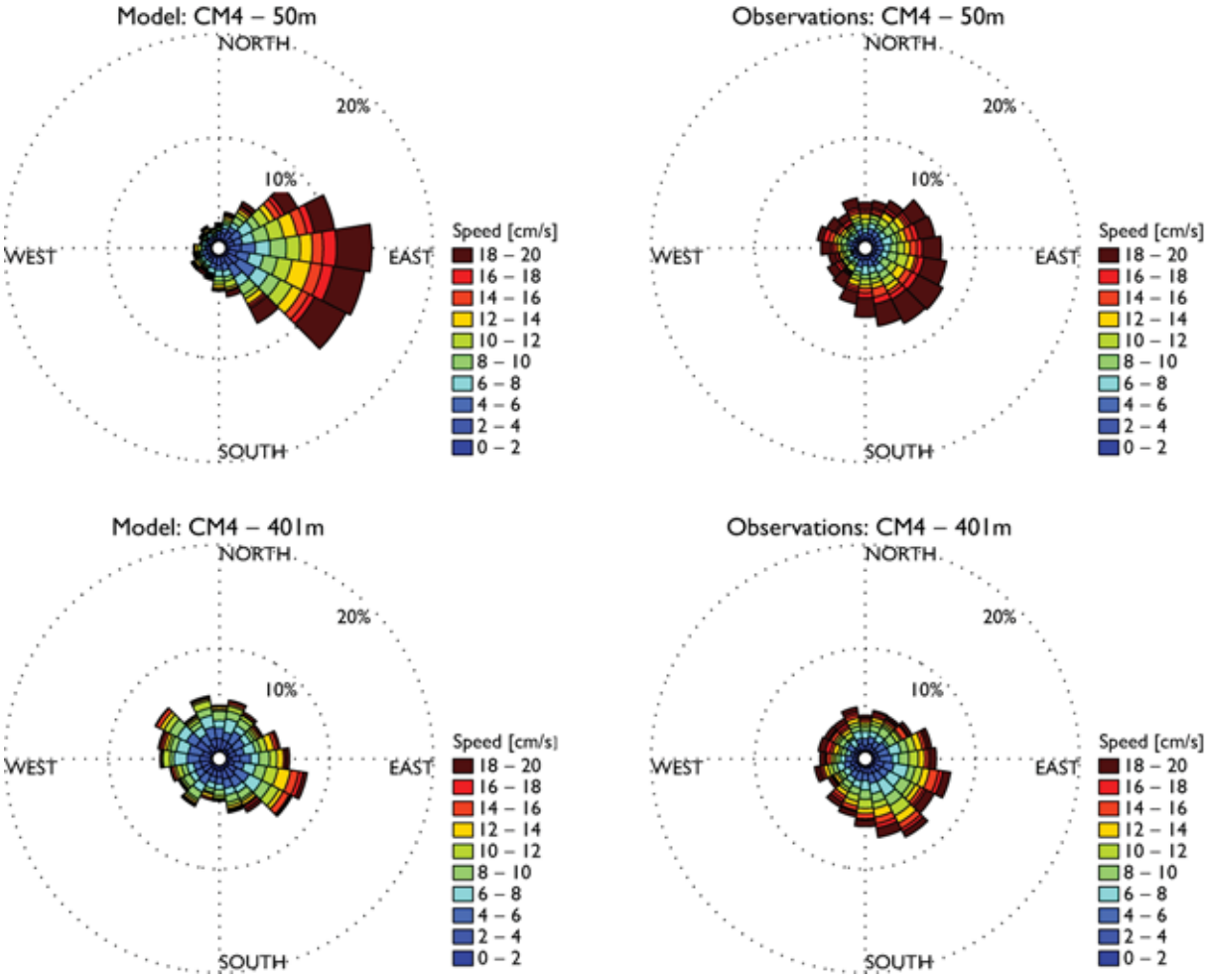

Figure 4.56. Current distribution at 50 meter depth (top) and near the sea floor (bottom) from model (left) and observations (right) at mooring station 4 in the Barents Sea Opening.

also suggested based on model results (Årthun et al. 2011). This model, however, shows a unidirectional west/southwestard flow throughout the water column at CM5 (Figure 4.57).

As for the Svinøy section, it needs to be taken into account that the observations are based on point measurements, while the model results are based on averages within a 4 by 4 km grid cell. However, the Atlantic flow through the Barents Sea Opening is wider and less energetic than along the Norwegian continental slope. As a consequence, the results are less sensitive to the position of the current.

4.2.3 Short Summary: Currents

Generally, the model resembles the observed current pattern, but the modelled currents tend to be slightly weaker and more strongly controlled by topography. Also, there are indications that there is less eddy activity in the model. This could, at least to some degree, be explained by the challenge of comparing point measurements with model grid cells representing 4 by 4 km squares, as well as the models inability to resolve processes at the dynamical length scale.

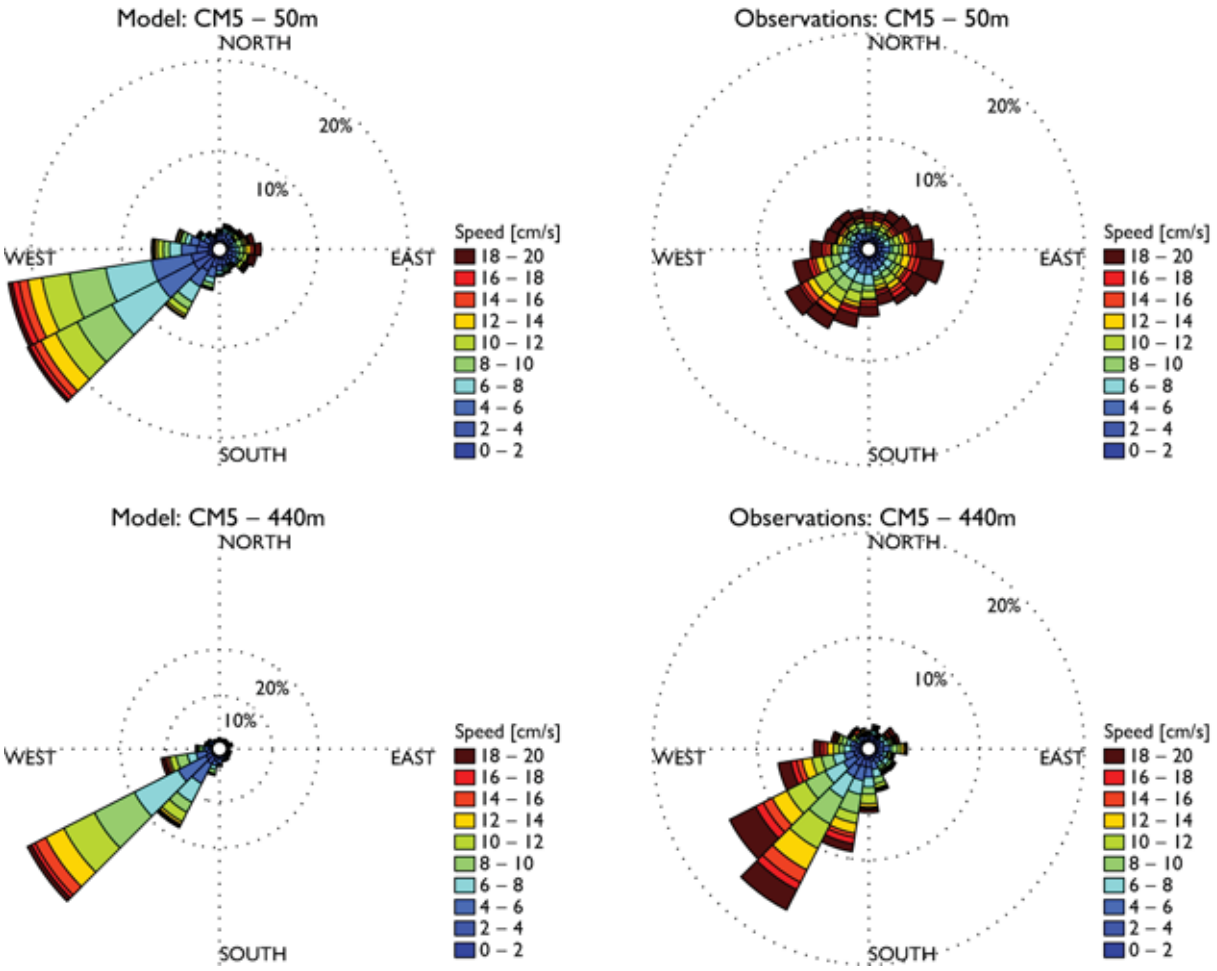

Figure 4.57. Current distribution at 50 meter depth (top) and near the sea floor (bottom) from model (left) and observations(right) at mooring station 5 in the Barents Sea Opening.

4.3 Volume and heat transports

4.3.1 Faroe-Shetland Channel

The Faroe-Shetland Channel is a main entrance for the Atlantic Water flowing into the Nordic Seas (e.g. Hansen and Østerhus (2000)), in which direct current measurements have been carried out since 1994 (Turrell et al. 2003). The modelled volume and heat transports through the section is shown in figures 4.58 and 4.59. There is, however, a substantial recirculation of Atlantic Water originating from the flow over the Iceland-Faroe Ridge. This complicates the observational-based estimation of Atlantic Water inflow through the Faroe-Shetland Channel. Here, we present both the total and net inflow and compare with similar observational-based estimates.

Table 4.5 summarizes the comparison between modelled and observed volume transports through the Faroe-Shetland Channel. The model results indicate considerably lower net inflow of Atlantic Water than the estimates found in literature. For the whole simulation period (1960-2011), the average net Atlantic inflow amounts to 2.0 Sv. However, looking at total rather than net Atlantic inflow increases the model-based estimate to 4.2 Sv for the whole simulation period and 4.0 Sv for the period which Rossby and Flagg (2012) used for

their estimate of 4.1 Sv based on ADCP measurements. The substantial difference between net and total Atlantic inflow indicates that a large recirculation takes place within the Faroe-Shetland Channel, and that this recirculation is exaggerated in the model.

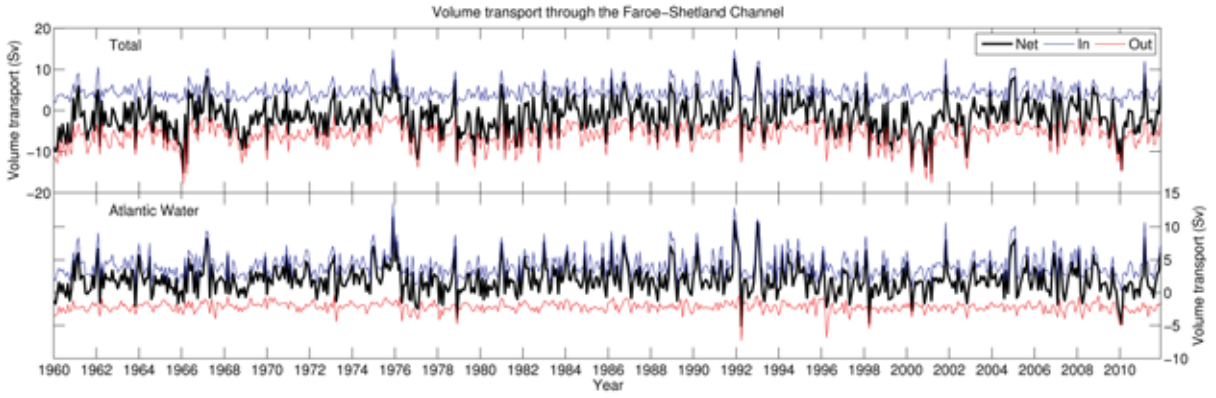

Figure 4.58. Volume transport through the Faroe-Shetland Channel from all water masses (top) and Atlantic water masses only (bottom). See table 3.3 for water mass definitions.

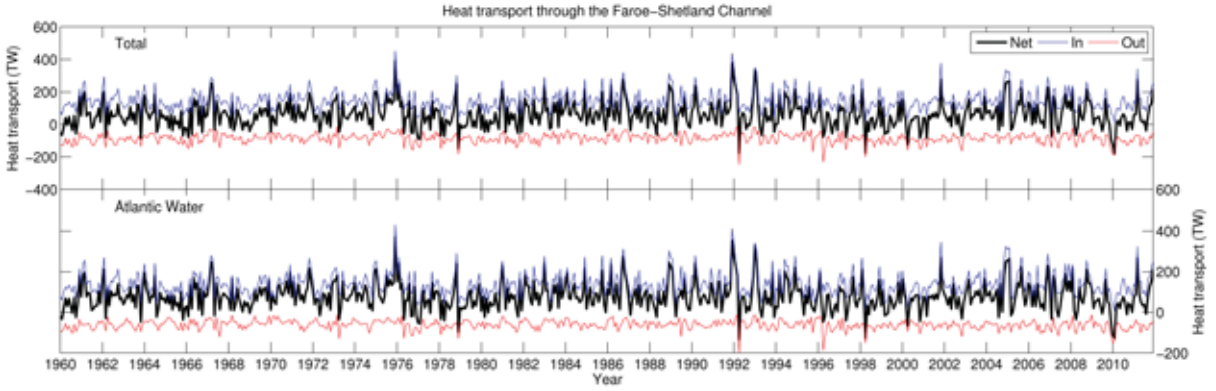

Figure 4.59. Heat transport through the Faroe-Shetland Channel from all water masses (top) and Atlantic water masses only (bottom). See table 3.3 for water mass definitions.

Rossby and Flagg (2012) estimated a net volume transport of 0.9 Sv above $\sigma\theta$ = 27.8, while Hansen and Østerhus (2007) estimated a southward flow of 1.9±0.3 Sv below $\sigma\theta$ = 27.8. This yields a total net of -1.0 Sv (i.e. southwards). The corresponding modelled net volume transport amounts to -2.3 Sv. The discrepancy is mostly due to a larger southward flow in the model (6.2 Sv in the model compared to 5.1 Sv from observations). By combining hydrographic data, altimetry and ADCP measurements Berx et al. (2013) obtained a net Atlantic volume transport (T > 5^{o}C) of 2.7 Sv during the period 1995-2009. The net volume transport was derived from a total northward Atlantic volume transport of 3.5 Sv and a southward transport of 0.8 Sv. In the model, the corresponding northward and southwards transports are 4.0 Sv and 2.3 Sv, respectively. However, a part of the dicrepancy could be due to the exclusion of the Faroese shelf in the observations-based estimates. The shelf circulation was excluded to omit the anti cyclonic circulation around the Faroe Islands (i.e. southward flow along the eastern side of the islands).

Table 4.5. Volume (top) and heat (bottom) transports estimates from the model hindcast (left) and observations (right) for similar periods in the Faroe-Shetland Channel. Values are in Sverdrups (volume) and Terawatts (heat). Note that total and net values are used, depending on the observations.

Period	Mod. Vol.	Obs. Vol.	Reference
1999-2001	1.3	3.8	Østerhus et al. (2005)
1994-2000	1.5	3.2	Turrell et al. (2003)
2008-2011	4.0	4.1	Rossby and Flagg (2012)
1995-2009	1.7	2.7	Berx et al. (2013)
Period	Mod. Heat	Obs. Heat	Reference
1999-2001	62	156	Østerhus et al. (2005)
2008-2011	128	133	Rossby and Flagg (2012)
1995-2009	73	107	Berx et al. (2013)

As for the volume transport, also the modelled net Atlantic heat transport only corresponds to about half of that based on observations (table 4.5). Looking at the whole simulation period yields a heat transport of 79 TW, which is somewhat larger than for the limited period 1999-2001, but still substantially lower than observation-based values. Looking at northward transport only, yields a heat transport of 140 TW and 146 TW for Atlantic Water and all water masses, respectively, averaged over the whole simulation period. For the period 1999-2001, we get 125 TW from Atlantic Water only. The average northward heat transports for the period March 2008 to March 2011 are 124 TW and and 128 TW for Atlantic Water and all water masses, respectively. These numbers are closer to the observation-based estimtes of 156 TW obtained by Østerhus et al. (2005) and 132.5 TW obtained by Rossby and Flagg (2012). Furthermore, Rossby and Flagg (2012) obtained a net heat transport of 42 TW for the period March 2008 to March 2011. The corresponding modelled estimate is 33 TW. Comparing with the observations-based estimates of 131 TW northward and 24 TW southward, yielding a net Atlantic heat transport of 107 TW northwards by Berx et al. (2013), the model yields a northward Atlantic heat transport of 139 TW and southward Atlantic heat transport of 66 TW, i.e. a net heat transport of 73 TW northwards, for the period 1995-2009. Note that Berx et al. (2013) used 0 ^{o}C as reference temperature, compared to the -0.1 ^{o}C used here. To summarize, the modelled heat transport in the Faroe-Shetland Channel yields realistic values, but a direct comparison between model and observations based on specific water mass characteristics is not straight forward.

Based on the model results, we find a seasonal amplitude of approximately 0.5 Sv, with a maximum in winter (December to February) and a minimum in summer (not shown). This is higher than the 0.2 Sv seasonal amplitude reported by Østerhus et al. (2005), although the modelled seasonal cycle is in phase with the observed cycle, displaying maxima in March (Østerhus et al. 2005) and November (Turrell et al. 2003). Using more extensive data from a longer time period, Berx et al. (2013) found seasonal amplitudes of 0.9 Sv and 0.7 Sv from ADCP-data and altimetry-data, respectively, with maxima in November (ADCP) and January (altimetry). However, the monthly averages calculated from the ADCP measurements exhibit large variability (std = 1.2 Sv), and the fitted sinusoidal seasonal curve explains only 21% of the total variability.

4.3.2 Iceland-Faroe Ridge

Opposite to the Faroe-Shetland Channel, the area between the Faroese Islands and Iceland is a ridge with complex topography and thus also complex circulation patterns. Hence, monitoring the inflow at the ridge by using moored current meters is difficult. In the following, it should therefore be noted that while Østerhus et al. (2005) base their estimates on measurements across the shelf north of the Faroes, Rossby and Flagg (2012) base their estimates on ADCP measurements along the ridge itself. In the model, we use a section following a straight line from the Faroese Islands towards Iceland (Figure 2.2).

The comparison of modelled and observation-based estimates of volume and heat transports across the Iceland-Faroe ridge is summarized in Table 4.6. Both the modelled volume (Figure 4.60) and heat (Figure 4.61) transports are lower than observed. Note that the estimates from Rossby and Flagg (2012) are based on the months June-August only, and therefore we have also only used these months in the comparison for that period. Considering northward transport only, reveals a substantial recirculation over the ridge. The modelled total Atlantic inflow amounts to 4.9 Sv for the whole simulation period, while the net Atlantic inflow is 3.0 Sv for the same period.

Table 4.6. Volume (top) and heat (bottom) transports estimates from the model hindcast (left) and observations (right) for similar periods over the Iceland-Faroe Ridge. Values are in Sverdrups (volume) and terawatts (heat).

Period	Mod. Vol.	Obs. Vol.	Reference
1999-2001	2.5	3.8	Østerhus et al. (2005)
1997-2001	2.8	3.5	Hansen et al. (2003)
2008-2011	2.8	4.6	Rossby and Flagg (2012)
Period	Mod. Heat	Obs. Heat	Reference
1999-2001	71	134	Østerhus et al (2005)
1997-2001	81	124	Hansen et al (2003)
2008-2011	88	134	Rossby and Flagg (2012)

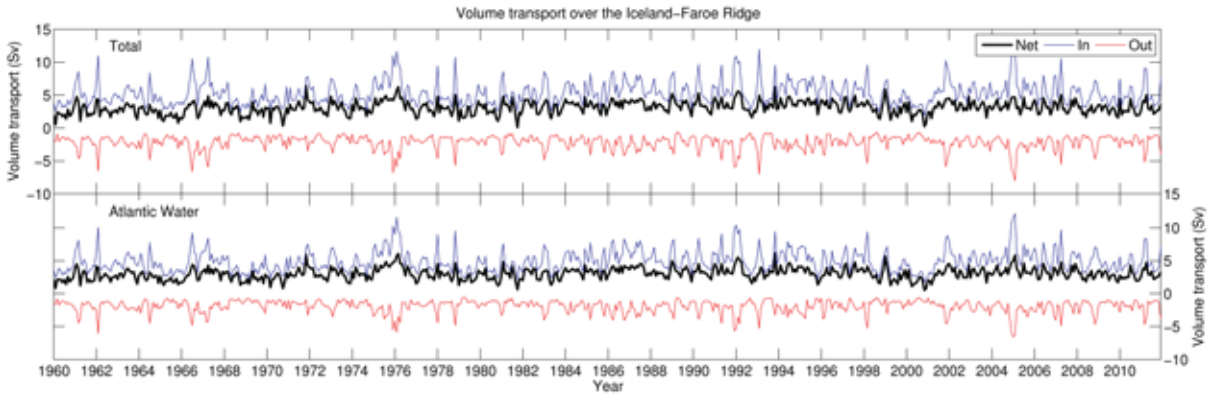

Figure 4.60. Volume transport over the Iceland-Faroe Ridge from all water masses (top) and Atlantic water masses only (bottom). See table 3.3 for water mass definitions.

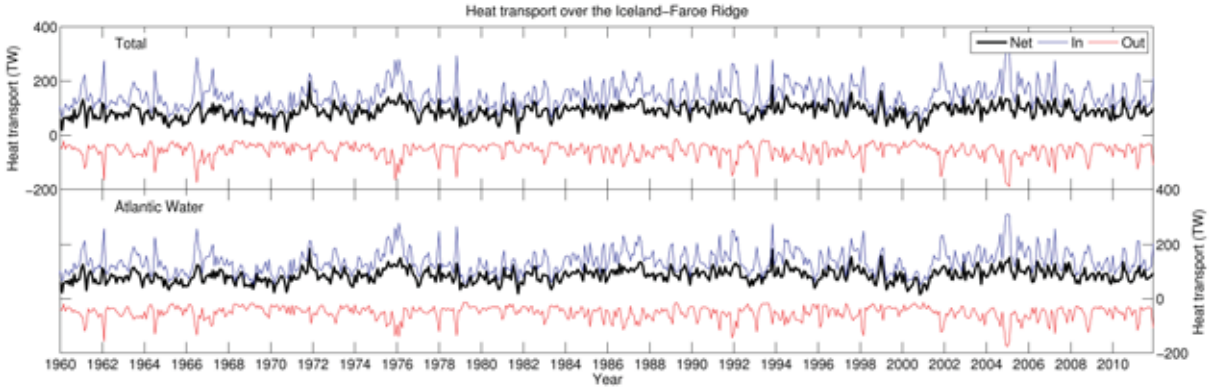

Figure 4.61. Heat transport over the Iceland-Faroe Ridge from all water masses (top) and Atlantic water masses only (bottom). See table 3.3 for water mass definitions.

The difference between total and net Atlantic inflow is also reflected in the heat transport, with 138 TW and 86 TW from total and net Atlantic inflow, respectively, for the whole simulation period. The total northward heat transport of 136 TW during the periods June-August 2008-2011 is somewhat lower than the observation-based estimate of 154 TW for the same period (Rossby and Flagg 2012).

Averaged over the whole simulation period (1960-2011), we find a seasonal amplitude of 0.4 Sv for the net Atlantic inflow (not shown), which is comparable to the 0.3 Sv reported by Østerhus et al. (2005). However, we find the modelled seasonal signal to be out of phase, with a maximum in February and minimum in October, as opposed to a maximum in October seen in observations.

4.3.3 Denmark Strait

The 600 m deep Denmark Strait between Greenland and Iceland is a major pathway for southward flowing dense water formed in the Arctic and Nordic Seas (Hansen and Østerhus 2000), while only little Atlantic Water is flowing northward through the strait (e.g. Østerhus et al. (2005)). Figure 4.62 shows the modelled volume transports through the Denmark Strait for the whole simulation period. Compared to observations, the model results indicate less northward flow of Atlantic Water than observed, and opposite for the southward flow of dense water ($\sigma\theta > 27.8$).

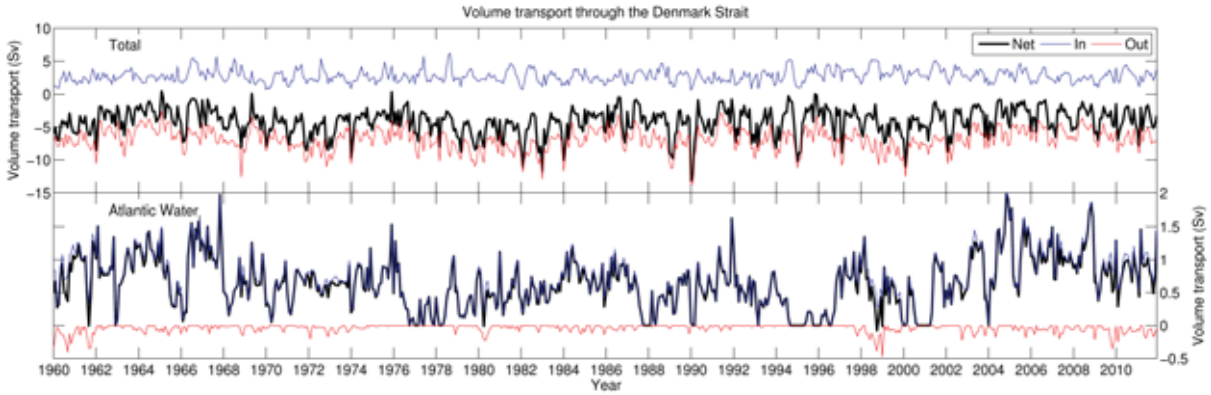

Figure 4.62. Volume transport through the Denmark Strait from all water masses (top) and Atlantic water masses only (bottom). See table 3.3 for water mass definitions.

According to Østerhus et al. (2005), the average temperature and salinity of the Atlantic Water inflow through the Denmark Strait is 6 ^{o}C and ~35.0, respectively. Here, we define Atlantic Water by $T > 5$ ^{o}C and $S > 34.9$ (Table 3.3), which is already close to the typical observed water mass characteristics. Moreover, the modelled Atlantic Water tends to be slightly less saline than observed; e.g. in the Barents Sea Opening we find that the model is biased 0.1 low in salinity. However, it should also be noted that Østerhus et al. (2005) based their estimates on a section north of Iceland, i.e. downstream of our model section representing the Denmark Strait, and as a consequence, we cannot rule out the possibility of a slight dilution of the Atlantic Water en route. These issues possibly influence the estimated Atlantic volume transport through the Denmark Strait in the model. This is seen by the rather frequent events of zero volume flux in the model results, indicating that no water masses are characterized as Atlantic Water.

Jónsson and Valdimarsson (2005) found an average Atlantic inflow of 0.75 Sv, using observations from 1994-2000, while an extended time series updated to 2010 yields an average of 0.88 Sv (Jónsson and Valdimarsson 2012). In the model, we find a net inflow of 0.36 Sv and 0.68 Sv, respectively, during the same periods. However, from Figure 4.62 we see that these periods include extended time spans of no Atlantic Water in the model, especially during 1995. Using the whole simulation period (1960-2011) and the period 2004-2011 yields a modelled net Atlantic inflow of 0.7 Sv and 1.0 Sv, respectively. This is comparable to the observations-based estimates by e.g. Østerhus et al. (2005). In the same period, the total modelled northward flow through the Denmark Strait is found to be 2.7 Sv, compared to 3.2 Sv for the period 1994-2000. Hence, it is an increase of the Atlantic fraction of the inflow rather than an increase of the inflow itself that accounts for the increase in modelled Atlantic inflow after 2003. This demonstrates the sensitivity to rigid water mass definitions when operating in water masses with core characteristics close to the definition bounds.

Using the whole simulation period, we find a seasonal amplitude of 0.1 Sv, with a maximum in December and minimum in March. Comparably, Jónsson and Valdimarsson (2012) report a seasonal amplitude of 0.3 Sv, mainly due to seasonal changes in the Atlantic water fraction, with a maximum in August and minimum in March.

Figure 4.63 shows the modelled southward transport of dense overflow water, defined by $\sigma\theta > 27.8$. On average, the modelled overflow is somewhat (~20%) larger than the observation-based estimates presented in Jochumsen et al (2012). Using the whole simulation period yields an average overflow of 4.3 Sv, while the maximum modelled monthly overflow is close to 10 Sv (February, 1990). The model results indicate a strong seasonal cycle (not shown) with an amplitude of ~0.7 Sv and a maximum in fall/winter and minimum in late spring. Based on ADCP-measurements, Jochumsen et al (2012) found no pronounced seasonal signal, with amplitudes below 0.2 Sv, although there were some signs of stronger flow in fall/winter and slightly weaker in spring/summer.

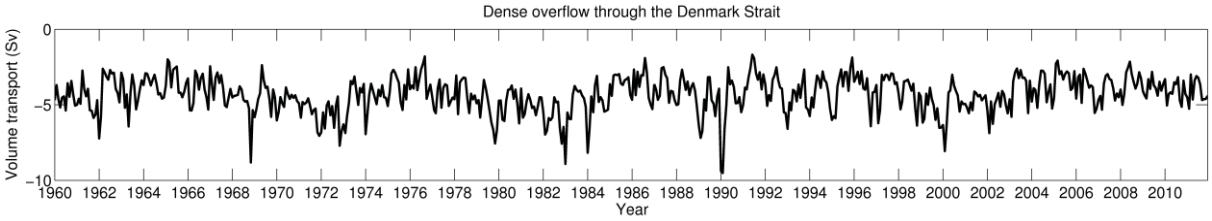

Figure 4.63. Dense water overflow through the Denmark Strait.

The heat transport through the Denmark Strait is shown in Figure 4.64, and a comparison with observations is summarized in Table 4.7. Due to the apparent sensitivity to water mass definitions, the heat carried by the Atlantic inflow is highly variable, with modelled estimates varying from about half to about equal to observed values, depending on the period selected. Using the whole simulation period, yields an average heat transport of 17 TW, which is ~25% lower than observation-based estimates, although based on a different period. The modelled monthly averages show a maximum net Atlantic volume transport of 2 Sv and a corresponding maximum heat transport of 55 TW (November, 2004). This is consistent with observations indicating a maximum volume transport of ~1.6 Sv and a corresponding heat transport of ~50 TW in late 2004 (Jónsson and Valdimarsson 2012). However, using a 13-month running average, we obtain a maximum yearly average net Atlantic volume transport of about 1.2 Sv and a corresponding heat transport of just above 30 TW in late 2004/early 2005. This is well above a year later than a similarly estimated maximum yearly average based on observations, indicating close to 1.5 Sv in volume and about 40 TW of heat in 2003 (Jónsson and Valdimarsson 2012). However, observed values are still comparable to the modelled values in 2005. Hence, the model results give realistic values of both the volume and heat transport through the Denmarsk Strait, although the estimates are sensitive to choices of water mass definitions.

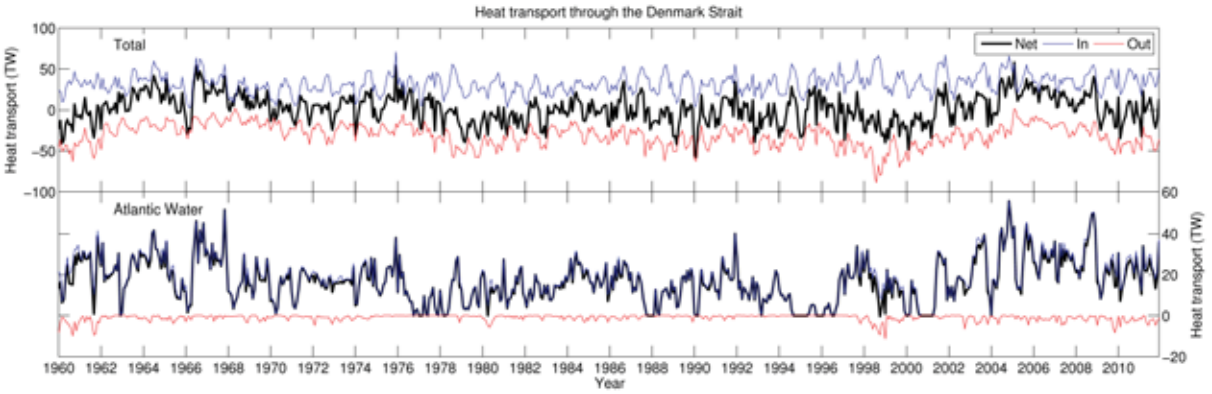

Figure 4.64. Heat transport through the Denmark Strait from all water masses (top) and Atlantic water masses only (bottom). See table 3.3 for water mass definitions.

Table 4.7. Volume (top) and heat (bottom) transports estimates from the model hindcast (left) and observations (right) for similar periods through the Denmark Strait. Values are in Sverdrups (volume) and terawatts (heat).

Water mass	Period	Mod. Vol.	Obs. Vol.	Reference
Atlantic water	1999-2001	0.4	0.8	Østerhus et al. (2005)
Atlantic water	1994-2010	0.7	0.9	Jónsson and Valdimarsson (2012)
Overflow	1996-2011	4.1	3.4	Jochumsen et al. (2012)
Water mass	Period	Mod. Heat	Obs. Heat	Reference
Atlantic water	1999-2001	10	22	Østerhus et al (2005)
Atlantic water	1994-2010	18	24	Jónsson and Valdimarsson (2012)

4.3.4 Short Summary: Atlantic-Nordic Seas Exchanges

Summarizing the modelled inflow to the Nordic Seas, we obtain a net Atlantic volume and heat transport of 5.7 Sv and 182 TW, respectively, averaged over the whole simulation period. This is substantially lower than the observations-based estimate of 8.5 Sv and 313 TW obtained by Østerhus et al. (2005). Using all water masses in the Faroe-Shetland Channel and the Iceland-Faroe Ridge, we get a net northward flow of 1.7 Sv and 150 TW and a total northward flow of 9.9 Sv and 291 TW. These estimates are in close agreement with the net northward estimates of 3.6 Sv and 176 TW and total northward estimates of 10.1 Sv and 287 TW obtained by Rossby and Flagg (2012) based on repeated ADCP measurements and hydrography.

4.3.5 Svinøy Section

Similar to Orvik et al. (2001), we define Atlantic Water in the Svinøy section by temperature (T >5 ^{o}C) and salinity (S >34.9). Note that we have compensated for the negative bias in model salinity (e.g. Figure 4.20) by reducing the salinity criterion by 0.1 units. Figure 4.65 shows the modelled volume transports through the Svinøy section using all water masses (top) and Atlantic Water only (bottom). In addition, we have divided the Atlantic Water into a western and an eastern branch, by using the 1000 m isobath to distinguish between the two (Figure 4.66). The corresponding heat transports are shown in Figure 4.68 and 4.69, respectively.

Based on direct current measurements, Orvik et al. (2001) estimated an annual mean volume transport in the eastern branch of 4.2 Sv and a standard deviation of 1.5 Sv in the period April 1997 to April 1998. Elaborating on this, Orvik and Skagseth (2005) estimated the transport anomalies for the period 1995 to 2005 to be in the range -0.46 Sv and 0.63 Sv which resulted in an estimated volume transport of 3.7 to 4.8 Sv. Correspondingly, we find an average modelled Atlantic volume transport of 4.3 Sv in total and a net transport of 3.8 Sv with a standard deviation of 2.6 Sv for the baseline period April 1997 to April 1998 (13 months). Also, we find a maximum monthly mean transport of 8.2 Sv and a minimum of 0.4 Sv during the same period, which is comparable to the 8.0 Sv and 2.0 Sv, respectively, reported by Orvik et al. (2001). Looking at the extended period 1995-2005, we get a net modelled Atlantic volume transport of 4.0 Sv and a standard deviation of 2.3 Sv, while using the whole simulation period (1960-2011) yields an average net Atlantic volume transport of 4.1 Sv. Both of these estimates are within the range reported by Orvik and Skagseth (2005).

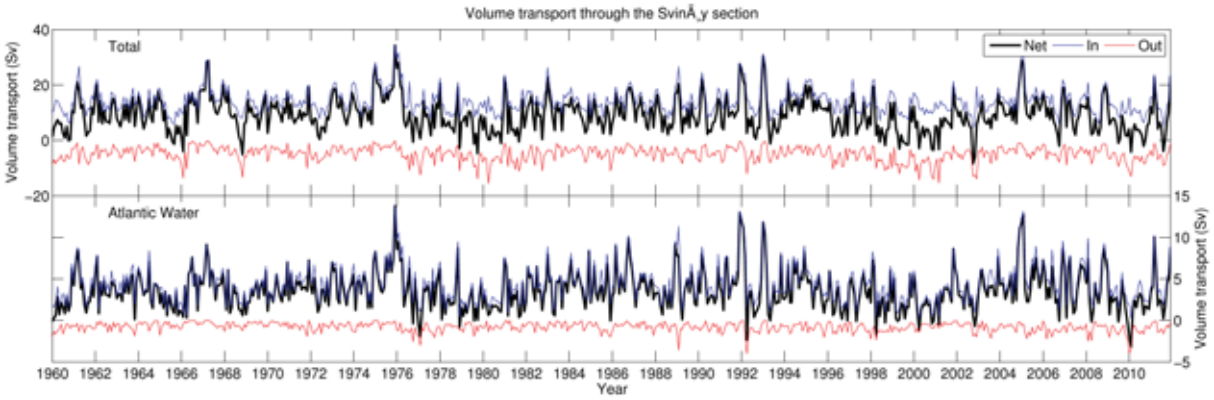

Figure 4.65. Volume transport through the Svinøy section from all water masses (top) and Atlantic water masses only (bottom). See table 3.3 for water mass definitions.

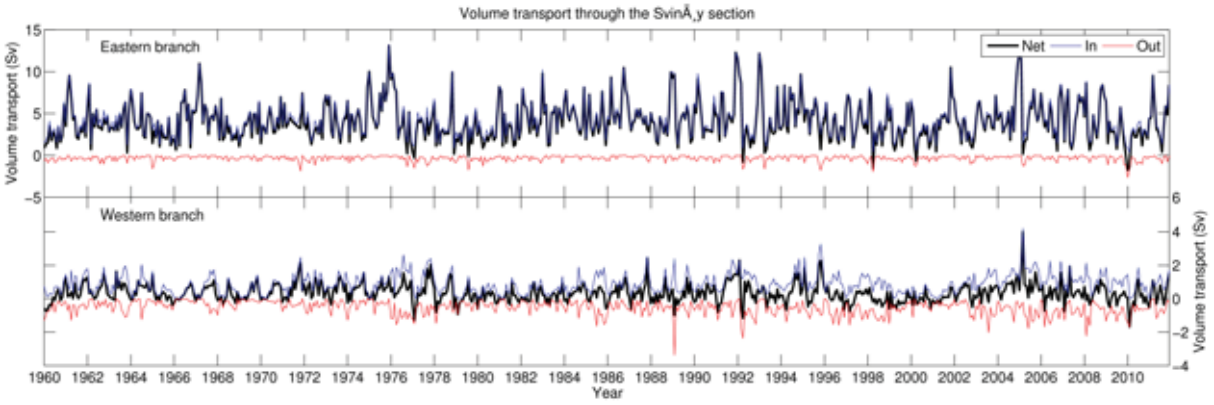

Figure 4.66 Volume transport of Atlantic Water through the Svinøy section east (top) and west (bottom) of the 1000 m isobath. See table 3.3 for water mass definitions.

Other estimates of the volume transport in the eastern branch of the Norwegian Atlantic Current include the work by Mork and Skagseth (2010), who combined altimetry and hydrography to obtain an estimate of 3.4±0.3 Sv for the period 1992-2009, while Hunegnaw et al. (2009) found a volume transport of 3.9 Sv based on gravimetry, altimetry and hydrography for the period 1993 to 1996. Their section covers a similar part of the Svinøy section as our eastern branch defined by the 1000 m isobath. By extending the section somewhat further out on the slope, they obtained an estimate of 4.3 Sv.

Estimates of volume transports, although less reliable, also exist for the western branch. Orvik et al. (2001) calculated an average transport of 3.4 Sv with a standard deviation of 1 Sv based on geostrophy and a single current meter mooring for the period 1995-1998. Using data from an ADCP transect, a transport of 4 Sv was found (Orvik et al. 2001). The geostrophic approach also revealed a significant seasonal signal, with a minimum close to 2 Sv in July and a maxima of ~4.5 Sv in January and October. Using the similar period 1995-1998, we find that the total modelled volume transport in the western branch is 1.0 Sv, while the net transport is as low as 0.2 Sv, with the corresponding standard deviations being 0.6 Sv for both. Using the whole simulation period, we get 0.9 Sv and 0.3 Sv, respectively, for total and net volume transport in the western branch.

Mork and Skagseth (2010) argue that earlier hydrography-based estimates are probably overestimating the transports. One factor is the problem of choosing a reference level of no motion. The circulation below the Atlantic layer in the Norwegian Basin (e.g. Rossby et al. (2009), Voet et al. (2010)), indicates that the geostrophic velocities are overestimated if one assumes no motion at intermediate level. Based on altimetry and hydrography, Mork and Skagseth (2010) estimated a volume transport of 1.7±0.2 Sv in the western branch. However, there is still a large discrepancy between our model-based estimate and the observation-based estimates. During testing, we have experienced anomalously low temperatures and salinities in upper layers the Norwegian Sea, probably originating from inflow of cold, lowsalinity waters from the Iceland Sea. This has also been reported to be a problem in earlier simulations using ROMS (e.g. Lien et al. (2006)). Here, we apply a salinity restoration towards the sea surface salinity in the SODA-dataset to eliminate the problem of too low salinities within the Norwegian Sea. However, the temperatures may still be affected and therefore too low (see also section 4.1.4). This will influence our estimate of the volume transport in the western branch by giving a negative bias in model temperature, and as a consequence, reduce the amount of water being characterized as Atlantic Water.

Figure 4.67 shows estimated monthly averaged volume transport in the eastern branch as standardized anomalies, based on the approach proposed by Orvik and Skagseth (2003) using a single current meter. Here, we have identified the model grid point that yields the highest correlation with observations. The observation-based estimate is superimposed (red curve) and a correlation analysis yields a correlation coefficient of $R = 0.63$ ($p < 0.01$). Thus, in statistical terms, the model reproduces 40% of the observed variability. Using seasonally adjusted anomalies reduces the correlation coefficient to $R = 0.45$ ($p < 0.01$). Hence, the seasonal variation contributes positively to the correlation, which is also reflected in the correlation between modelled and observed seasonal variation ($R = 0.83$; $p < 0.01$), implying that 69% of the observed seasonal cycle is resembled in the model results.

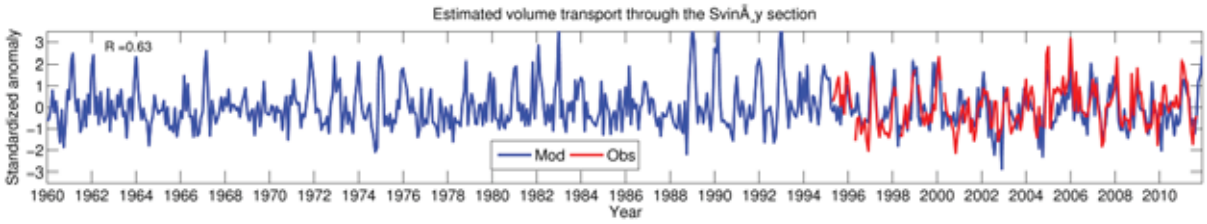

Figure 4.67. Estimated standardized volume transport anomaly in the eastern branch of the Norwegian Atlantic Current based on current speed in the grid point that yields the maximum correlation with single-point based observational estimate.

The modelled heat transport through the Svinøy section is shown in Figures 4.68 and 4.69 for the whole section and divided into separate branches, respectively. As for the volume transports, some heat transport estimates exist for the eastern branch, while only less reliable heat transport estimates are available for the western branch. However, due to the low volume transport in the modelled western branch, a direct comparison with observationbased estimates is of less interest. We therefore focus on the main, eastern branch. Orvik and Skagseth (2005) find an overall heat transport of 133 TW, with a range of 117 TW to 148 TW

during the period 1995-2005. Comparably, for the similar period we get 127 TW net and 137 TW total Atlantic heat transport with standard deviations of 71 TW and 66 TW, respectively, based on the model results. This indicates that there is only little resirculation within the eastern branch. Using the whole simulation period yields 128 TW and 137 TW for net and total, respectively, Atlantic heat transport.

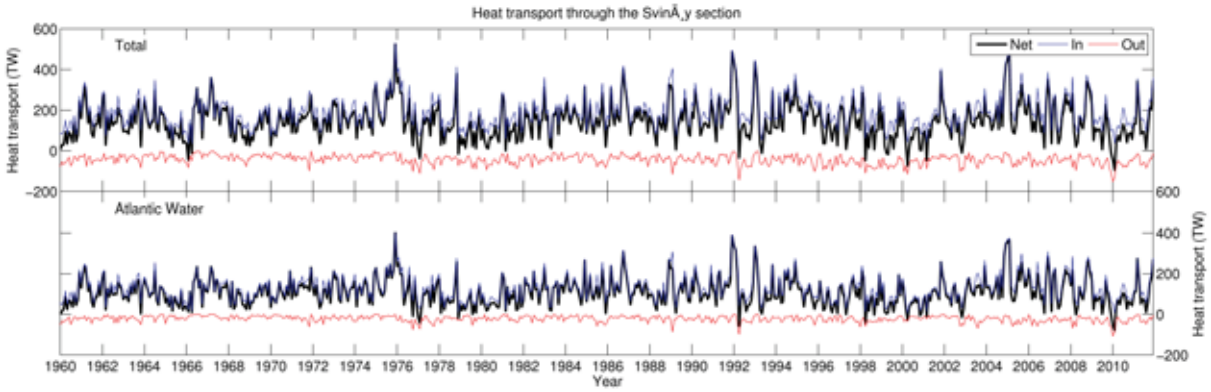

Figure 4.68. Heat transport through the Svinøy section from all water masses (top) and Atlantic water masses only (bottom). See table 3.3 for water mass definitions.

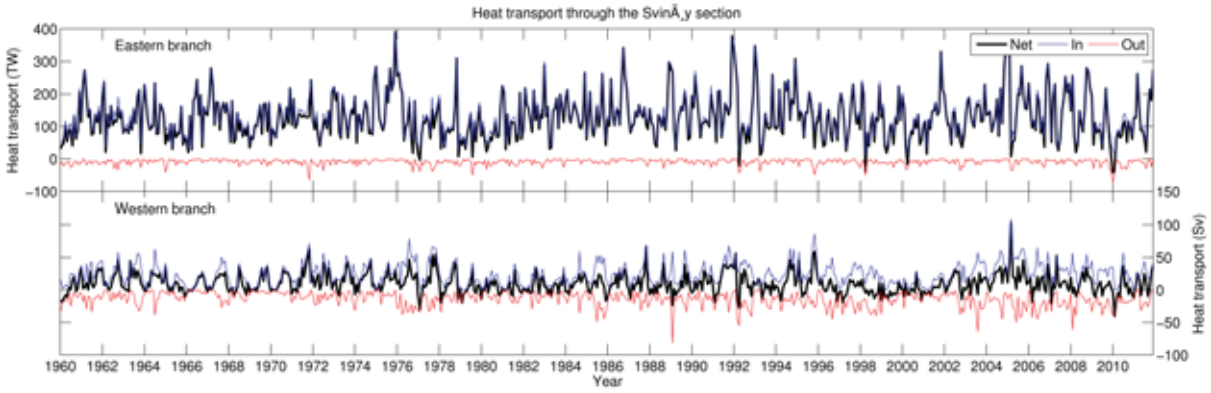

Figure 4.69. Heat transport of Atlantic Water through the Svinøy section east (top) and west (bottom) of the 1000 m isobath. See table 3.3 for water mass definitions.

4.3.6 Barents Sea Opening

The inflow of warm Atlantic Water through The Barents Sea Opening is important for the heat content and thus the climate as well as the sea-ice extent within the Barents Sea (Loeng 1991, Årthun et al. 2012, Smedsrud et al. 2013). Furthermore, the Atlantic Water transports nutrients and zooplankton from the Norwegian Sea into the Barents Sea (Sundby 2000).

The Barents Sea Opening has been continuously monitored by moored direct current meters since 1997 (Skagseth et al. 2008). However, a direct comparison between the model and observations is not straightforward. The current meter moorings covers the part of the section between 71^o 30'N and 73^o 30'N. Hence, the Norwegian Coastal Current and the flow on the slope south of Bjørnøya is not accounted for. Due to less reliable salinity measurements (especially in the early years of direct current measurements) and the fact that the moorings to a large degree covers the "Atlantic" part of the section, Atlantic Water is defined by $T > 3$ ^{o}C in the observations (Ingvaldsen et al. 2004). For the model results, we use both temperature

(T > 3 ^{o}C) and salinity (S > 34.9) but without geographical bounds (using the whole section; see Table 3.3) to define Atlantic Water. Usually, Atlantic Water is defined by S > 35.0. However, because the model is biased low in salinity (see Figure 4.20), we use the criterion S > 34.9. While the modelled temperature is also biased low (*rmse* = 0.81), we consider the temperature criterion to be weaker, i.e. the temperature bound is well within ”mixed waters”. Therefore we excpect the results to be less sensitive to the temperature criterion compared to the salinity criterion (note that the average modelled salinity is actually slightly lower than 35.0, while the average modelled temperature is 4.8 ^{o}C).

Based on moored current meter data for the period August 1997 to August 2001, Ingvaldsen et al. (2004) found a net average Atlantic volume transport of 1.5 Sv, with slightly higher transports in winter (1.7 Sv) and lower in summer (1.3 Sv). Extending the time series to 2006, Skagseth et al. (2008) estimated the net Atlantic inflow to be 1.8 Sv. Using similar periods, we get 1.5 Sv and 1.9 Sv, respectively, while using the whole simulation period yields 2.0 Sv.

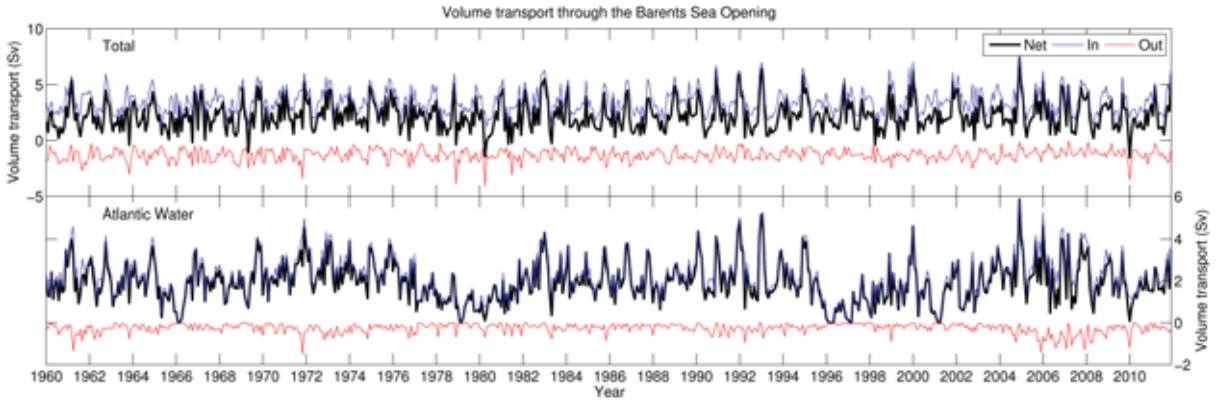

Figure 4.70. Volume transport through the Barents Sea Opening from all water masses (top) and Atlantic water masses only (bottom). See table 3.3 for water mass definitions.

We find a maximum net Atlantic volume transport in winter (2.6 Sv in December) and a minimum in spring (1.3 Sv in May), which is in agreement with observations, although the modelled winter maximum is higher than in observations (Ingvaldsen et al. 2004). Based on monthly mean estimates of net Atlantic volume transport for the period 1997-2011 (Randi Ingvaldsen; Pers. comm.), we find a winter maximum in January of 2.7 Sv and a minimum in spring (April) of 1.5 Sv. Overall, we get a correlation between modelled and observed seasonal cycle of R = 0.61 (p = 0.03). Using the same data reveals a correlation of R = 0.41 (p<0.01) between observed and modelled Atlantic volume transports. Removing the seasonal signal reduces the correlation slightly to R = 0.39 (p < 0.01). Thus, in statistical terms, only less than 20% of the observed variability is resembled in the model results. Looking at mean and standard deviation only, we get 1.9±1.0 Sv and 2.0±1.0 Sv from the model and observations, respectively, for the similar period (1997-2011). Hence, the modelled Atlantic inflow variability has a realistic amplitude, while the phase is to a less degree captured in the model.

For the heat transport (Figure 4.71), we find an estimated modelled transport of 42 TW, compared to 48 TW reported by Skagseth et al. (2008), for the period 1997-2006. For the whole simulation period we obtain 43 TW. The seasonality in the heat transport resembles that of the volume transport, with about twice the heat transport during the winter maximum (~55 TW) compared to the spring minimum (~ 25 TW).

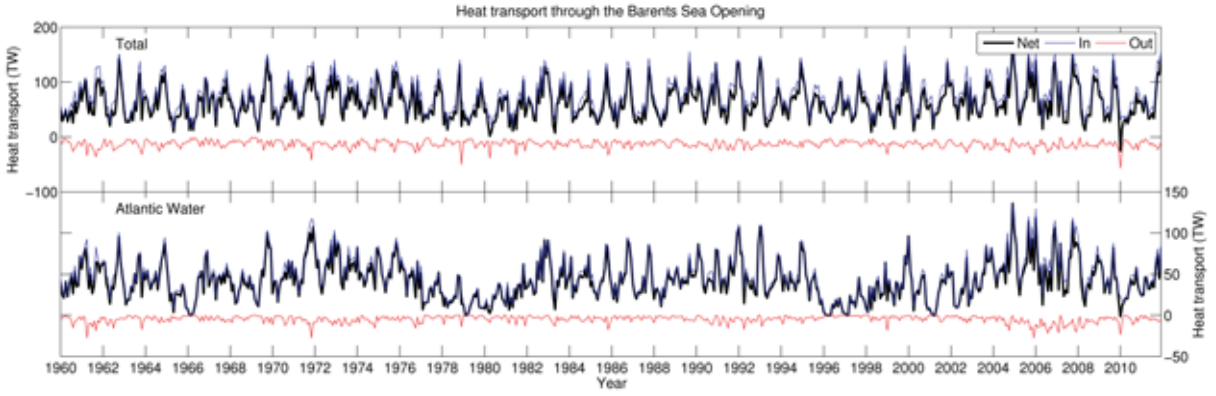

Figure 4.71. Heat transport through the Barents Sea Opening from all water masses (top) and Atlantic water masses only (bottom). See table 3.3 for water mass definitions.

Few reliable and consistent Norwegian Coastal Current volume transport estimates exist. Moreover, they only represent shorter periods and are therefore less suitable for estimating the long term variability. According to the model, the long term average volume transport in the Norwegian Coastal Current is 0.8 Sv, with a standard deviation of 0.5 Sv (Figure 4.72). There is a seasonal cycle (not shown) with lower transport in spring/summer (0.4 Sv in May) and higher transport in autumn and early winter (1.3 Sv in November). This is consistent with the seasonal cycle reported by Skagseth et al. (2011), except that they found slightly lower velocity in summer (July-August-September) compared to spring (April-May- June), while the model indicates lower transport in spring. The modelled average volume transport is close to the estimates reported by Blindheim (1989) and Björk et al. (2001), while it is low compared to the estimated average volume transport of 1.8 Sv reported by Skagseth et al. (2011). Blindheim (1989) used current meter measurements from a single month only, while Skagseth et al. (2011) based their estimates on measurements from the period July 2007 - July 2008. Using this latter period only, we find a modelled volume transport of 0.5 Sv.

A likely explanation for at least a part of the discrepancy between modelled and observed estimates is the salinification of the Norwegian Coastal Current due to the sea surface salinity relaxation scheme (see sections 4.1.4 and 4.1.5). This contributes to decrease the amount of water being classified as coastal water, and therefore reduces the total amount of volume and heat of the water masses classified as coastal water. However, an expected increase of the modelled Atlantic inflow due to this artificial transformation of coastal water into Atlantic Water does not seem to occur, as the amount of inflowing Atlantic Water is in close agreement with observations.

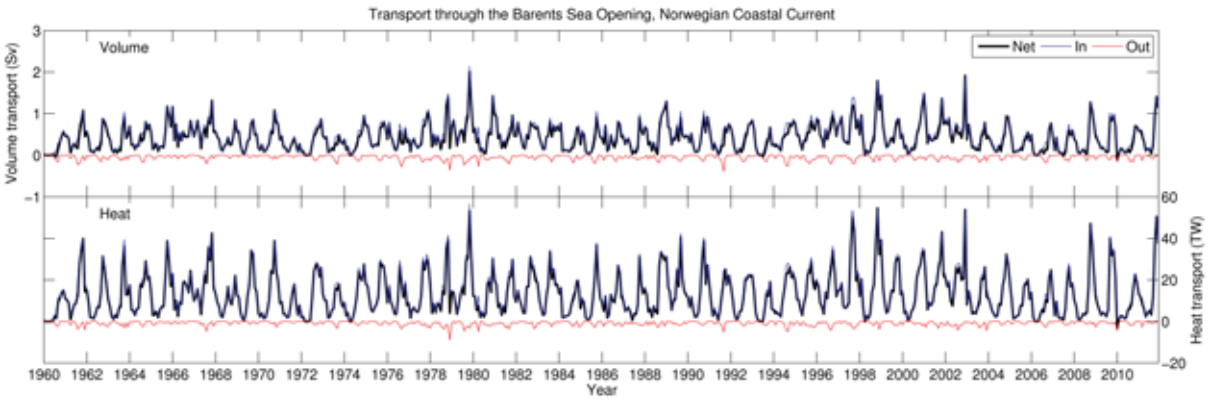

Figure 4.72. Volume (top) and heat (bottom) transport by the Norwegian Coastal Current through the Barents Sea Opening. See table 3.3 for water mass definitions.

The lower than observed modelled volume transport estimate also affects the modelled heat transport. For the whole simulation period and the period July 2007 to July 2008, we find a net heat transport of 23 TW and 15 TW, respectively, which is lower than the 34 TW reported for the slope part only (Skagseth et al. 2011).

Combining the volume and heat transport estimates of the inflow of Atlantic and coastal water, we get a net inflow of 2.8 Sv and 65 TW through the Barents Sea Opening. Including all water masses in the section, we get 2.2 Sv and 63 TW, which is close to the 2.3 Sv and 70 TW indicated by Smedsrud et al. (2013).

4.3.7 Novaya Zemlya - Franz Josef Land

The major part of the flow through the Barents Sea toward the Arctic Ocean flows through the Barents Sea Exit (e.g. Schauer et al. (2002)). Only two time series of direct current observations exist (1991-92 and 2007-08), but only the former (1991-92) is yet available. The current measurements revealed a small fraction of Atlantic Water originating from the Fram Strait branch of the Atlantic flow towards the Arctic (Schauer et al. 2002), while the main part of the flow consisted of locally formed Cold Bottom Water (Gammelsrød et al. 2009).

Using the direct current measurements from October 1991 to September 1992, Gammelsrød et al. (2009) estimated a net eastward volume transport of 1.6±0.5 Sv, of which 1.0 Sv was classified as Cold Bottom Water ($T < 0$ ^{o}C; $S > 34.75$). There was a small fraction of Atlantic Water (0.2 Sv) being advected both in and out and thereby cancelling each other. However, because the current meter mooring array only covered a part of the section, Gammelsrød et al. (2009) used model results from two numerical ocean models to estimate the volume transport through the whole section to 2.0±0.6 Sv.

From the model results (Figure 4.73), we get an average net volume transport of 2.1 Sv for the whole section during the period October 1991 to September 1992. Dividing into different water masses, the major part of the flow consists of dense water (T <0 ^{o}C; $\sigma\theta > 27.9$), with a net modelled volume transport of 1.8 Sv (Figure 4.74). This is substantially larger than the observed values, although some of the discrepancy may be due to the lack of observations in

the northern part of the section, which is dominated by cold water masses (Lien and Trofimov 2013). However, Gammelsrød et al. (2009) found that the ROMS model was overestimating the flow of Cold Bottom Water. In addition, we get 0.2 Sv eastward flow of Atlantic Water (both total and net; see Table 3.3 for water mass definitions). Hence, the modelled Atlantic Water is advected from the Barents Sea and not the Fram Strait branch, as reported by Schauer et al. (2002). Using the whole model simulation period, we get a net volume transport of 1.8 Sv from all water masses, of which 0.1 Sv is classified as AtlanticWater. Looking at Figure 4.73, we see that the modelled volume transport of Atlantic Water has the form of events rather than a weak but steady flow, and periods of no traceable Atlantic Water flow following periods of so-called Great Salinity Anomalies, which is also usually associated with lower than normal temperatures (e.g. mid-1960s, late 1970s and late 1990s (Dickson et al. 1988, Belkin et al. 1998, Sundby and Drinkwater 2007)).

The modelled heat transport through the Barents Sea Exit is displayed in Figure 4.75. Note that positive direction for the flow is still eastward. However, negative values can either imply westward flow of water masses warmer than the reference temperature (T_{ref} = -0.1; Aagaard and Greisman (1975)), or eastward flow of water masses colder than the reference temperature. Similar to Gammelsrød et al. (2009), we get a negative heat transport eastward from the Barents Sea towards the Arctic Ocean. Our estimate of -5.2 TW for the period October 1991 to September 1992 is slightly larger in absolute value than that based on observations (-3.6 TW), but again the limited coverage by the current meter moorings probably bias the observations low, due to an underrepresentation of water masses colder than 0 ^{o}C. The small fraction of Atlantic Water accounts for a minor 0.2 TW positive heat transport towards the Arctic Ocean. Using the whole simulation period, we get -4.7 TW and 0.3 TW, respectively, for total net and net Atlantic heat transport.

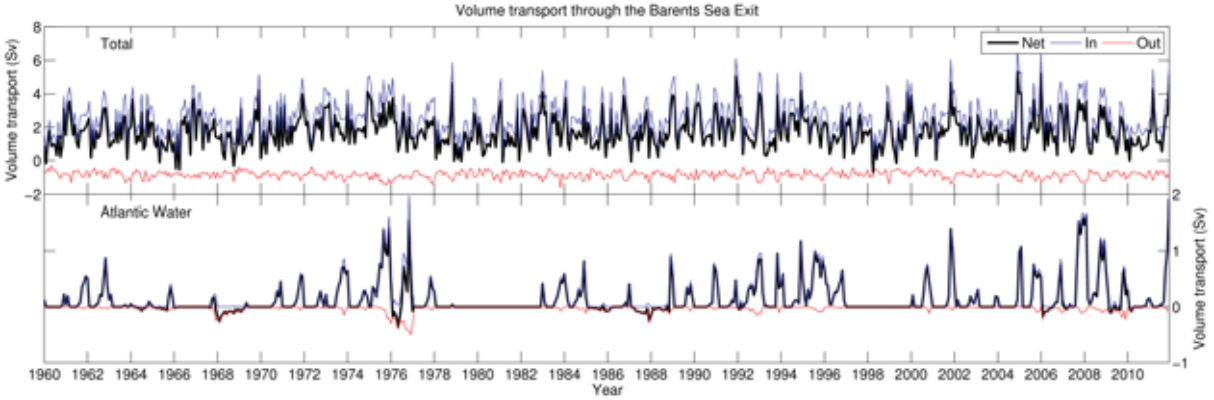

Figure 4.73. Volume transports through the Barents Sea Exit from all water masses (top) and Atlantic Water only (bottom), see table 3.3 for water mass definitions. Positive direction (in) towards east.

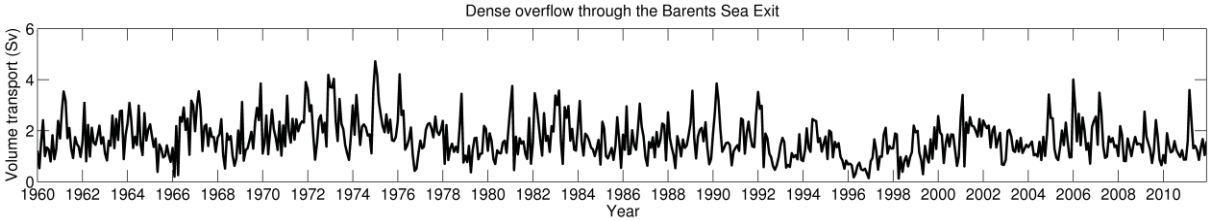

Figure 4.74. Eastward flow of dense bottom water (T <0 ^{o}C; $\sigma\theta$> 27.9) through the Barents Sea Exit.

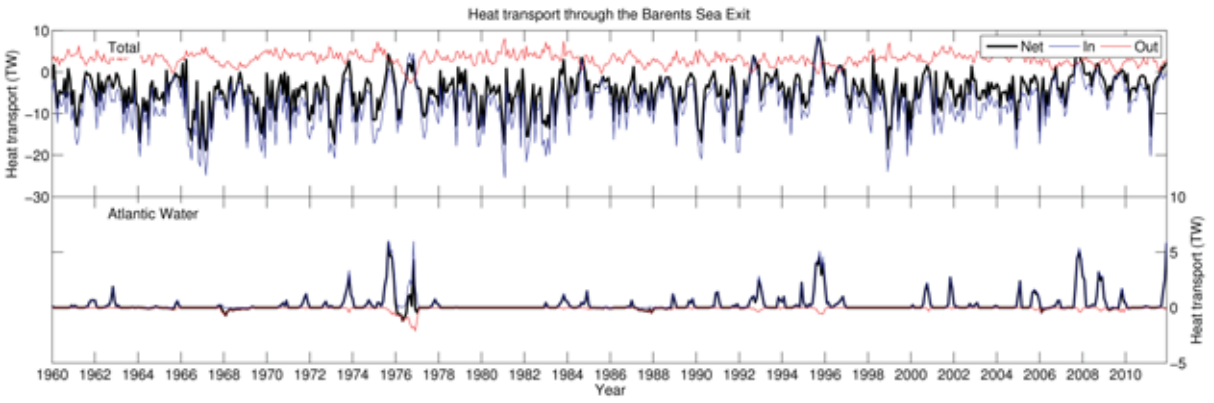

Figure 4.75. Heat transports through the Barents Sea Exit. See Table 3.3 for water mass definitions. Positive direction (in) towards east.

4.3.8 Fram Strait

The Fram Strait is the only deep passage between the Nordic Seas and the Arctic Ocean. However, complex topography together with a Rossby radius of ~10 km in a section of 500 km width makes accurate estimates of volume and heat transports through the section difficult (Beszczynska-Möller et al. 2011). Moreover, heavy ice conditions along the Greenland continental shelf further complicates the estimates of the southward-flowing East Greenland Current.

Considering the part of the section covered by the moorings, i.e. excluding most of the shallow Greenland shelf, Schauer et al. (2008) estimated northward and southward volume transports of 12 Sv and 14 Sv, respectively, yielding a net southward volume transport of 2±2.7 Sv for the period 1997-2006. For the similar period, we get modelled-based estimates of 9.3 Sv and 14.0 Sv northward and southward, respectively, yielding a net southward volume transport of 4.8 Sv - about twice the observation-based estimate. Dividing into separate years, Schauer et al. (2004) estimated the volume transports to be 13±2 Sv southward and 9±2 Sv northward, with a net transport of 4±2 Sv southward, for the period 1997-98. For 1998-99 the numbers were 12±1 Sv southward and 10±1 Sv northward, yielding a net southward transport of 2±2 Sv. Corresponding estimates based on the model are: 13.0 Sv southward and 9.8 Sv northward (3.2 Sv net southward) for 1997/98; 18.4 Sv southward and 8.6 Sv northward (9.8 Sv net southward) for 1998-99. Hence, although the modelled estimates are close to observation-based estimates, the modelled northward flow tends to be on the low side, while the southward flow tends to be on the high side, yielding a slightly exaggerated net southward flow.

The net southward transport through the Fram Strait more or less balances the net inflow to the Arctic Ocean through the Barents Sea (e.g. Rudels et al. (1994)). However, from the model results, we find a long-term net inflow to the Barents Sea of 2.2 Sv, compared to a longterm net southward flow through the Fram Strait of 4.3 Sv, leaving 2.1 Sv to be explained by other sources. The only two other passages between the Arctic Ocean and the world oceans is the Bering Strait and through the Canadian archipelago. The net volume transport through the Bering Strait has been found to vary between 0.7 Sv in 2001 to 1.1 Sv in 2011 towards the Arctic (Woodgate et al. 2012). The Canadian archipelago more than balances the Bering Strait

inflow, and volume transport estimates yield a net southward transport in the range 2.3 Sv (Curry et al. 2011) to 2.6 Sv (Cuny et al. 2005). Hence, there is a deficiency of ~3.5 Sv in the Arctic Ocean volume budget if one uses observed values through the openings not represented in the model. However, in this model set up, the northern boundary crosses the Arctic Ocean just north of Greenland, and as a consequence, the volume of the Arctic Ocean need not be conserved due to the non-conservative boundary conditions. We speculate that the imposed southward flow at the boundary north of Greenland is exaggerated due to lack of sea ice in SODA, causing exaggerated ocean drag from wind forcing. The northward transport through the Fram Strait is, however, determined by ROMS which only to a very low degree ”feels” the drag from the possibly exaggerated downstream velocities in the interior Arctic Ocean. The reason for this is the different nudging time scales applied in the open boundary conditions for the incoming (0.25 days) and outgoing (25 days) water masses.

A part of the northward flow through the Fram Strait consists of relatively warm Atlantic Water. According to Beszczynska-Möller et al. (2011), the volume transport carried by the warm West Spitsbergen Current amounts to 1.8±0.1 Sv, of which 1.3±0.1 Sv included Atlantic Water warmer than 2 ^{o}C, for the period 1997-2010. Similarly, we find a net northward volume transport of water warmer than 2 ^{o}C (see Table 3.3) of 1.3 Sv both for the period 1997-2010 and the whole simulation period. The total modelled northward Atlantic volume transport in the two periods are 1.4 Sv and 1.6 Sv, respectively. However, from Figure 4.76, we clearly see that the modelled northward Atlantic volume transport, at least partly due to the strict temperature criterion, ocurrs periodically. Qualitatively, it appears that the Atlantic Water transport ceases following the passing of great salinity anomalies. Although there is a close agreement between modelled and observed Atlantic Water volume transport, the extent of the 2 ^{o}C-isotherm is substantially less in the model compared to in the observations (not shown).

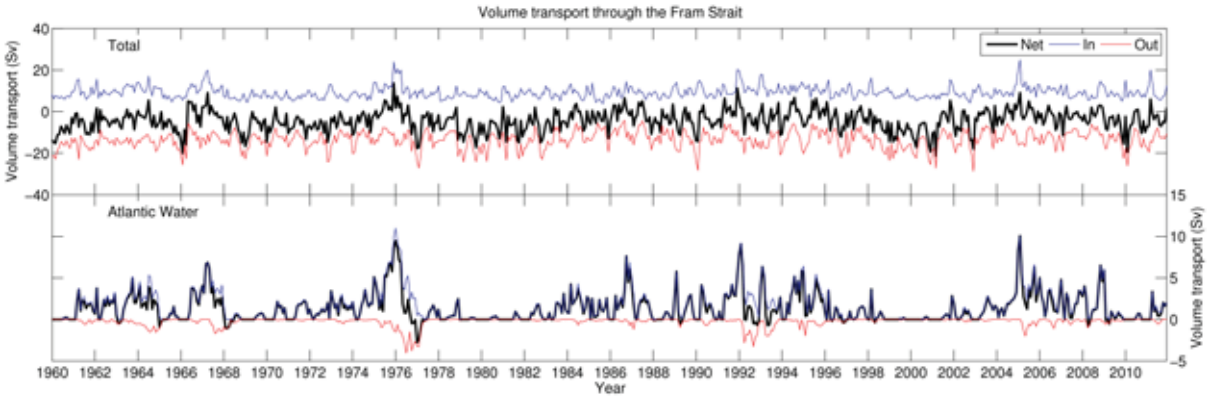

Figure 4.76. Volume transports through the Fram Strait from all water masses (top) and Atlantic Water only (bottom), see table 3.3 for water mass definitions. Positive direction (in) towards north.

To estimate the heat transport through the Fram Strait based on observations is a challenging task. See Schauer et al. (2008) and Schauer and Beszczynska-Möller (2009) for a throrough discussion on this matter. Here, we apply the traditional procedure by estimating the heat transport relative to a fixed reference temperature. Although less reliable, we apply this

method for a closer comparison with historic heat transports referenced in the literature. However, it makes a comparison with recent estimates of Fram Strait heat transports difficult. We therefore compare the modelled heat transports with the estimates made by Schauer et al. (2004), for the period mentioned above (1997-98 and 1998-99). We then get a total northward heat transport of 25 TW in total and 10 TW for Atlantic Water only, compared to 32±6 TW and 35±3 TW, respectively, based on observations. For the year 1998-99, Schauer et al. (2004) found the heat transport to increase to 55±4 TW in total and 57±3 TW for the Atlantic Water. In the model, however, a drop in the temperature causes a substantial decrease in northward heat transport to 6 TW for all water masses, while virtually no Atlantic Water (T > 2 ^{o}C) is detected (Figure 4.77). However, it should be noted that Schauer et al. (2004) used T > 1 ^{o}C to define Atlantic Water. Hence, the observed heat transport is expected to be somewhat larger than our model estimate. Furthermore, as the temperature in the Fram Strait is close to the reference temperature (T = -0.1 ^{o}C), the estimated heat transport is sensitive to the bias in modelled temperature. E.g. a change in average temperature of 0.8 ^{o}C (similar to the bias in the Barents Sea Opening) from 0.5 ^{o}C to 1.3 ^{o}C yields a change in heat transport from 22 TW to 56 TW, given a volume transport of 9 Sv. Nevertheless, as opposed to the observations, the model indicates a decrease in heat transport from 1997-98 to 1998-99.

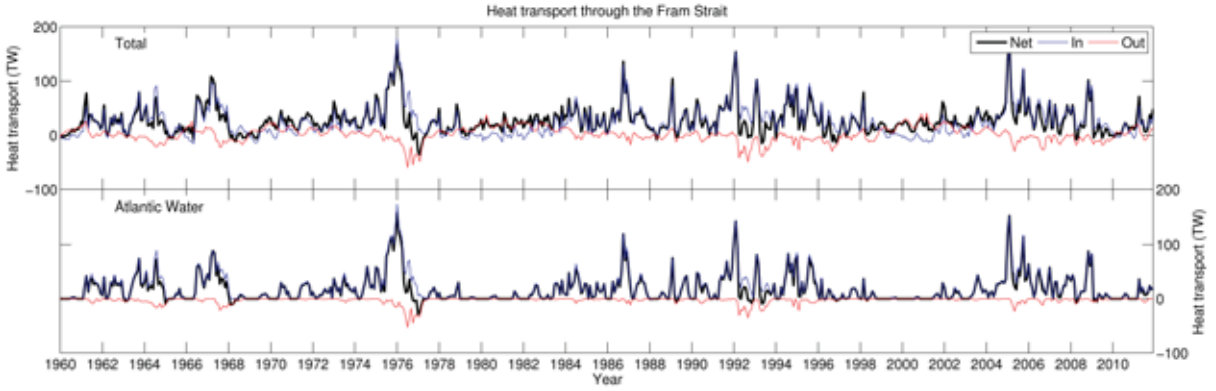

Figure 4.77. Heat transports through the Fram Strait from all water masses (top) and Atlantic Water only (bottom), see table 3.3 for water mass definitions. Positive direction (in) towards north.

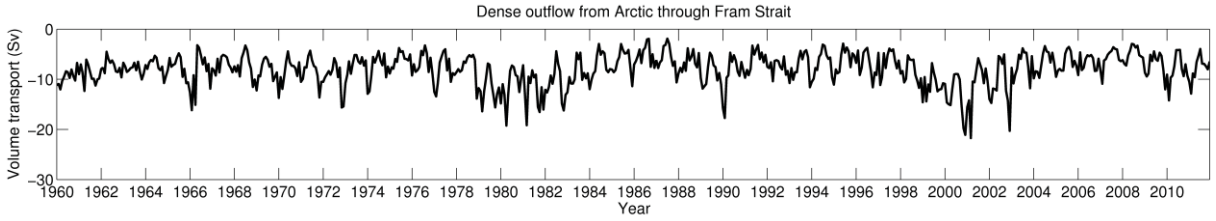

Figure 4.78. Total southward volume transport of dense water only (T <0 ^{o}C; $\sigma\theta$> 27.9) through the Fram Strait. (NB! Positive direction towards north)

To summarize, both the northward and southward volume transports through the Fram Strait are realistic, i.e. within or close to the uncertainty range of the observation-based estimates. However, the net southward flow is somewhat larger than the observed net transport, although still more or less within uncertainty ranges due to the large absolute uncertainty arising from the complex dynamics and large geographical extent of the Fram Strait. The modelled heat

transports are lower than observed, which can be at least partly explained by the negative bias in the modelled Atlantic Water temperature downstream, e.g. as seen in the Barents Sea Opening (see Figure 4.20).

The Fram Strait is close to the northern boundary of the model domain, which increase the model results dependency of the boundary conditions in this area. In addition, the boundary conditions and forcing applied in this area are not consistent. Due to the lack of sea ice in SODA, we have applied sea-ice boundary conditions based on sea-ice data from another numerical ocean model (MICOM), which in turn is not entirely consistent with the atmospheric forcing used here. Hence, we expect that this area is vulnerable to continuous adjustment processes due to inconsistencies in the applied volume, heat and freshwater fluxes. Unfortunately, a general lack of data from this area prevents a necessary extensive model evaluation here. As a consequence, the model results from downstream of the Arctic Ocean, i.e. along the eastern coast of Greenland and probably to some extent the Greenland Sea, should be used with care.

4.3.9 East Greenland Current

The East Greenland Current flows southward along the eastern coast of Greenland, carrying sea ice and low-salinity water from the Arctic Ocean through the Fram Strait to the North Atlantic through the Denmark Strait. Several estimates for volume transport in the East Greenland Current exist from various geographical locations, from Fram Strait in the north to the Cape Farewell at the southern tip of Greenland. Here, we use a section at 75^{o}N (Table 3.1), corresponding to the mooring section presented by Woodgate et al. (1999), which extends from the coast of Greenland to the central part of the Greenland Sea. Thus, our transport estimates include the gyre circulation within the Greenland Sea, and as a result, our estimates are substantially higher than those based on observations in the Fram Strait and the Denmark Strait (e.g. Foldvik et al. (1988)).

Based on one year of measurements (summer 1994 to summer 1995), Woodgate et al. (1999) estimated a net southward volume transport of 25±4 Sv, using 8^{o}W as the eastern boundary. The seasonal variation was large, with a maximum in winter (41±7 Sv) and a minimum in summer (14±7 Sv). Corresponding volume transport estimates based on the model results (Figure 4.79) are 18.3 Sv net southward, with a maximum of 34.7 Sv in january and a minimum of 8.2 Sv in October.

Due to the depth of the Greenland Sea, approximately 3000 m at the eastern end of the section, the transport estimates are sensitive to the extent of the section as well as even small velocities within the deep ocean. By moving the eastern extent one degree westward, to 9^{o}W, Woodgate et al. (1999) found a reduction in the net southward transport of 4 Sv (21±3 Sv), with seasonal ranges of 37±5 Sv to 11±5 Sv maximum and minimum, respectively. In the model, however, the velocities in the central part of the Greenland Sea are very small, and as consequence, moving the eastern boundary from 8^{o}W to 9^{o}W only reduces the estimated volume transport by approximately 1 Sv. In addition, the model section extends further onto the Greenland shelf than does the mooring section. According to the model, there is a

northward flow at the shelf (not shown). However, the velocities are relatively small and the shelf is rather shallow, and therefore the effect of including this coastal current is small (<1 Sv).

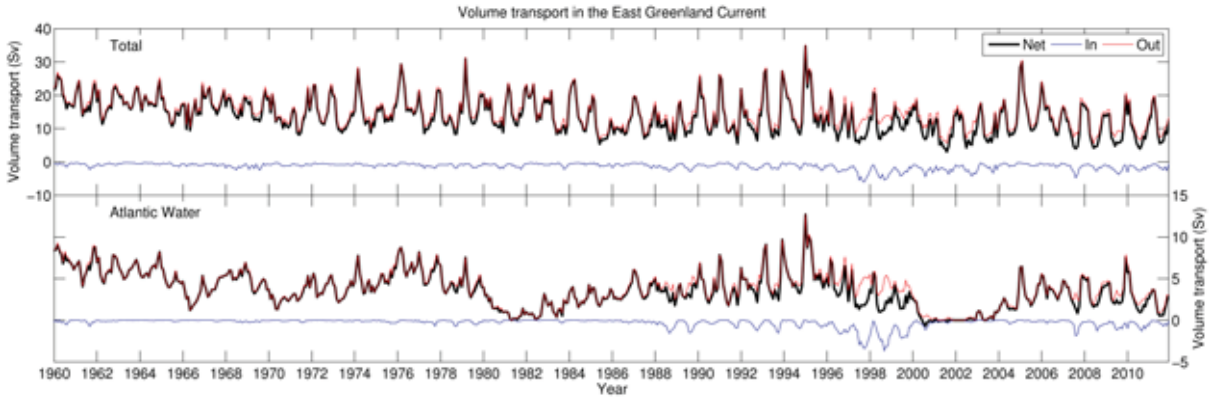

Figure 4.79: Volume transports in the East Greenland Current from all water masses (top) and Atlantic Water only (bottom), see table 3.3 for water mass definitions. Positive direction (in) towards south.

In addition to cold and relatively fresh water from the Arctic, the East Greenland Current carries a substantial amount of modified Atlantic Water, mostly recirculated in the Fram Strait, but also remnants of Atlantic Water that has circulated around the Polar Basin in the Arctic Ocean. For comparison with Woodgate et al. (1999), we have chosen to define Atlantic Water (or more correctly modified Atlantic Water) by the same temperature criterion (T > 0^{o}C). For the annual average 1994-95, Woodgate et al. (1999) estimated a net southward transport of Atlantic Water of 8±1 Sv, with no clear seasonal signal. Correspondingly, the model yields 7.1 Sv and a large seasonal amplitude, with winter values being up to three times higher than summer values. Using direct current observations from several years, Woodgate et al. (1999) found an approximated net southward transport of 20±2 Sv for the period 1988-1995. From the model, we find a net southward transport of 14.2 Sv during the same period. For the whole simulation period, we find net southward volume transports of 13.9 Sv and 3.6 Sv, respectively, for all water masses and Atlantic Water only. For comparison, based on hydrography and acoustic doppler current profiler data in a section spanning 13^o W to ~8^o 30'W, Cisewski et al. (2003) estimated the East Greenland Current volume transport to 12.2 Sv and 11.9 Sv during the summers of 1997 and 1998, respectively. Similarly, accounting only for water masses warmer than T > 0 ^{o}C, they found volume transports of 7.6 Sv and 7.4 Sv, respectively. These estimates are comparable to the modelled long term estimates.

However, due to the seasonality in the model in both total and Atlantic volume transport, the modelled transports are lower during summer. Hence, the modelled volume transports are somewhat lower than the observation-based estimates, mostly due to lower transports in the gyre circulation of the Greenland Sea.

According to the model, the 1990s was a period of high transports in the East Greenland Current, with an all time high transport of 34.7 Sv in january 1995. According to Woodgate et al. (1999), January 1995 was the month with the highest estimated wind-driven Sverdrup transport in the period 1991-95. This coincides with the high North Atlantic Oscillation index

(Hurrell 1995) during the first half of the 1990s, culminating with a very high index during winter 1994-95 (see e.g. http://www.cru.uea.ac.uk/ timo/datapages/naoi.htm).

Looking at heat transports (Figure 4.80), the modelled long term heat transport by all water masses combined yields -8.3 TW, i.e. southward transport of water masses with average temperature lower than T_{ref} = -0.1 ^{o}C. For Atlantic Water only, the figure is 9.2 TW. Hence, heat transport by water masses colder than T = 0 ^{o}C is -17.5 TW. As for the volume transports, Cisewski et al. (2003) estimated the Atlantic Water heat transport to be about twice the modelled long term average (24.5 TW in 1997 and 15.1 TW in 1998). However, looking at summer season only for the two separate years yields even lower modelled estimates, due to both too low modelled volume transports as well as too low temperatures. A CTD-section in July 1994 indicates a maximum temperature of just above 2 ^{o}C in the core of the Atlantic Water (Woodgate et al. 1999), while the modelled maximum temperature is just above 1 ^{o}C.

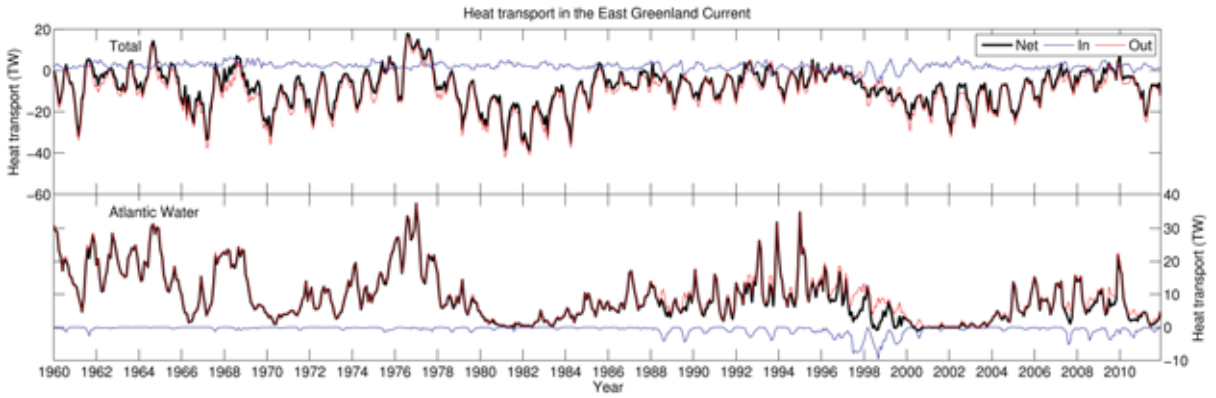

Figure 4.80. Heat transports in the East Greenland Current from all water masses (top) and Atlantic Water only (bottom), see table 3.3 for water mass definitions. Positive direction (in) towards south.

4.3.10 Short Summary: Transports

Generally, the northward transport within Norwegian Atlantic slope Current, as well as the southward transport in the East Greenland Current is well represented in the model. The exchange between the northern North Atlantic and the Nordic Seas is in agreement with observations-based estimates, although issues such as recirculation make a straight forward comparison difficult. Further out on the continental slope, the flow of Atlantic Water is grossly underestimated in the model. However, few reliable observation-based estimates inhibits firm conclusions. Estimating the transports through the Fram Strait is a challenging task. Adding to this, the proximity of the model domain boundary adds sources of errors to the Fram Strait estimates, which is reflected by the variable agreement between model-based and observation-based transport estimates.

4.4 Sea ice

The analysis of sea ice results is restricted to the period 2000-01-01 – 2001-12-31. Evaluation of the results are performed both for the entire model domain, as well as for the Barents Sea subdomain. These domains are shown in Figure 4.81, along with the shelf break region.

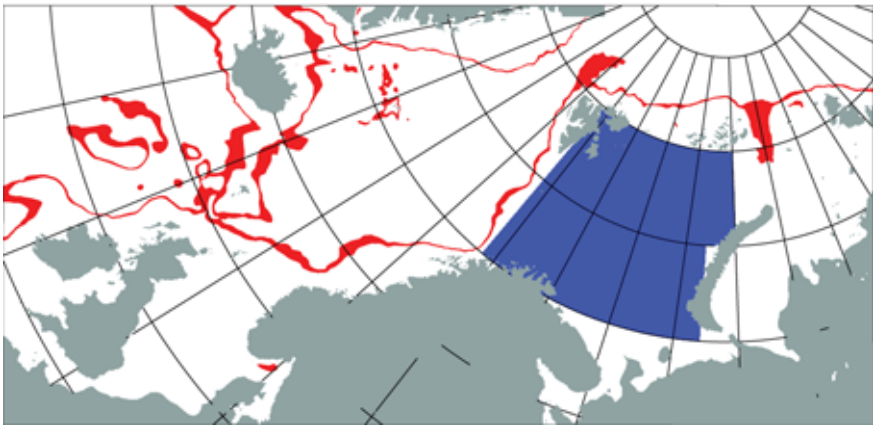

Figure 4.81. Barents Sea subdomain. Shown here is the Barents Sea subdomain (blue), inside the full model domain. The shelf break, displayed in red, is here defined as the region where the bottom depth is between 500 m and 1000 m.

4.4.1 Integral properties

We set the sea-ice concentration at the ice edge to be $SIC_{edge} = 0.15$, and define the gridded ice edge as the grid cells where the sea-ice concentration > SIC_{edge} in the OSI-SAF product, and which has at least one neighbor node where the sea-ice concentration < SIC_{edge}. We find that the *rms* position offsets between the observed ice edge and the models' ice edges are 180 km and 55 km in the full domain and in the Barents Sea subdomain, respectively (Table 4.8). The contrasting quality suggests that the sea ice cover is better restrained in a semi-enclosed shelf-sea such as the Barents Sea than in the Arctic Ocean.

Next, we examine the sea-ice area and the sea-ice extent. The sea-ice area is defined as the integral of the sea-ice concentration (multiplied by the area), while the sea-ice extent is the area where the sea-ice concentration exceeds the limit that defines the ice edge.

The two-year averages of these quantities are given in Table 4.8. We find that the model results reproduce observations very well, and particularly in the Barents Sea. There is a very slight underestimation of sea ice in the Barents Sea, though.

Product	**Domain**	
	Barents Sea	**Full**
	Ice edge offset (*rms*)	
Model	55	180
	Sea-ice area	
OSI-SAF	66	2320
Model	62	2200
	Sea-ice extent	
OSI-SAF	85	2680
Model	82	2760

Table 4.8: Root mean square offset in ice edge position (in km), mean sea-ice area and mean sea-ice extent (both in units of 1000 km^2) during 2000-2001. OSI-SAF is the product derived from satellite data, as described in Section 3.3. The Barents Sea subdomain is depicted in Figure 4.81.

4.4.2 Distribution

Table 4.9 reveals that the model does a fair job of reproducing the distribution of the various categories of sea-ice concentration. We note, though, that the model somewhat overestimates

the region with the highest sea-ice concentration category. This category, which corresponds to a near-continuous ice cover (80-100%), on average occupies 45% of the Barents Sea in the model results, but only 35% in the observations, after the region where no or very little ice has been removed.

Furthermore, with the exception of very low and very high sea-ice concentration values (i.e., categories 0-10% and 80-100%, respectively), the geographical distribution of the model results for the various sea-ice concentration categories is inaccurate.

Table 4.9: Confusion matrix for five categories of daily sea-ice concentrations during 2000-2001. Values are fraction of relative occurence, after discarding grids where concentrations in both model and observations were <10%. This corresponds to removal of 64% and 69% of all wet grid cells in the full domain and in the Barents Sea subdomain, respectively.

		Observations					Model
		0-10%	10-30%	30-50%	50-80%	80-100%	sum
Full domain	0-10%		0,050	0,030	0,024	0,012	0,12
	10-30%	0,025	0,010	0,007	0,009	0,008	0,06
	30-50%	1,018	0,008	0,006	0,012	0,011	0,06
	50-80%	0,024	0,011	0,011	0,031	0,049	0,13
	80-100%	0,043	0,020	0,016	0,070	0,492	0,64
Observations	Sum	0,11	0,10	0,07	0,15	0,57	1
Barents Sea	0-10%		0,135	0,026	0,014	0,001	0,18
	10-30%	0,035	0,030	0,016	0,014	0,003	0,10
	30-50%	0,021	0,024	0,018	0,024	0,007	0,09
	50-80%	0,027	0,025	0,030	0,065	0,032	0,18
	80-100%	0,016	0,014	0,022	0,099	0,302	0,46
Observations	Sum	0,10	0,23	0,11	0,22	0,35	1

4.4.3 Temporal variability

Finally, we examine the temporal evolution of sea ice in the observations and in the model results. We restrict this presentation to results for the domain of the Barents Sea region as shown by Figure 4.81. The results are displayed in Figure 4.82.

Unsurprisingly, the model describes the seasonal cycle very well. A more detailed examination bolsters our conclusion that the model reproduces the temporal variability of sea-ice area and extent: The shorter duration and higher values for sea ice maximum in 2001 compared to 2000 is reproduced well by the model. The episodic maximum in November 2001 observations does not have a counterpart in the observations from November 2000. This contrasting evolution during the freezing season is reproduced well by the model. Similar high-frequency variability in observations and models is also seen during other episodes. The only significant shortcoming is that the sea-ice area and extent during the melting season of 2001 is somewhat over-estimated by the model.

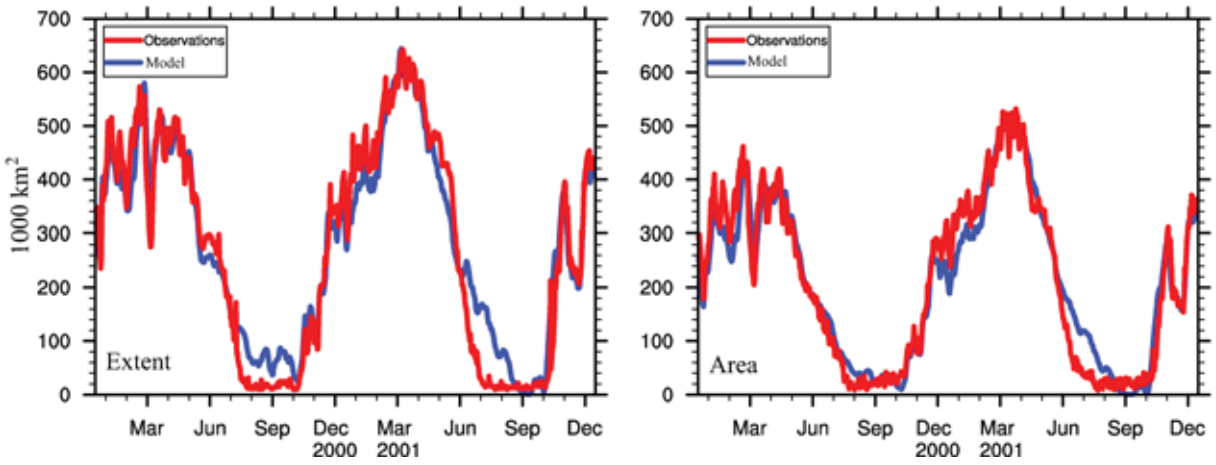

Figure 4.82. Time series of sea-ice extent (left) and sea-ice area (right), in the Barents Sea subdomain. Areas are given in units of 1000 km^2.

5 Concluding remarks

Overall, we find that the water masses that are directly influenced by Atlantic Water are realistically represented in the model, both in terms of hydrography and dynamics. Inshore of the Norwegian Atlantic slope Current, the salt relaxation scheme applied negates variability in salinity within the Norwegian Coastal Current. This is most pronounced in the upper part of the water column. The temperature variability in the near-shore waters is, however, resembled in the model. Offshore of the Norwegian Atlantic slope Current, within the two Norwegian Sea basins, the heat/freshwater content is unrealistically low/high, probably due to too little slope-basin eddy-flux exchange between the slope current and the interior basins.

In shelf areas (e.g. the Barents Sea and the North Sea), we find that the model resembles the variability within the Atlantic-influenced water masses, while the salinity relaxation inhibits variability in the salinity within water masses dominated by coastal water.

The simulation evaluated herein is planned for continuous updates. However, based on the results from the presented evaluation, we find evidence of specific areas that need improvement. Most importantly, the surface salinity relaxation needs refinement in order to allow for the relatively low salinity within the Norwegian Coastal Current. Improved input of freshwater run-off from land will also likely contribute to a more realistic representation of the Norwegian Coastal Current. Furthermore, mechanisms for slope-basin exchanges will need attention for more realistic simulation of the interior basins. This calls for future improvement of the existing model set-up and ultimately a re-run of the whole simulation period when adequate solutions to the above issues are found. Such improvement, along with parallell updates of the existing simulation, is to be undertaken in the near future.

Bibliography

Aagaard, K. and P. Greisman, Toward new mass and heat budgets for the Arctic Ocean, J.Geophys. Res., 80, 3821-3827 (1975)

Andersen, S., L.-A. Breivik, S. Eastwood et al.: OSI SAF Sea Ice Product Manual. EUMETSAT OSI SAF Ocean and Sea Ice Satellite Application Facility, Ed.: S. Eastwood. SAF/OSI/met.no/TEC/MA/125 38 pp. (2012)

Belkin, I.M., S. Levitus, J. Antonov and S.-A. Malmberg, "Great Salinity Anomalies" in the North Atlantic, Prog. Oceanogr., 41, 1-68 (1998)

Belkin, I.M., Propagation of the "Great Salinity Anomaly" of the 1990s around the northern North Atlantic, Geophys. Res. Lett., 31, L08306 (2004)

Berx, B., B. Hansen, S. Østerhus, K.M. Larsen, T. Sherwin and K. Jochumsen, Combining in situ measurements and altimetry to estimate volume, heat and salt transport variability through the Faroe-Shetland Channel, Ocean Sci., 9, 639-654 (2013)

Beszczynska-Möller, A., R.A. Woodgate, C. Lee, H. Melling and M. Kärcher, A Synthesis of Exchanges Through the Main Oceanic Gateways to the Arctic Ocean, Oceanography, 24(3), 82-99 (2011)

Björk, G., B.G. Gustafsson and A. Stigebrandt, Upper layer circulation in the Nordic Seas as inferred from the spatial distribution of heat and freshwater content and potential energy, Polar Res., 20, 161-168 (2001)

Blindheim, J. and H. Loeng, On the variability of Atlantic influence in the Norwegian and Barents Seas, Fiskeridirektoratets Skrevne Serie for Havundersøkelser, 17, 161-189 (1981)

Blindheim, J., Cascading of Barents Sea bottom water into the Norwegian Sea, Rapp. P.-V. Reun. Cons. Int. Explor. Mer, 188, 49-58 (1989)

Bochkov, Y.A., Water temperature in the 0-200 m layer in the Kola-Meridian section in the Barents Sea, 1900-1981, Sb. Nauchn. Trud. PINRO, 46, 113-122 (in russian) (1982)

Budgell, W.P., Numerical simulation of ice-ocean variability in the Barents Sea region: Towards dynamical downscaling, Ocean Dynam., 55, 370-387 (2005)

Carton, J.A., G. Cherupin, X. Cao and B.S. Giese, A simple ocean data assimilation analysis of the global upper ocean 1950-95. Part I: methodology, J. Phys. Oceanogr., 30, 294-309 (2000)

Carton, J.A. and B.S. Giese, A Reanalysis of Ocean Climate Using Simple Ocean Data Assimilation (SODA), Mon. Wea. Rev., 136, 2999-3017 (2008)

Chapman, D.C., Numerical treatment of cross-shelf open boundaries in a barotropic coastal ocean model, J. Phys. Oceanogr., 15, 1060-1075 (1985)

Cisewski, B., G. Budéus and G. Krause, Absolute transport estimates of total and individual water masses in the northern Greenland Sea derived from hydrographic and acoustic Doppler current profiler measurements, J. Geophys. Res., 108, 3298 (2003)

Cuny, J., P. Rhines and R. Kwok, Davis Strait volume, freshwater and heat fluxes, Deep-Sea Res. Part I, 52(3), 519-542 (2005)

Curry, B., C.M. Lee and B. Petrie, Volume, freshwater, and heat fluxes through Davis Strait, 2004-05, J. Phys. Oceanogr., 41, 429-436 (2011)

Dickson, R.R., J. Meincke, S.-A. Malmberg and A.J. Lee, The Great Salinity Anomaly in the northern North-Atlantic 1968-1982, Prog. Oceanogr., 20, 103-151 (1988)

Eastwood, S., K.R. Larsen, T. Lavergne, E. Nielsen and R. Tonboe, OSI SAF Global Sea Ice Concentration Reprocessing, User Manual. EUMETSAT OSI SAF Ocean and Sea Ice Satellite Application Facility, SAF/OSI/met.no/TEC/MA/138 38 pp. (2011)

Flather, R.A., A tidal model of the northwest European continental shelf, Mem. Soc. Roy. Sci. Liege, 6(10), 141-164 (1976)

Foldvik, A., K. Aagaard and T. Tørresen, On the velocity field of the East Greenland Current, Deep-Sea Res., 35, 1335-1354 (1988)

Gammelsrød, T., Ø. Leikvin, V. Lien, W.P. Budgell, H. Loeng and W. Maslowski, Mass and heat transports in the NE Barents Sea: Observations and models, J. Mar. Sys., 75, 56-69 (2009)

Hansen, B. and S. Østerhus, North Atlantic - Nordic Seas Exchanges, Prog. Oceanogr., 45, 109-208 (2000)

Hansen, B., S. Østerhus, H. Hátun, R. Kristiansen and K.M.H. Larsen, The Iceland-Faroe inflow of Atlantic water to the Nordic Seas, Prog. Oceanogr., 59, 443-474 (2003)

Hansen, B. and S. Østerhus, Faroe Bank Channel overflow 1995-2005, Prog. Oceanogr., 75, 817-856 (2007)

Hunegnaw, A., F. Siegismund, R. Hipkin and K.A. Mork, Absolute flow field estimation for the Nordic seas from combined gravimetric, altimetric, and in situ data, J. Geophys. Res., 114, C02022 (2009)

Hurrell, J.W., Decadal trends in the North-Atlantic Oscillation - regional temperatures and precipitation, Science, 269, 676-679 (1995)

Ingvaldsen, R., L. Asplin and H. Loeng, The seasonal cycle in the Atlantic transport to the Barents Sea during the years 1997-2001, Cont. Shelf Res., 24, 1015-1032 (2004)

Ingvaldsen, R.B., Width of the North Cape Current and the location of the Polar Front in the western Barents Sea, Geophys. Res. Lett., 32, L16603 (2005)

Isachsen, P.E., I. Koszalka and J.H. LaCasce, Observed and modeled surface eddy heat fluxes in the eastern Nordic Seas, J. Geophys. Res., 117, C08020 (2012)

Jakobsen, T. and V.K. Ozhigin, The Barents Sea - Ecosystem, Resources, Management, Trondheim: Tapir Academic Press (2011)

Jochumsen, K., D. Quadfasel, H. Valdimarsson and S. Jónsson, Variability of the Denmark Strait overflow: Moored time series from 1996-2011, J. Geophys. Res., 117, C12003 (2012)

Johannessen, O.M. and L.A. Foster, Note on topographically controlled oceanic Polar Front on Barents Sea, J. Geophys. Res., 83, 4567-4571 (1978)

Jónsson, S. and H. Valdimarsson, The flow of Atlantic water to the North Icelandic Shelf and its relation to the drift of cod larvae, ICES J. Mar. Sci., 62, 1350-1359 (2005)

Jónsson, S. and H. Valdimarsson, Water mass transport variability to the North Icelandic shelf, 1994-2010, ICES J. Mar. Sci., 69, 809-815 (2012)

Kangas, T.V., E. Svendsen and Ø. Strand, Normalverdier for saltholdighet og temperatur i Havforskningsinstituttets faste snitt, Fisken og Havet, 6/2006, 53pp, in norwegian (2006)

Lien, V.S., P. Budgell, B. Ådlandsvik and E. Svendsen, Validating results from the model ROMS (Regional Ocean Modelling System), with respect to volume transports and heat fluxes in the Nordic Seas, Fisken og Havet, 2/2006, 58pp (2006)

Lien, V.S. and B. Ådlandsvik, Bottom water formation as a primer for spring-blooms on Spitsbergenbanken?, J. Mar. Sys., in press (2011)

Lien, V.S., F.B. Vikebø and Ø. Skagseth, One mechanism contributing to covariability between Atlantic inflow branches to the Arctic, Nat. Commun., 4, 1488 (2013)

Lien V.S. and A.G. Trofimov, Formation of Barents Sea Branch Water in the north-eastern Barents Sea, Polar Res., 32, 18905 (2013)

Loeng, H., Features of the physical oceanographic conditions of the Barents Sea, Polar Res., 10(1), 1-18 (1991)

Marchesiello, P., J.C. McWilliams and A.F. Shchepetkin, Open boundary conditions for longterm integration of regional oceanic models, Ocean Model., 3, 1-20 (2001)

Marchesiello, P., L. Debreu and X. Couvelard, Spurious diapycnal mixing in terrain-following coordinate models: The problem and a solution, Ocean Model., 26, 156-169 (2009)

Mork, K.A. and Ø. Skagseth, A quantitative description of the Norwegian Atlantic Current by combining altimetry and hydrography, Ocean Sci., 6, 901-911 (2010)

Orvik, K.A., Ø. Skagseth and M. Mork, Atlantic inflow to the Nordic Seas: current structure and volume fluxes from moored current meters, VM-ADCP and SeaSoar-CTD observations, Deep-Sea Res., 48, 937-957 (2001)

Orvik, K.A. and P. Niiler, Major pathways of Atlantic water in the northern North Atlantic and Nordic Seas toward Arctic, Geophys. Res. Lett., 29 (19), 1896 (2002)

Orvik, K.A. and Ø. Skagseth, Monitoring the Norwegian Atlantic slope current using a single moored current meter, Cont. Shelf. Res., 23, 159-176 (2003)

Orvik, K.A. and Ø. Skagseth, Heat flux variations in the eastern Norwegian Atalntic Current toward the Arctic from moored instruments, 1995-2005, Geophys. Res. Lett., 32, L14610 (2005)

Palmer, M.D. and K. Haines, Estimating oceanic heat content change using isotherms, J. Climate, 22, 4953-4969 (2009)

Reistad, M., Ø. Breivik, H. Haakenstad, O.J. Aarnes, B.R. Furevik and J.R. Bidlot, A highresolution hindcast of wind and waves for the North Sea, the Norwegian Sea, and the Barents Sea, J. Geophys. Res.-Oceans, 116, C05019 (2011)

Rossby, T., M.D Prater and H. Søiland, Pathways of inflow and dispersion of warm waters in the Nordic seas, J. Geophys. Res., 114, C04011 (2009)

Rossby, T. and C.N. Flagg, Direct measurements of volume flux in the Faroe-Shetland Channel and over the Iceland-Faroe Ridge, Geophys. Res. Lett., 39, L07602 (2012)

Rudels, B., E.P. Jones, L.G. Anderson and G. Kattner, On the intermediate depth waters of the Arctic Ocean. The Polar Oceans and their role in shaping the global environment, Geophysical Monograph Series, 85, 33-46 (1994)

Sandø, A.B., J.E.Ø. Nilsen, T. Eldevik and M. Bentsen, Mechanisms for variable North Atlantic-Nordic seas exchanges, J. Geophys. Res., 117, C12006 (2012)

Schauer, U., H. Loeng, B. Rudels, V.K. Ozhigin and W. Dieck, Atlantic Water flow through the Barents and Kara Seas, Deep-Sea Res. I, 49, 2281-2298 (2002)

Schauer, U., E. Fahrbach, S. Østerhus and G. Rohardt, Arctic warming through the Fram Strait: Oceanic heat transport from 3 years of measurements, J. Geophys. Res., 109, C06026 (2004)

Schauer, U., A. Beszczynska-Möller, W.Walczowski, E. Fahrbach, J. Piechura and E. Hansen, Variation of Measured Heat Flow Through the Fram Strait Between 1997 and 2006, in: Arctic Subarctic ocean fluxes: Defining the Role of the Northern Seas in Climate, Dickson, R., J. Meincke and P. Rhines (Eds.), pp. 65-86, Springer, New York (2008)

Schauer, U. and A. Beszczynska-Mõller, Problems with estimation and interpretation of oceanic heat transport: Conceptual remarks for the case of Fram Strait in the Arctic Ocean, Ocean Sci., 5, 487-494 (2009)

Shchepetkin, A.F. and J.C. McWilliams, The Regional Ocean Modeling System (ROMS): A split-sxplicit, free-surface, topography-following coordinates ocean model, Ocean Model., 9, 347-404 (2005)

Skagseth, Ø., T. Furevik, R. Ingvaldsen, H. Loeng, K.A. Mork, K.A. Orvik and V. Ozhigin, Volume and Heat Transports to the Arctic Ocean via the Norwegian and Barents Seas, in: Arctic Subarctic ocean fluxes: Defining the Role of the Northern Seas in Climate, Dickson,R., J. Meincke and P. Rhines (Eds.), pp. 45-64, Springer, New York (2008) Skagseth, Ø. and K.A. Mork, Heat content in the Norwegian Sea, 1995-2010, ICES J. Mar. Sci., 69(5), 826-832 (2012)

Skagseth, Ø., K.F. Drinkwater and E. Terrile, Wind- and buoyancy-induced transport of the Norwegian Coastal Current in the Barents Sea, J. Geophys. Res., 116, C08007 (2011)

Smedsrud, L.H., I.N. Esau, R.B. Ingvaldsen, T. Eldevik, P.M. Haugan, C. Li, V.S. Lien, A. Olsen, A. Omar, O.H. Otterå, B. Risebrobakken, A.B. Sandø, V. Semenov and S.A. Sorokina, The role of the Barents Sea in the Arctic climate system, Rev. Geophys., 51, 2012RG000418 (2013)

Sundby, S., Recruitment of Atlantic cod stocks in relation to temperature and advection of copepod populations, SARSIA, 85, 277-298 (2000)

Sundby, S. and K. Drinkwater, On the mechanisms behind salinity anomaly signals of the northern North Atlantic, Prog. Oceanogr., 73, 190-202 (2007)

Sætre, R., J. Aure and D.S. Danielsen, Long-term hydrographic variability patterns off the Norwegian coast and in the Skagerrak, ICES Mar. Sci. Symp., 219, 150-159 (2003)

Tereshchenko, V.V., Seasonal and year-to-year variation in temperature and salinity of the main currents along the Kola section in the Barents Sea, Murmansk: PINRO Publ., 71pp (in russian) (1997)

Troupin, C., A. Barth, D. Sirjacobs, M. Ouberdous, J.M. Brankart, P. Brasseur, M. Rixen, A. Alvera-Azcarate, M. Belounis, A. Capet, F. Lenartz, M.E. Toussaint and J.-M- Beckers, Generation of analysis and

consistent error fields using the Data Interpolating Variational Analysis (DIVA), Ocean Model., 52-53, 90-101 (2012)

Turrell, W.R., B. Hansen, S. Hughes and S. Østerhus, Hydrographic variability during the decade of the 1990's in the northeastern Atlantic and southern Norwegian Sea, ICES Mar. Sci. Symp. (2003)

Umlauf, L. and H. Burchard, A generic length-scale equation for geophysical turbulence models, J. Mar. Res., 61, 235-265 (2003)

Umlauf, L., H. Burchard and K. Hutter, Extending the k − ω turbulence model towards oceanic applications, Ocean Model., 5, 195-218 (2003)

Uppala, S. and Co-authors, The ERA-40 re-analysis, Q.J.R. Meteorol. Soc., 131, 2961-3012 (2005)

Uppala, S., D. Dee, S. Kobayashi, P. Berrisford and A. Simmons, Towards a climate data assimilation system: status update of ERA-Interim, ECMWF Newsletter, 115, 7pp (2008)

Voet, G., D. Quadfasel, K.A. Mork and H. Søiland, The mid-depth circulation of the Nordic Seas derived from profiling float observations, Tellus, 62, 516-529 (2010)

Warner, J.C., C.R. Sherwood, H.G. Arango and R.P. Signell, Performance of four turbulence closure models implemented using a generic length scale method, Ocean Model., 8, 81-113 (2005)

Warner, J.C., W.R. Geyer and J.A. Lerczak, Numerical modeling of an estuary: A comprehensive skill assessment, J. Geophys. Res.-Oceans, 110, C05001 (2005)

Woodgate, R.A., E. Fahrbach and G. Rohardt, Structure and transports of the East Greenland Current at 75^{o}N from moored current meters, J. Geophys. Res., 104, 18059-18072 (1999)

Woodgate, R.A., T.J. Weingartner and R. Lindsay, Observed increases in Bering Strait oceanic fluxes from the Pacific to the Arctic Ocean from 2001 to 2011 and their impacts on the Arctic Ocean water column, Geophys. Res. Lett., 39, L24603 (2012)

Østerhus, S. and T. Gammelsrød, The abyss of the Nordic Seas is warming, J. Climate, 12, 3297-3304 (1999)

Østerhus, S., W.R. Turrell, S. Jónsson and B. Hansen, Measured volume, heat and salt fluxes from the Atlantic to the Arctic Mediterranean, Geophys. Res. Lett., 32, L07603 (2005)

Årthun, M., R.B. Ingvaldsen, L.H. Smedsrud and C. Schrum, Dense water formation and circulation in the Barents Sea, Deep-Sea Res. I, 58, 801-817 (2011)

Årthun, M., T. Eldevik, L.H. Smedsrud, Ø. Skagseth and R.B. Ingvaldsen, Quantifying the Influence of Atlantic Heat on Barents Sea Ice Variability and Retreat, J. Climat., 25, 4736-4743 (2012)

Retur: Havforskningsinstituttet, Postboks 1870 Nordnes, NO-5817 Bergen

HAVFORSKNINGSINSTITUTTET
Institute of Marine Research
Nordnesgaten 50 – Postboks 1870 Nordnes
NO-5817 Bergen
Tlf.: +47 55 23 85 00 – Faks: +47 55 23 85 31
E-post: post@imr.no

HAVFORSKNINGSINSTITUTTET
AVDELING TROMSØ
Sykehusveien 23, Postboks 6404
NO-9294 Tromsø
Tlf.: +47 77 60 97 00 – Faks: +47 77 60 97 01

HAVFORSKNINGSINSTITUTTET
FORSKNINGSSTASJONEN FLØDEVIGEN
Nye Flødevigveien 20
NO-4817 His
Tlf.: +47 37 05 90 00 – Faks: +47 37 05 90 01

HAVFORSKNINGSINSTITUTTET
FORSKNINGSSTASJONEN AUSTEVOLL
NO-5392 Storebø
Tlf.: +47 55 23 85 00 – Faks: +47 56 18 22 22

HAVFORSKNINGSINSTITUTTET
FORSKNINGSSTASJONEN MATRE
NO-5984 Matredal
Tlf.: +47 55 23 85 00 – Faks: +47 56 36 75 85

AVDELING FOR SAMFUNNSKONTAKT
OG KOMMUNIKASJON
Public Relations and Communication
Tlf.: +47 55 23 85 00 – Faks: +47 55 23 85 55
E-post: informasjonen@imr.no

www.imr.no

HAVFORSKNINGSINSTITUTTET
INSTITUTE OF MARINE RESEARCH